MONTHLY NOTICES

OF THE

ROYAL ASTRONOMICAL SOCIETY

Vol. 109 No. 3

MEETING OF 1949 MARCH 11

Professor W. M. Smart, President, in the Chair

The election by the Council of the following Fellows was duly confirmed :—

H. K. Binks, Kirichwa Road, Nairobi, Kenya (proposed by R. d'E. Atkinson) ;

David Yule Devine, 36 Kingshurst Avenue, King's Park, Glasgow, S.4 (proposed by W. M. Smart) ;

Charles T. Melvin, 109 Kenilworth Avenue, Glasgow, S. 1 (proposed by W. M. Smart) ;

Thomas Keith Metcalfe, 16 High Street, Poole, Dorset (proposed by F. M. Wingate) ; and

John Francis Pell, 11a Cheltenham Road, Orpington, Kent (proposed by H. Wildey).

The election by the Council of the following Junior Member was duly confirmed :—

Ian Leslie Martin-Jones, 17 Croham Park Avenue, South Croydon (proposed by C. A. Ronan).

Eighty-nine presents were announced as having been received since the last meeting, including :—

Sir W. M. Flinders Petrie, Astronomical Charts and Manuscripts (presented by Lady Flinders Petrie) ;

C. T. Moss, *The Telescopes of Sir William Herschel* (presented by the author);

Report of the Scientific Information Conference, 1948 *June* 21–*July* 2 (presented by the Royal Society);

M. A. R. Khan, *Synopsis of Meteor Observations in* 1945 *at Begumpet, Deccan, India* (presented by the author); and

Centennial Symposia, Harvard Observatory Monograph No. 7 (presented by Harvard Observatory).

MEETING OF 1949 APRIL 8

Professor W. M. Smart, President, in the Chair

The election by the Council of the following Fellows was duly confirmed :—

Walter D. Lambert, Ph.D., Box 687, Canaan, Connecticut, U.S.A. (proposed by H. Jeffreys) ;

L. Llewellyn Lloyd, 164 Whitchurch Road, Cardiff, South Wales (proposed by A. Buxton) ;

Ernst Julius Öpik, D.Ph., Armagh Observatory, Armagh, Northern Ireland (proposed by E. M. Lindsay) ;

Chandrika Prasad, M.Sc., Queen's College, Oxford (proposed by E. A. Milne) ; and

William Trevor Trewartha, B.Sc., Science Department, Technical College, Gloucester (proposed by W. J. Jones).

Seventy-one presents were announced as having been received since the last meeting, including :—

Sir Richard Gregory, *Gods and Men* (presented by the author);

F. J. M. Stratton, *The History of the Cambridge Observatories* (presented by the author); and

Helen Wright, *Sweeper in the Sky: the Life of Maria Mitchell* (presented by Miss Margaret Harwood).

The President announced that the Council had elected the following as Associates of the Society :—

Dr Daniel Chalonge, Institut d'Astrophysique, 98 Boulevard Arago, Paris ; and

Dr Charlotte E. Moore Sitterly, U.S. Bureau of Standards, Washington, D.C., U.S.A.

ON THE OPTICS OF THE SCHMIDT CAMERA

E. H. Linfoot

(Received 1949 January 18)

Summary

A fifth-order aberration function is derived for the ordinary Schmidt camera. Colour correction is also considered and a proof is given of J. G. Baker's formulae for the first three coefficients in the aspheric plate profile of a system with minimized axial colour-spreads. Finally aberration functions are used to design a modified system in which the monochromatic aberrations are balanced over a finite field, and the performance of this system is compared with that of the ordinary Schmidt camera by means of spot diagrams.

---

1. *Introduction.*—Although its performance must be rated as high by ordinary standards, the Schmidt camera in its classical form possesses the disadvantage that its aberrations are not balanced over its field. The images are smallest in the centre of the field and increase in size towards the edge. In most of the existing astronomical Schmidt cameras this is probably of little practical consequence, since the confusion patches, even at the edge of the field, are smaller than the diameter of the tremor disk of a star under conditions of moderate seeing. Nevertheless, it seems worth while to consider what improvements in optical performance can be made by modifying the design of the system so as to balance its monochromatic aberrations over a given field. In the present paper a general aberration theory of the Schmidt camera is set out and is applied to the discussion of this question.

In Section 2 the theory of the Schmidt camera is developed *ab initio*, the fifth-order aberration function of the system is derived, and the performance of the camera is shown to be substantially unchanged when the plate is turned round and readjusted to annul Seidel coma. In Section 3 the question of axial colour correction is discussed, a proof is given of J. G. Baker's formulae for the first three coefficients in the expansion of the plate profile and the off-axis aberrations in light of different wave-lengths are determined.

Finally, in Section 4, aberration functions are used to design a modified camera with balanced monochromatic aberrations and to compare its performance with that of the ordinary Schmidt camera. It appears that some improvement in performance is obtained ; in particular, the maximum size of the geometrical images in light from a selected point of the spectrum can be reduced by a factor $\frac{2}{5}$ and the image quality is nearly uniform over the whole field. The small amount of "figuring" introduced on the mirror does not seriously increase the amount of work involved in constructing the system, since its depth is less than four fringes even in a 48–72-inch $f/2{\cdot}5$ telescope.

2. *The aberration function of the Schmidt camera.*—First, suppose that the aspheric face of the plate is towards the mirror. The imaging properties of the system for objects at infinity are then independent of the plate-thickness. Take rectangular coordinates (x, y, z) with origin at the pole of the aspheric surface, which is also the centre of curvature C of the spherical mirror, and z-axis along

the axis CA of the camera, as shown in Fig. 1. Then the Cartesian equation of the aspheric surface can be written

$$z = T(x,y) - T(0,0) = a_1h^2 + a_2h^4 + a_3h^6 + \ldots, \tag{1}$$

where $h^2 = x^2 + y^2$ and $T(x,y)$ denotes the thickness of the plate at the point (x,y). The values of the coefficients $a_1, a_2, a_3, \ldots$ are discussed in the next section, and it is shown there that, if the terms in $h^6, h^8, \ldots$ are small enough for their sum to be neglected,

$$T(x,y) = T(0,0) + \frac{1}{n-1}\frac{1}{32f^3}(h^4 - aH^2h^2) + O(H^6/32f^5), \tag{2}$$

where n is the refractive index of the plate, f the focal length of the camera and H the radius of the aperture stop on the plate. The focal ratio F of the camera is equal to $f/2H$.

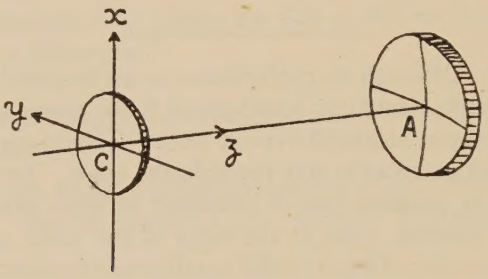

Fig. 1.

A notation better adapted to the discussion of the off-axis errors is obtained on setting

$$\lambda = H/2f. \tag{3}$$

Then 2λ is the numerical aperture of the system and

$$\lambda = 1/4F, \tag{4}$$

where F is its focal ratio. We introduce the dimensionless variables u, v and r by means of the equations

$$x = 2\lambda f u, \quad y = 2\lambda f v, \quad h = 2\lambda f r\ ; \tag{5}$$

thus $r^2 = u^2 + v^2$ and the aperture stop is defined by the inequality $u^2 + v^2 \leqq 1$. In order to keep the formulae as simple as possible, we suppose for the time being that $f = \frac{1}{2}$; this is equivalent to taking as unit of length the quantity $2f$, which is very nearly equal to the radius of curvature of the mirror. Equation (2) now becomes

$$T(x,y) - T(0,0) = \frac{1}{n-1} \cdot \tfrac{1}{4}\lambda^4(r^4 - ar^2) + O(\lambda^6). \tag{6}$$

In an $f/3$ camera $\lambda^2 = 1/144$, while $r \leqq 1$ always and the value of a is between 1 and 2 in a practical case. Therefore the error-term in this equation amounts to only a few per cent of the maximum size of the leading term.

Let d_0 be the least thickness of the plate. Then the plate is equivalent to a plane-parallel plate of thickness d_0, together with a "figuring layer", of which the thickness is $T(0,0) - d_0$ at the centre of the plate and decreases to zero at its

"neutral zone". Let the thickness of the figuring layer at the point (x, y) be denoted by

$$U(x, y) = T(x, y) - d_0. \tag{7}$$

Then it follows from (6) that

$$U(x, y) = O(\lambda^4) \tag{8}$$

at all points (x, y) of the aperture.

First, suppose the system to consist of the mirror and the figuring layer only. The effect on the images of adding in the remainder of the plate-thickness will be considered later ; it is evidently zero when the aspheric side of the plate is towards the mirror.

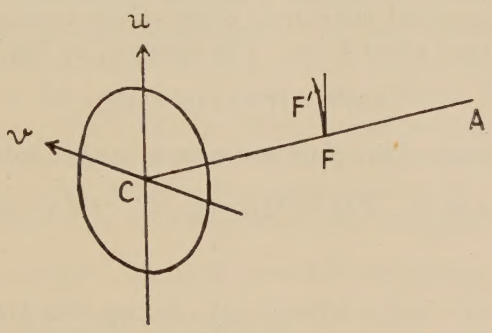

FIG. 2A.

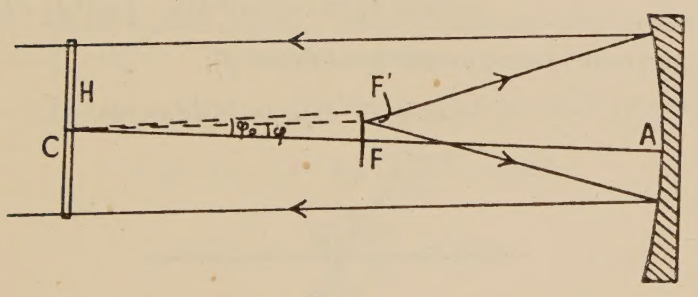

FIG. 2B.

Let c be the central obstruction ratio of the system. Then if $2\phi_0$ is the angular diameter of the field,

$$\sin\phi_0 = cH/f = 2c\lambda,$$

approximately. In cases (such as the 24–36-inch $f/3{\cdot}5$ Burrell telescope and the 48–72-inch $f/2{\cdot}5$ Palomar Schmidt) where the mirror-diameter is $\frac{3}{2}$ times the clear aperture, we have, to within one per cent,

$$c = \tfrac{1}{4}, \quad \sin\phi_0 = \tfrac{1}{2}\lambda.$$

In an $f/3{\cdot}5$ system this gives $\sin\phi_0 = 1/28$ and the unvignetted field has a diameter of just over 4 degrees; in an $f/2{\cdot}5$ system the unvignetted field is 6 degrees in diameter. In all the large Schmidt telescopes so far built, the value of c lies between $\frac{1}{4}$ and $\frac{1}{2}$.

A parallel pencil entering the camera at an angle ϕ with the axis forms an image on the photographic plate if $0 \leqslant \phi \leqslant \phi_0$. The new variable V, defined by the equation

$$\sin\phi = 2c\lambda V, \tag{9}$$

runs from 0 at the centre of the field to approximately 1 at its edge.

The new variables have the property that u, v, r, V all range from -1 to 1 or from 0 to 1, while λ^2 is usually less than 0·01. The numerical order of magnitude of the different terms in our expression is therefore indicated by the powers of λ which they contain.*

Consider a pencil of rays, and their orthogonal surfaces the associated wave-fronts, issuing from a point F′ in the field surface such that $\widehat{FCF'}=\phi$ and F′ lies in the plane uCz. See Figs. 2A, 2B. If the system had no off-axis aberrations, these wave-fronts would emerge from it as plane surfaces; their actual deviations from flatness indicate the aberrations of the system.

These deviations arise in the following way.† In the first place, the retardation imposed by a plane-parallel plate upon plane waves meeting it at an angle ϕ is greater when $\phi\neq 0$ than when $\phi=0$. The increase, by Fig. 3, is

$$n\,.\,\mathrm{PQ}-[\mathrm{PM}+(n-1)d],$$

where d is the thickness of the plate and n its refractive index. Since

$$\mathrm{PQ}=d\sec\eta,\quad \mathrm{PM}=\mathrm{PQ}\cos(\phi-\eta),\quad \sin\eta=(\sin\phi)/n$$

it follows that

$$\begin{aligned} n\,.\,\mathrm{PQ}-[\mathrm{PM}+(n-1)d] &= nd(\sec\eta-1)-d(\cos\phi+\sin\phi\tan\eta-1)\\ &= d(\sin^2\phi)/2n-d((\sin^2\phi)/n-\tfrac{1}{2}\sin^2\phi)+O(d\sin^4\phi), \end{aligned}$$

since $\sin\phi\tan\eta=\sin^2\phi\sec\eta/n=\sin^2\phi/n+O(\sin^4\phi)$,

$$=\sin^2\phi\,.\,(n-1)d/2n+O(d\sin^4\phi). \qquad (10)$$

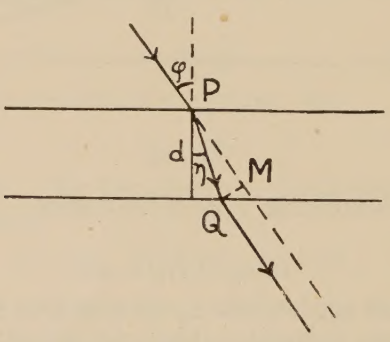

FIG. 3.

Now suppose that the wave-fronts are nearly plane, with angular deviations $O(\lambda^3)$ from flatness, the plate nearly plane-parallel, with thickness $O(\lambda^4)$ and surface-slope deviations $O(\lambda^3)$, and the angle of incidence ϕ such that $\sin\phi=O(\lambda)$. This change in the hypotheses introduces an inaccuracy $O(\lambda^8)$ in the retardations and (10) can therefore be replaced by the expression

$$\sin^2\phi\,.\,(n-1)d/2n+O(\lambda^8). \qquad (11)$$

* The device of introducing an auxiliary parameter λ, so as to make visible the numerical orders of magnitude of the terms, is due to J. L. Synge, *J.O.S.A.*, **33**, 129–136, 1943.

† Compare C. Carathéodory, *Hamb. Math. Einzelschrift*, **28**, paragraphs 25–29, 1940.

By (6), (7) the new hypotheses are applicable to any element δS of the aspheric surface of the figuring layer surrounding the point $(x, y, U(x, Y) - U(0, 0))$. It follows that the retardation imposed by the figuring layer on that part of the oblique, near-flat wave-front which crosses its aspheric surface in the element δS exceeds the retardation imposed on a wave-front arriving square on by an amount

$$\sin^2\phi \,.\, (n-1)U(x,y)/2n + O(\lambda^8)$$

$$= 4\lambda^2 c^2 V^2 \,.\, (n-1)U(x,y)/2n + O(\lambda^8), \tag{12}$$

by (9).

A further contribution to the change in retardation of the wave-fronts arises from "foreshortening", in the following way. Consider that ray γ traced out from F (Fig. 2A) which, after reflection at the spherical mirror, meets the plane $z = 0$ of the aperture stop in the point $(x, y, 0)$ and, consequently, the aspheric surface in a point $(x + O(\lambda^7), y + O(\lambda^7), O(\lambda^4))$. If the pencil issuing from F be rotated bodily through an angle ϕ about the axis Cv, it becomes a pencil issuing from F′; let γ' be the ray of this new pencil which corresponds to γ. After reflection in the sphere, γ' meets the plane of the aperture stop in a point of coordinates

$$(x\sec\phi + O(\lambda^3) \,.\, O(x\sin\phi),\ y + O(\lambda^3) \,.\, O(x\sin\phi),\ 0)$$

$$= (x\sec\phi + O(\lambda^5),\ y + O(\lambda^5),\ 0)$$

and meets the aspheric surface in a point whose coordinates differ from these values by $O(\lambda^4) \,.\, O(\sin\phi) = O(\lambda^5)$. This causes a change

$$(n-1)U(x\sec\phi + O(\lambda^5),\ y + O(\lambda^5)) - (n-1)U(x + O(\lambda^5),\ y + O(\lambda^5))$$

$$= (n-1)(\sec\phi - 1)x\frac{\partial U(x,y)}{\partial x} + O(\lambda^8)$$

$$= 4c^2\lambda^2 V^2 \,.\, (n-1)\tfrac{1}{2}x\frac{\partial U}{\partial x} + O(\lambda^8) \tag{13}$$

in the retardation of the emerging wave-front by the plate.

The cross terms between the two effects (12) and (13) being $O(\lambda^8)$, their resultant is

$$4(n-1)c^2\lambda^2 V^2\left(\frac{1}{2n} + \tfrac{1}{2}x\frac{\partial}{\partial x}\right)U(x,y) + O(\lambda^8). \tag{14}$$

Since the rays from the axial focal point F become a parallel beam after passing through the aspheric surface, (14) gives the deviations from flatness of the wave-fronts corresponding to the pencil from F′ after passing out through the figuring layer of thickness $O(\lambda^4)$. If we assume (what is true in a practical case) that the overall thickness of the Schmidt plate is at most $O(\lambda)$, then the deviation from flatness of a wave-front after passing through the whole plate differs by $O(\lambda^8)$ from its deviation, at the corresponding point of its surface, after passing (into air) through the figuring layer only; it is therefore still given by (14).

This means that the "aberration function" of the Schmidt camera working backwards can be written

$$\lambda^6\Phi(x, y, V) = 4(n-1)c^2\lambda^2 V^2\left(\frac{1}{2n} + \tfrac{1}{2}x\frac{\partial}{\partial x}\right)U(x,y) + O(\lambda^8). \tag{15}$$

If the plate is turned round, with its aspheric face away from the mirror, and placed so that its plane face is $1/n$ times the axial plate thickness inside C, then with a plate-thickness $O(\lambda)$ the effect on the error function is $O(\lambda^8)$.* Thus (15) gives the error-function in this case also.

The mathematical form of the function

$$\lambda^6\Phi(x,y,V)=4\lambda^2(n-1)c^2V^2\left(\frac{1}{2n}+\tfrac{1}{2}x\frac{\partial}{\partial x}\right)U(x,y)+O(\lambda^8)$$

$$=\tfrac{1}{2}\lambda^6c^2V^2\left(\frac{1}{n}+u\frac{\partial}{\partial u}\right)(r^4-ar^2)+O(\lambda^8)\dagger \tag{16}$$

embodies a description of the optical aberrations of the system when working backwards. The quantities

$$\left(\lambda^6\frac{\partial\Phi}{\partial x},\lambda^6\frac{\partial\Phi}{\partial y}\right)=\left(\lambda^5\frac{\partial\Phi}{\partial u},\lambda^5\frac{\partial\Phi}{\partial v}\right) \tag{17}$$

measure, in radians, the radial and tangential aberration displacements corresponding to the point (u,v) of the aperture stop $u^2+v^2\leqq 1$, at any given distance from the centre of the field in the u-direction. So far as leading terms are concerned, these displacements are the same whether we consider rays traced out from a single focal point or rays traced in from a single parallel pencil. It follows that (16) also describes the optical aberrations of the Schmidt camera working normally with object at infinity, and is valid with the corrector plate either way round, provided the thickness of this plate is $O(\lambda)$. Since (16) holds with the system working either forwards or backwards, it follows that the curves $\Phi(x,y,V)=$ constant give the fringes seen on the plate when the camera is tested, on and off axis, by autostigmatism on an interferometer.

By (17), the angular displacement components in the field surface are

$$\tfrac{1}{2}c^2\lambda^5V^2\left(\frac{n+1}{n}\frac{\partial}{\partial u}+u\frac{\partial^2}{\partial u^2},\ \frac{1}{n}\frac{\partial}{\partial v}+u\frac{\partial^2}{\partial u\,\partial v}\right)(r^4-ar^2)+O(\lambda^7)$$

$$=c^2\lambda^5V^2\left(\frac{n+1}{n}[2u(u^2+v^2)-au]+2u(3u^2+v^2)-au,\right.$$

$$\left.\frac{1}{n}[2v(u^2+v^2)-av]+4u^2v\right)+O(\lambda^7) \tag{18}$$

and the linear components are obtained on multiplying these by the focal length of the system. When $n=\frac{3}{2}$, the angular displacements take the values

$$\tfrac{4}{3}c^2\lambda^5V^2(7u^3+4uv^2-2au,\ 4u^2v+v^3-\tfrac{1}{2}av)+O(\lambda^7). \tag{19}$$

We call the leading term on the right of (16), namely

$$\tfrac{1}{2}\lambda^6c^2V^2\left(\frac{1}{n}+u\frac{\partial}{\partial u}\right)(r^4-ar^2), \tag{20}$$

* In the on-axis pencil, the only effect is on the zonal aberration of the plane-parallel part of the plate in the nearly parallel pencil coming from the mirror ; this contributes a wave-distortion $O(\lambda^{14})$. In the off-axis pencils, there is also a contribution $O(\lambda^3)\,.\,O(\lambda)\,.\,O(\lambda^4)=O(\lambda^8)$ due to lateral shift of the wave-fronts impinging on the aspheric surface.

† By (6) and (7). Since the error-term in (6) is the tail end of a convergent power series in r^2, its partial derivative with respect to u is likewise $O(\lambda^6)$.

the *fifth-order monochromatic aberration function* of the Schmidt camera and denote it by $\lambda^6\Phi^*(u, v, V)$. The quantities

$$\lambda^5\frac{\partial\Phi^*}{\partial u}, \quad \lambda^5\frac{\partial\Phi^*}{\partial v}$$

$$= c^2\lambda^5V^2\left(\frac{n+1}{n}[2u(u^2+v^2)-au]+2u(3u^2+v^2)-au,\right.$$

$$\left.\frac{1}{n}[2v(u^2+v^2)-av]+4u^2v\right) \qquad (21)$$

will be called the *fifth-order monochromatic aberration displacements* of the system.* When the focal ratio of the system is 1 : 3 or longer, $\gamma^2 \leq 1/144$ and the fifth-order aberrations describe the size and shape of the geometrical image with an error of only two or three per cent. It will be seen that only the second- and fourth-power terms in the plate profile expansion contribute to these aberrations.

In the derivation of the expressions (18)–(21), it was assumed that the unit of length was twice the focal length of the system. When this assumption is dropped, (18)–(21) retain their form unchanged, since all the letters in these expressions represent dimensionless quantities.

3. *Corrector plate profile and colour error in the classical Schmidt camera.*— To calculate, with accuracy sufficient for all practical purposes, the off-axis aberrations of a Schmidt telescope of focal ratio 1 : 3 or longer, it is enough to know the coefficients of the squared and fourth-power terms in the expansion of the aspheric plate profile. For, knowing these and knowing also that the axial image is stigmatic, we can, by the last section, write down the fifth-order aberration displacements (21) which describe the light distribution in the geometrical image.

Provided a suitable optical test is used during the final figuring, it is also possible to neglect sixth and higher powers in the aspheric grinding of the plate. For example, in an *f*/3 Schmidt telescope of 25 inches aperture, the omission of these terms from the calculated profile creates a turn-down edge only one fringe deep, an error which can easily be corrected during the optical figuring of the system under an autocollimation test.

However, the same procedure applied to a 25-inch *f*/2 Schmidt would give 11 fringes of turn-down error on the plate as calculated, and applied to an 8-inch *f*/1 Schmidt would give 37 fringes. The removal of these errors by polishing would be a very laborious task.

Since the amount of turn-down caused by dropping sixth and higher powers in the plate profile varies rapidly with the focal ratio (namely as its sixth power) and much less rapidly with the aperture, it appears from the above that we may adopt the rough working rule that sixth powers should be taken into account whenever the focal ratio is shorter than *f*/3.

To calculate the plate profile as far as the sixth-power term, consider a ray QP entering the system, parallel to the axis, through the "neutral zone" of the corrector plate, as shown in Fig. 4. After reflection at the point P of the mirror surface, this ray comes into the axial focal point F. Let C denote the centre of curvature of the mirror, A its pole and CQ a perpendicular through C to the axis

* This differs from the usual terminology, according to which terms in au, av would be classed as third-order displacements. Such a classification by means of total degree in u, v, V has practical value only in an optical system whose Seidel errors are not "corrected", i. e. balanced against its higher errors. For only in such uncorrected systems do the total degrees of the terms give a true picture of their numerical sizes, by which the performance of the system is determined.

of the system. If the plate is turned with its aspheric face towards the mirror, then this face passes through C and Q is very close to it and just outside the glass. If the plate is turned with its plane face towards the mirror, then C and Q are inside the glass, at a distance from the plane surface equal to $1/n$ of the central thickness of the plate.

Let R denote the radius of curvature of the mirror, H the radius of the aperture stop and set

$$\mu = H/R. \tag{22}$$

Since the focal length f of the system is nearly equal to $\frac{1}{2}R$, it follows that μ is nearly equal to the parameter λ of Section 2. Coordinates u, v in the aperture stop, defined by the equations

$$x = Hu, \quad y = Hv, \tag{23}$$

are identical with those of Section 2, since the aperture stop again has the circle $u^2+v^2=1$ as boundary. To simplify the formulae, we now choose R as the unit of length, setting $R=1$. Then $H=\mu$, by (22), and equations (23) become

$$x = \mu u, \quad y = \mu v. \tag{24}$$

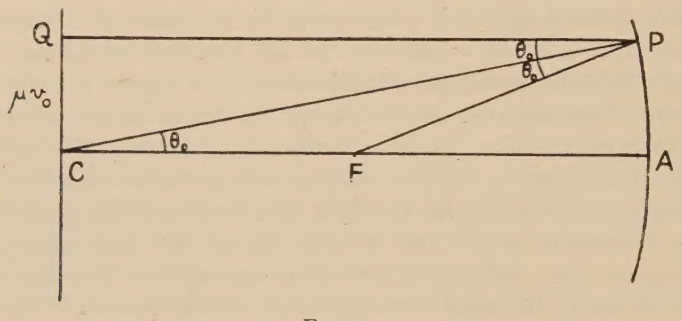

FIG. 4.

Fig. 4 can be taken to represent a section of the system by the plane $u=0$. Set

$$CQ = \mu v_0, \quad \widehat{CPQ} = \widehat{CPF} = \widehat{PCF} = \theta_0\,; \tag{25}$$

the value $\frac{1}{2}\sqrt{3}$ for v_0 corresponds to the usual "colour-minimized" plate profile with neutral zone of radius $\frac{1}{2}\sqrt{3}$ times that of the full aperture.

From the geometry of the figure,

$$f = CF = \tfrac{1}{2}\sec\theta_0, \tag{26}$$

$$\sin\theta_0 = \mu v_0, \tag{27}$$

$$\cos\theta_0 = (1-\mu^2 v_0^2)^{\frac{1}{2}} = 1 - \tfrac{1}{2}\mu^2 v_0^2 - \tfrac{1}{8}\mu^4 v_0^4 - \ldots,$$

$$1-\cos\theta_0 = \tfrac{1}{2}\mu^2 v_0^2(1+\tfrac{1}{4}\mu^2 v_0^2 + \ldots). \tag{28}$$

By Gaussian optics, the paraxial focal length f_P of the plate is given by

$$\frac{1}{f_P} + \frac{1}{\frac{1}{2}} - \frac{CA}{\frac{1}{2}f_P} = \frac{1}{f},$$

$$2 - \frac{1}{f_P} = 2\cos\theta_0,$$

$$\frac{1}{f_P} = 2(1-\cos\theta_0). \tag{29}$$

Let the equation of the plate profile be

$$s = a_1\mu^2v^2 + a_2\mu^4v^4 + a_3\mu^6v^6 + \ldots, \tag{30}$$

where $s = z/R$ is the z of Section 2 measured in the new units.

Then we have,

(1) by considering coefficients of v^2

$$(n-1)a_1\mu^2 = -\mu^2/2f_P,$$
$$a_1 = -(1-\cos\theta_0)/(n-1). \tag{31}$$

(2)

$$\mathrm{FA}+\mathrm{AC} = 2 - \tfrac{1}{2}\sec\theta_0,$$
$$\mathrm{FP}+\mathrm{PQ} = \tfrac{1}{2}\sec\theta_0 + \cos\theta_0,$$
$$(\mathrm{FP}+\mathrm{PQ})-(\mathrm{FA}+\mathrm{AC}) = \sec\theta_0 + \cos\theta_0 - 2$$
$$= \sec\theta_0(1-\cos\theta_0)^2.$$

Since the wave-fronts issuing from a point source at F, and reflected at the mirror, emerge from the system as a set of planes perpendicular to the axis CA, it follows that the plate-thickness at the neutral point Q must be less than its thickness at C by the amount

$$\sec\theta_0(1-\cos\theta_0)^2/(n-1).$$

That is to say

$$a_1\mu^2v_0^2 + a_2\mu^4v_0^4 + a_3\mu^6v_0^6 = -\sec\theta_0(1-\cos\theta_0)^2/(n-1) + O(\mu^8),$$
$$a_2\mu^4v_0^4 + a_3\mu^6v_0^6 = -a_1\mu^2v_0^2 - \sec\theta_0(1-\cos\theta_0)^2/(n-1) + O(\mu^8). \tag{32}$$

(3) Since the plate-slope $ds/\mu\,dv$ vanishes * for $v = v_0$, (30) gives

$$2a_1\mu^2v_0 + 4a_2\mu^4v_0^3 + 6a_3\mu_6v_0^5 = O(\mu^8),$$
$$2a_2\mu^4v_0^4 + 3a_3\mu^6v_0^6 = -a_1\mu^2v_0^2 + O(\mu^8). \tag{33}$$

From (32), (33)

$$a_2\mu^4v_0^4 = -2\mu^2v_0^2a_1 - 3\sec\theta_0(1-\cos\theta_0)^2/(n-1) + O(\mu^8), \tag{34}$$
$$a_3\mu^6v_0^6 = a_1\mu^2v_0^2 + 2\sec\theta_0(1-\cos\theta_0)^2/(n-1) + O(\mu^8). \tag{35}$$

Equations (31), (34), (35) give the plate-coefficients explicitly in terms of $\mu v_0 = \sin\theta_0$ and $(1-\mu^2v_0^2)^{\frac{1}{2}} = \cos\theta_0$, with an error $O(\mu^8)$. On substituting the power-series expansions of $\sec\theta_0$ and $1-\cos\theta_0$ in terms of μv_0, the expressions for the coefficients become

$$a_1 = \frac{-1}{n-1}\left(\tfrac{1}{2}\mu^2v_0^2 + \tfrac{1}{8}\mu^4v_0^4 + \ldots\right),$$
$$a_2 = \frac{1}{n-1}\left(\tfrac{1}{4} - \tfrac{1}{2}\mu^2v_0^2 + \ldots\right), \tag{36}$$
$$a_3 = \frac{1}{n-1}\left(\tfrac{3}{8} + \ldots\right)$$

and the plate profile is obtained in the form

$$(n-1)s = \tfrac{1}{4}\mu^4(v^4 - 2v^2v_0^2) + \mu^6\left(\tfrac{3}{8}v^6 - \tfrac{1}{2}v^4v_0^2 - \tfrac{1}{8}v^2v_0^4\right) + O(\mu^8), \tag{37}$$

* The idea of using path differences and deviation changes simultaneously was suggested to me by Dr E. Wolf, who has used it to reduce the amount of trigonometrical ray-tracing needed in the computation of Schmidt-Cassegrain plate profiles. However, Dr Wolf tells me that in this case he has found the method not very well adapted to numerical work. It seems better suited to discussions of a more algebraic character.

or

$$(n-1)s=\tfrac{1}{4}\mu^4(v^2-v_0^2)^2(1+\tfrac{5}{2}v_0^2\mu^2)+\tfrac{3}{8}\mu^6(v^2-v_0^2)^3+\text{constant}+O(\mu^8). \quad (38)$$

(38) has been derived without specifying whether the aspheric surface of the plate is on the side towards or away from the mirror. It therefore holds with the plate either way round.

By (26), (27)

$$f/R=\tfrac{1}{2}(1-\mu^2v_0^2)^{-\frac{1}{2}}=\tfrac{1}{2}(1+\tfrac{1}{2}\mu^2v_0^2+\tfrac{3}{8}\mu^4v_0^4+\dots). \quad (39)$$

By (3), (22), (27)

$$\lambda=\frac{H}{2f}=\frac{H}{R}\cdot\frac{R}{2f}=\mu\cos\theta_0=\mu(1-\mu^2v_0^2)^{\frac{1}{2}}; \quad (40)$$

thus in an $f/3$ system with $v_0=\frac{1}{2}\sqrt{3}$, λ and μ differ in value by less than $\frac{1}{3}$ per cent.

The Baker formulae.—In a system with $\mu=\frac{1}{4}$ and $v_0=\frac{1}{2}\sqrt{3}$, the difference between λ and μ amounts to about $2\frac{1}{2}$ per cent of the value of each of them, and the aperture of the system is very near to $f/1$. The coefficients of v^2, v^4 and v^6 in (38) are respectively $-\frac{3}{8}\mu^4-\frac{9}{128}\mu^6=-0{\cdot}0015$, $\frac{1}{4}\mu^4-\frac{3}{8}\mu^6=0{\cdot}0009$ and $\frac{3}{8}\mu^6=0{\cdot}0001$. Thus, at the edge of the plate, the slope-contribution from the sixth-power term is about $\frac{1}{6}$ of that from the fourth-power term or $\frac{2}{3}$ of that from the squared and fourth-power terms taken together. This suggests that the value $v_0=\frac{1}{2}\sqrt{3}$ of the radius of the neutral zone, which minimizes the axial colour-spread of the system when sixth-power and higher terms in the plate profile are negligible, could be increased with advantage when the aperture ratio approaches $f/1$. Let

$$v_0=\tfrac{1}{2}\sqrt{3}(1+c'\mu^2+\dots) \quad (41)$$

be the modified choice of the neutral zone radius. We wish to choose c' so that the profile-slope at the edge of the plate is equal to that at the steepest part of the central bulge. See Fig. 5.

FIG. 5.—*Profile-curve of Schmidt plate.*

By (38),

$$(n-1)\frac{ds}{dv}=\mu^4v(v^2-v_0^2)(1+\tfrac{5}{2}v_0^2\mu^2)+\tfrac{9}{4}\mu^6v(v^2-v_0^2)^2+\dots, \quad (42)$$

$$(n-1)\frac{d^2s}{dv^2}=\mu^2(3v^2-v_0^2)(1+\tfrac{5}{2}v_0^2\mu^2)+\tfrac{9}{4}\mu^6(v^2-v_0^2)(5v^2-v_0^2)+\dots. \quad (43)$$

Substituting from (41) into (43) and neglecting powers of u higher than the sixth, we find that the slope is stationary where

$$(v^2-\tfrac{1}{4})(1+\tfrac{15}{8}\mu^2)=\tfrac{1}{2}c'\mu^2-\tfrac{3}{4}\mu^2(v^2-\tfrac{3}{4})(5v^2-\tfrac{3}{2}),$$

i.e. where

$$v=\tfrac{1}{2}(1+c'\mu^2+\tfrac{3}{8}\mu^2)+\dots.$$

By (42), the value of the slope at this point is

$$-\tfrac{1}{4}\mu^4(1+3c'\mu^2+\tfrac{3}{4}\mu^2)+\ldots, \tag{44}$$

while its value at the edge of the plate, found by substituting from (41) into (42) and setting $v=1$, is

$$\tfrac{1}{4}\mu^4(1-6c'\mu^2+\tfrac{39}{16}\mu^2)+\ldots. \tag{45}$$

Since (44) increases with c', while (45) decreases as c' increases, it follows that the colour is minimized when

$$\tfrac{1}{4}\mu^4(1+3c'\mu^2+\tfrac{3}{4}\mu^2)+\ldots=\tfrac{1}{4}\mu^4(1-6c'\mu^2+\tfrac{39}{16}\mu^2)+\ldots,$$

$$c'=\tfrac{3}{16}, \tag{46}$$

and that the value of the greatest slope is then

$$\tfrac{1}{4}\mu^4(1+\tfrac{21}{16}\mu^2)+\ldots, \tag{47}$$

while the neutral zone is at the radius

$$v_0=\tfrac{1}{2}\sqrt{3}(1+\tfrac{3}{16}\mu^2)+\ldots, \tag{48}$$

On substituting this value for v_0 into (36), the values of the plate profile coefficients a_1, a_2, a_3 become

$$a_1=\frac{-1}{n-1}(\tfrac{3}{8}\mu^2+\tfrac{27}{128}\mu^4+\ldots),$$

$$a_2=\frac{1}{n-1}(\tfrac{1}{4}-\tfrac{3}{8}\mu^2+\ldots), \tag{49}$$

$$a_3=\frac{1}{n-1}(\tfrac{3}{8}+\ldots),$$

while the focal length

$$f=\tfrac{1}{2}\sec\theta_0=\tfrac{1}{2}+\tfrac{3}{16}\mu^2+\tfrac{45}{256}\mu^4+\ldots. \tag{50}$$

These formulae were given, without proof and in a slightly different notation, by J. G. Baker in his valuable and interesting paper "The solid glass Schmidt camera and a new-type nebular spectrograph".* They are especially useful at focal ratios shorter than $f/1$, for which indeed they were developed. At longer focal ratios, such as $f/3$, the choice of v_0 is not very critical. For example, colour-compensation by taking $v_0=\frac{1}{2}\sqrt{3}$ gives maximum slope $-\frac{1}{4}\mu^4(1+\frac{15}{61}\mu^2)+\ldots$ on the central bulge of the plate, and slope $\frac{1}{4}\mu^4(1+\frac{39}{16}\mu^2)+\ldots$ at its edge. The worst slope is therefore at the edge, and in an $f/1$ system ($\mu=\frac{1}{4}$) this is about 16 per cent greater than the worst slope when v_0 is chosen according to (48). In an $f/2$ system ($\mu=\frac{1}{8}$) the corresponding loss is only 2 per cent, so that in systems of focal ratio $f/2$ or longer the value $v_0=\frac{1}{2}\sqrt{3}$ is sufficient for all practical purposes. On substituting this value in (37), the plate profile becomes

$$(n-1)s=\tfrac{1}{4}\mu^4(v^4-\tfrac{3}{2}v^2)+\mu^6(\tfrac{3}{8}v^6-\tfrac{3}{8}v^4-\tfrac{9}{128}v^2)+O(\mu^8). \tag{51}$$

Proof of equation (2).—If the focal ratio is $f/3$ or longer, terms in μ^6 can be neglected in practice and (38) becomes

$$(n-1)s=\tfrac{1}{4}\mu^4(v^2-v_0^2)^2+\text{constant}+O(\mu^6)$$

$$=\tfrac{1}{4}\mu^4(v^4-2v_0^2v^2)+O(\mu^6), \tag{52}$$

* J. G. Baker, *Proc. Am. Phil. Soc.*, **82**, 323–338, 1940; Baker's h, y become $\mu, \mu v$ respectively in the notation used here. In a footnote to p. 332 of the same paper, expansions up to μ^{10} for the first five coefficients a, b, c, d, e in the power series representing the plate profile are given, again without proof. These expansions, useful in the design of very fast Schmidt cameras, can be derived by an obvious extension of the present method.

since $s=0$ when $v=0$. We also have from (50)

$$f=\tfrac{1}{2}+\tfrac{3}{16}\mu^2+O(\mu^4). \tag{53}$$

On reintroducing x, y, z, H by means of (22), (23), dropping the assumption that $R=1$, and writing z/R, f/R for s, f to allow for the change of unit, (52) and (53) take the form

$$(n-1)z=(y^4-2v_0^2H^2y^2)/4R^3+O(H^6/R^5), \tag{54}$$

$$f=\tfrac{1}{2}R+\tfrac{3}{16}\frac{H^2}{R}+O(H^4/R^3). \tag{55}$$

These equations give the equation of the plate profile and the focal length of the system in terms of R, H and v_0. On replacing y by $h=R(x^2+y^2)^{\frac{1}{2}}$, setting $a=2v_0^2$ and eliminating f between (54) and (55), we obtain

$$(n-1)z=\frac{1}{32f^3}(h^4-aH^2h^2)+O(H^6/R^5)$$

as the Cartesian equation of the plate-surface when terms of order H^6/R^5 can be neglected. This establishes (2) ; the parameter

$$a=2v_0^2$$

takes the value $\frac{3}{2}$ when $v_0=\frac{1}{2}\sqrt{3}$, i. e. when the neutral zone is given a diameter equal to 0·866 of the full aperture. When v_0 is given the Baker value (48), or, more generally, whenever $v_0=\frac{1}{2}\sqrt{3}+O(\mu^2)$, the error committed by retaining the value $a=\frac{3}{2}$ in (2) is $O(H^6/R^5)$ and hence is absorbed in the error term. It follows that the fifth-order monochromatic aberration function of the colour-minimized Schmidt camera is obtained on setting $a=\frac{3}{2}$ in (16), whether the axial colour-compensation is done according to the simple recipe $v_0=\frac{1}{2}\sqrt{3}$ or in a more refined way by giving v_0 the value (48).

The chromatic aberration function.—The axial colour-spread of a Schmidt telescope is comparable with the monochromatic error-spread at the edge of the field when the obstruction ratio c is between $\frac{1}{4}$ and $\frac{1}{2}$. For example, in an $f/3$ camera covering a 5-degree field the obstruction-ratio is $\frac{1}{4}$, the monochromatic error-spread at the edge of the field is 0·36 seconds of arc and the axial colour-spread, when the plate is figured in F-light, is 1 second of arc over the spectral range C–h. In such a system the colour-deviations are of numerical size $O(\lambda^5)$, and the error involved in treating them as constant over the field is of numerical size $O(\lambda^7)$, that is to say negligible in the fifth-order theory.

To the same order of accuracy, the value of $a=\frac{1}{2}v_0^2$ may be taken as $\frac{3}{2}$ in calculating the aberrations, even when it is actually given by (48). For, as already remarked, this approximation introduces an error of only $O(\lambda^7)$ in the monochromatic aberrations and it introduces only an error-factor $1+O(\lambda^2)$ into the axial colour-spreads.

It follows that, to the order of numerical accuracy involved in neglecting monochromatic aberrations beyond the fifth order, the aberration function $\lambda^6\Phi(u, v, V\,;\,n')$, in light of index n', of a Schmidt camera designed to give axial stigmatism in light of index n is given by the equation

$$\begin{aligned}\lambda^6\Phi(u, v, V\,;\,n')&=\lambda^6\Phi^*(u, v, V)+(n'-n)[T(x, y)-T(0, 0)]+O(\lambda^8)\\&=\lambda^6\Phi^*(u, v, V)+\frac{n'-n}{n-1}[\tfrac{1}{4}\lambda^4(r^4-ar^2)+O(\lambda^6)]+O(\lambda^8),\end{aligned}$$

by (6),

$$=\lambda^6[\tfrac{1}{2}c^2V^2\left(\frac{1}{n}+u\frac{\partial}{\partial u}\right)+k_{n,n',\lambda}](r^4-ar^2)+O(\lambda^8), \qquad (56)$$

where

$$k_{n,n',\lambda}=\frac{n'-n}{4\lambda^2(n-1)}=O(1) \qquad (57)$$

in a practical case. We call the leading term on the right of (56) the *fifth-order aberration function* of the Schmidt camera and denote it by $\lambda^6\Phi^*(u, v, V\,;\, n')$.

If the Schmidt plate, of a hard crown glass or of plate glass, is figured in F-light, the value of the coefficient $k_{n,n',\lambda}$ is approximately

$$1/240\lambda^2 = F^2/15$$

at either end of the spectral range C–h. In this last formula F stands for the focal ratio ; in the large Schmidt cameras so far made, $F^2/15$ lies between 0·25 and 1.

From (56) it is easy to calculate the fifth-order angular aberration components

$$\lambda^5\frac{\partial}{\partial u}\Phi^*(u, v, V\,;\, n'), \quad \lambda^5\frac{\partial}{\partial v}\Phi^*(u, v, V\,;\, n')$$

of the ray entering the system through the points (u, v) of the aperture stop, at an angle $\Phi=\arcsin 2c\lambda V$ with the axis, in light from any part of the spectrum. By plotting, for given V, n', the values of the aberration displacements corresponding to a lattice of points

$$u, v=0,\ \pm 0{\cdot}1,\ \pm 0{\cdot}2, \ldots$$

in the aperture stop $u^2+v^2\leqq 1$, we obtain a point-cluster or "spot diagram" which represents fairly closely the light distribution in the geometrical image.* Fig. 6 shows spot diagrams in F, G′ and h-light at selected points of the field-surface of an $f/3{\cdot}5$ Schmidt camera in which the plate is designed to give axial stigmatism in G′-light ; the effect of the central obstruction is ignored.† It will be seen that, over the spectral range F–h, which includes the brightest part of the mean astrographic spectrum, the geometrical images are comparable in size with the Airy disk corresponding to a 24-inch aperture. Even over the spectral range C–h, the geometric images only reach about three times the size of the Airy disk. Thus the optical aberrations of a 24-inch $f/3{\cdot}5$ Schmidt camera working over a field of 5 degrees diameter are negligible for practical purposes. The case is otherwise, however, with a 48-inch $f/2{\cdot}5$ Schmidt camera. See Fig. 8.

4. *A Schmidt camera with balanced monochromatic aberrations.*—The methods of Section 2 can be applied to discuss the problem of "balancing" the fifth-order aberrations of the Schmidt camera by the introduction of small, controlled amounts of Seidel astigmatism and of primary spherical aberration.

To introduce these balancing aberrations we put a figuring

$$\tfrac{1}{8}m_1\lambda^6(r^4-ar^2) \qquad (58)$$

---

* Compare D. G. Hawkins and E. H. Linfoot, *M.N.*, **105**, 334, 1945 ; M. Herzberger, *J.O.S.A.*, **37**, 485, 1947.

† Since the Airy disk corresponding to the central obstruction is several times larger than the geometrical images corresponding to the full aperture, the effect of the obstruction on the physical images cannot be approximately represented by deleting the corresponding points in the spot diagrams.

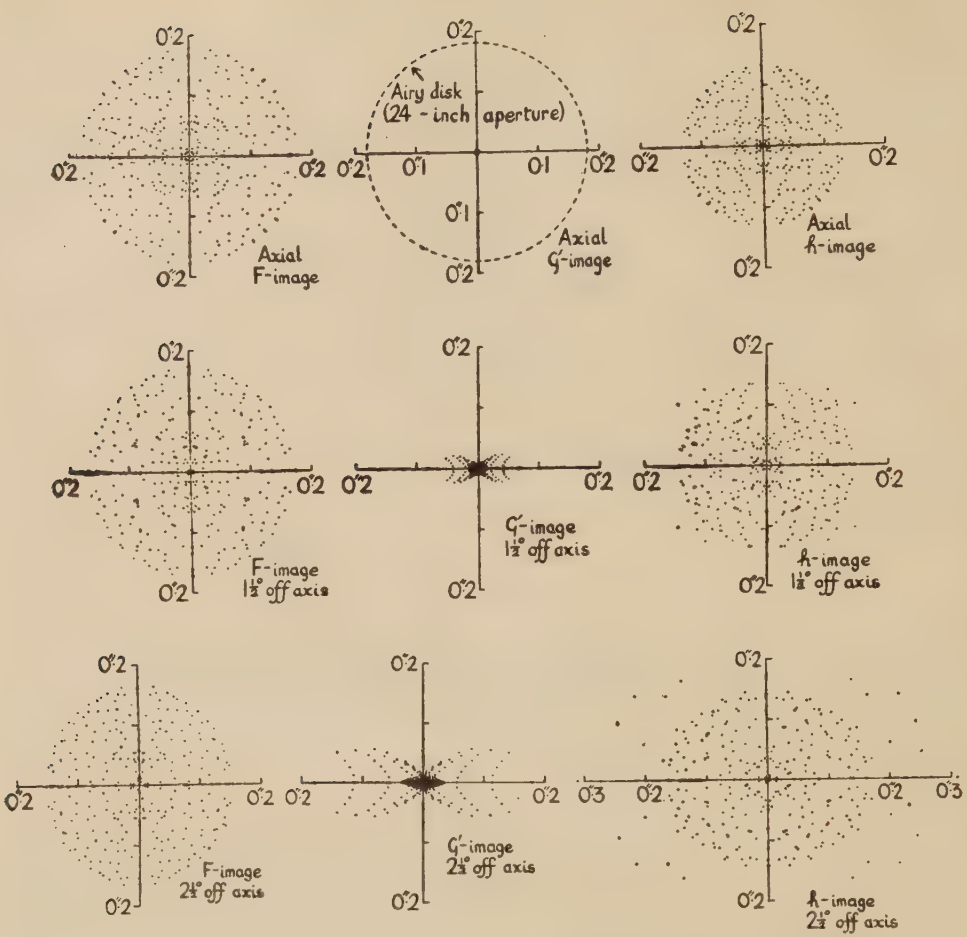

FIG. 6.—*Geometrical images by f/3·5 Schmidt camera (axially stigmatic in G′-light ;* $a=\frac{3}{2}$, $n_{G'}=1{\cdot}55$, $(n_F-n_{G'})/(n_{G'}-1)=-0{\cdot}0094$, $(n_h-n_{G'})/(n_{G'}-1)=0{\cdot}0070$).

on the surface of the spherical mirror * and a figuring

$$\frac{1}{n-1}\tfrac{1}{4}(\lambda^4+m_3\lambda^6)(r^4-ar^2)+\frac{1}{n-1}\tfrac{3}{8}\lambda^6r^6 \tag{59}$$

on the aspheric surface of the plate.† We also move the plate towards the mirror to a distance $m_4\lambda^2$ behind the aperture stop. Lastly we change slightly the adopted field curvature, so as to add a term

$$\begin{aligned}&\tfrac{1}{4}m_2\lambda^4r^2\sin^2\phi+O(\lambda^8)\\&=m_2c^2\lambda^6V^2r^2+O(\lambda^8)\end{aligned} \tag{60}$$

to the aberration function of the emerging wave-fronts. As in the first part of Section 2, f has been given the value $\frac{1}{2}$ and the camera is supposed for the time being to be working backwards and with its aspheric plate surface facing the

* It makes no difference to the final formulae whether the thickness of the figuring layer is measured normally to the mirror surface or parallel to the x-axis, since the discrepancy is $O(\lambda^6)[1-\cos\{O(\lambda)\}]=O(\lambda^8)$.

† The coefficient of the term in λ^6r^6 is obtained from (49).

mirror. The contributions to the distortion of an emerging wave-front are now as follows :

(i) From the "shearing" of mirror surface against stop and the change in adopted field curvature, a contribution

$$\tfrac{1}{4}m_1\lambda^6[(r_V^4 - ar_V^2) - (r^4 - ar^2)] + m_2\lambda^6c^2V^2r^2 + O(\lambda^8), \tag{61}$$

where

$$r_V^2 = (u + 2f\sin\phi/\lambda)^2 + v^2 = r^2 + 4cVu + 4c^2V^2. \tag{62}$$

On substituting for r_V^2 from (62), we obtain (61) in the form

$$m_1\lambda^6(cVu + c^2V^2)(2r^2 + 4cVu + 4c^2V^2 - a) + m_2\lambda^6c^2V^2r^2 + O(\lambda^8). \tag{63}$$

(ii) From the "foreshortening" of the aperture stop against the wave-fronts arriving from the sphere, a contribution

$$\tfrac{1}{2}\lambda^6c^2V^2u\frac{\partial}{\partial u}(r^4 - ar^2) + O(\lambda^8). \tag{64}$$

(iii) From the oblique passage of the wave-fronts through the plate, a contribution

$$\tfrac{1}{2}\lambda^6c^2V^2(r^4 - ar^2)/n + O(\lambda^8)$$

in accordance with (12).

(iv) From the shearing of the plate against the aperture stop, a contribution

$$\tfrac{1}{4}(\lambda^4 + m_3\lambda^6)[(r_V'^4 - ar_V'^2) - (r^4 - ar^2)] + O(\lambda^8),$$

where

$$r_V'^2 = (u + m_4\lambda^2\sin\phi)^2 + v^2 = (u + 2m_4\lambda^2cV)^2 + v^2$$

and the contribution can therefore be written

$$2m_4\lambda^6cVu(r^2 - \tfrac{1}{2}a) + O(\lambda^8). \tag{65}$$

It follows that the total distortion of the emerging wave-fronts is

$$\begin{aligned}&\tfrac{1}{4}(m_1 + m_3)\lambda^6(r^4 - ar^2) + m_1\lambda^6(cVu + c^2V^2)(2r^2 + 4cVu + 4c^2V^2 - a)\\ &\quad + m_2\lambda^6c^2V^2r^2 + \tfrac{1}{2}\lambda^6c^2V^2\left(\frac{1}{n} + u\frac{\partial}{\partial u}\right)(r^4 - ar^2)\\ &\quad + 2m_4\lambda^6cVu(r^2 - \tfrac{1}{2}a) + O(\lambda^8).\end{aligned} \tag{66}$$

Terms independent of u and v in this expression may be dropped, since they have no effect on the aberrations. To get rid of primary coma in the images, we have to annul the terms in ur^2, namely

$$2(m_1 + m_4)\lambda^6cVur^2 ;$$

that is, we must set $m_4 = -m_1$. Then the aberration function can be written

$$\begin{aligned}\lambda^6\Phi(u, v, V) = \lambda^6&\left[\tfrac{1}{4}(m_1 + m_3)(r^4 - ar^2) + \tfrac{1}{2}c^2V^2\left(\frac{1}{n} + u\frac{\partial}{\partial u}\right)(r^4 - ar^2)\right]\\ &+ \lambda^6c^2V^2[2m_1(2u^2 + r^2) + m_2r^2]\\ &+ 8\lambda^6c^3V^3m_1u + O(\lambda^8).\end{aligned} \tag{67}$$

The term in u represents a bodily shift of the image sideways ; it follows that the *distortion of the system*, in radians, is

$$8m_1\lambda^5c^3V^3 + O(\lambda^2). \tag{68}$$

Dropping the term in u, we obtain

$$\lambda^6\Psi(u,v,V)=\lambda^6\Big[\tfrac{1}{4}(m_1+m_3)(r^4-ar^2)+\tfrac{1}{2}c^2V^2\Big(\frac{1}{n}+u\frac{\partial}{\partial u}\Big)(r^4-ar^2)$$
$$+2c^2V^2m_1(2u^2+r^2)+c^2V^2m_2r^2\Big]+O(\lambda^8) \qquad (69)$$

as the aberration function for the image-errors, other than distortion, on the adopted field-surface. The corresponding angular aberration displacements are

$$\lambda^5\frac{\partial\Psi}{\partial u}=\lambda^5\Big[4c^2V^2u^3+\Big(m_1+m_3+\frac{2n+1}{2n}4c^2V^2\Big)(r^2-\tfrac{1}{2}a)u$$
$$+2c^2V^2(6m_1+m_2)u\Big]+O(\lambda^7),$$
$$\lambda^5\frac{\partial\Psi}{\partial v}=\lambda^5\Big[4c^2V^2u^2v+\Big(m_1+m_3+\frac{1}{2n}4c^2V^2\Big)(r^2-\tfrac{1}{2}a)v$$
$$+2c^2V^2(2m_1+m_2)v\Big]+O(\lambda^7). \qquad (70)$$

Consideration of the forms of the off-axis errors suggests that something near to the best balancing of the performance over the whole field will be obtained by making the aberration-displacements vanish for $V=1$, $(u,v)=(\pm 1,0)$ and $(0,\pm 1)$. This is equivalent to pulling in four selected margin-points of the image at the edge of the field, so that they meet in the centre of the image, which becomes folded over. The values of m_1, m_2, m_3 which achieve this are easily found to be

$$m_1=-1+\tfrac{1}{4}a,\quad m_2=4-\tfrac{3}{2}a,\quad m_3=1-\tfrac{1}{4}a-\frac{2n+1}{2n}.4c^2, \qquad (71)$$

and on inserting these values in (69), the aberration function becomes

$$\lambda^6\Psi(u,v,V)=\lambda^6c^2[(u^4-v^4)-2(u^2-v^2)$$
$$+(1-V^2)\{-2u^2r^2+ar^2+2(u^2-v^2)-(r^4-ar^2)/2n\}]+O(\lambda^8). \qquad (72)$$

The scale restriction $f=\frac{1}{2}$, under which this formula has been established, may be dropped if a multiplying factor $2f$ is inserted on the right-hand side. By (59), the plate profile is

$$s=\frac{1}{n-1}\tfrac{1}{4}\Big[\lambda^4+\Big(1-\tfrac{1}{4}a-\frac{2n+1}{2n}.4c^2\Big)\lambda^6\Big](r^4-ar^2)+\frac{1}{n-1}.\tfrac{3}{8}\lambda^6r^6, \qquad (73)$$

so that the change in plate strength only amounts to a few per cent of its original value. The figuring on the mirror, namely

$$-\tfrac{1}{8}\lambda^6(1-\tfrac{1}{4}a)(r^4-ar^2),$$

is of the same type as that on a paraboloid and when $a=\frac{3}{2}$ it amounts to only $\frac{2}{5}$ fringe in the case of an $f/3{\cdot}5$ system working with a 24-inch plate and a 36-inch mirror; in the case of an $f/2{\cdot}5$ system with a 48-inch plate and 72-inch mirror it amounts to $3\frac{1}{5}$ fringes.

Polychromatic aberrations.—From (72) and (73) it follows, by the same arguments as those used to derive (56), that the fifth-order aberration function in light of index n' of the above system is

$$\lambda^6\Psi^*(u,v,V)=\lambda^6c^2\Big[V^2\{(u^4-v^4)-2(u^2-v^2)\}-\frac{2n+1}{2n}(1-V^2)(r^4-ar^2)\Big]$$
$$+\lambda^6k_{n,n',\lambda}(r^4-ar^2)+O(\lambda^8), \qquad (74)$$

where $k_{n,n',\lambda}$ is again given by (57).

The fifth-order aberration displacements in n'-light, measured in radians, are then

$$\lambda^5 \frac{\partial \Psi^*}{\partial u}, \lambda^5 \frac{\partial \Psi^*}{\partial v} = 4\lambda^5 c^2 V^2(-u+u^3, v-v^3)$$
$$+4\lambda^5 \left\{ k_{n,n',\lambda} - \frac{2n+1}{2n} c^2(1-V^2) \right\} (r^2 - \tfrac{1}{2}a)(u,v). \qquad (75)$$

The distortion (68) of the system is not included in the aberration function (74). To include it, we only need to add a term

$$8m_1\lambda^6 c^3 V^3 u = -\lambda^6 c^3 V^3 (1-\tfrac{1}{4}a)u \qquad (76)$$

on the right of (74), since the variation of distortion with wave-length is $O(8m_1\lambda^6 c^3 V^3(n'-n)) = O(\lambda^8)$, which is negligible in the present approximation.

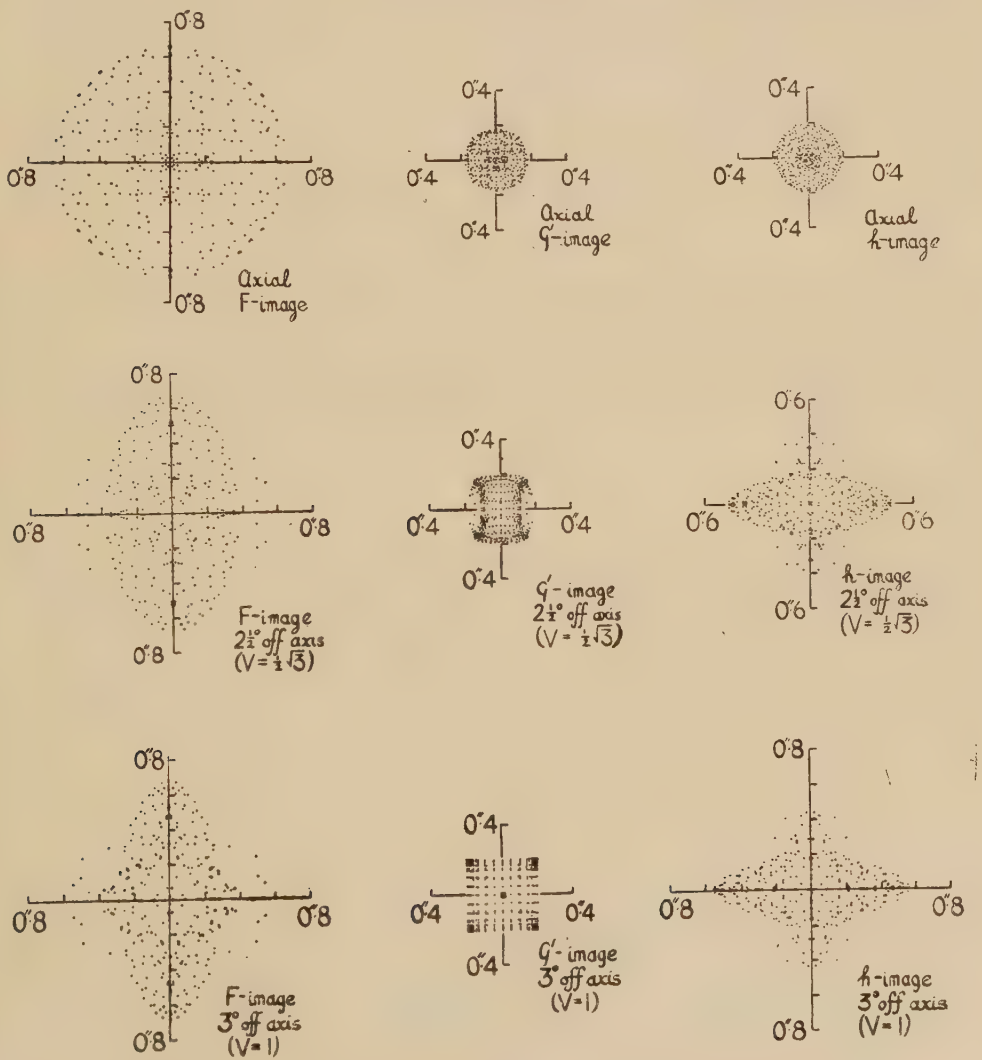

FIG. 7.—*Geometrical images by f/2·5 modified Schmidt camera, aberrations balanced in G'-light over a 6° field* ($a=3/2$, $n_{G'}=1{\cdot}55$, $(n_F-n_{G'})/(n_{G'}-1) = -0{\cdot}0094$, $(n_h-n_{G'})/(n_{G'}-1) = 0{\cdot}0070$).

For the same reasons as in Section 2, the leading terms in the aberration function remain unchanged when the plate, of paraxial thickness $d = O(\lambda)$, is turned round and its distance from the mirror readjusted in the manner there described (namely, by moving the plate-mounting a distance d/n towards the mirror when the plate is turned round so as to bring its aspheric surface to the side away from the mirror).

Further, the leading terms in the expressions for the angular aberration displacements are the same whether the system works backwards or in the normal manner.

Finally, a shift $O(\lambda^2)$ of the aperture stop, since it alters the boundary of any entering pencil by at most $O(\lambda^3)$, changes the values of the aberration displacements by at most $O(\lambda^7)$; it therefore leaves the leading terms in the expressions for these displacements unaltered. The same formulae (74), (75) therefore describe the fifth-order aberrations of the system working forwards or backwards, with the plate either way round, and with the stop either on the plate or at the centre of curvature of the mirror.

In a 48–72-inch $f/2{\cdot}5$ system with $a = \frac{3}{2}$ and $c = \frac{1}{4}$, the distortion (76) amounts at the edge of the field to

$$8m_1\lambda^5c^3V^3 = -8(1-\tfrac{1}{4}\cdot\tfrac{3}{2})10^{-5}(\tfrac{1}{4})^3$$

$$= -0{\cdot}16 \text{ second of arc.}$$

(Zero distortion would mean that great circles on the sky are imaged into great circles on the spherical field-surface.)

Fig. 7 shows the spot diagrams of this system, calculated from (74) and (75), for the images in F, G′ and h-light, at selected points of the field. The effect of

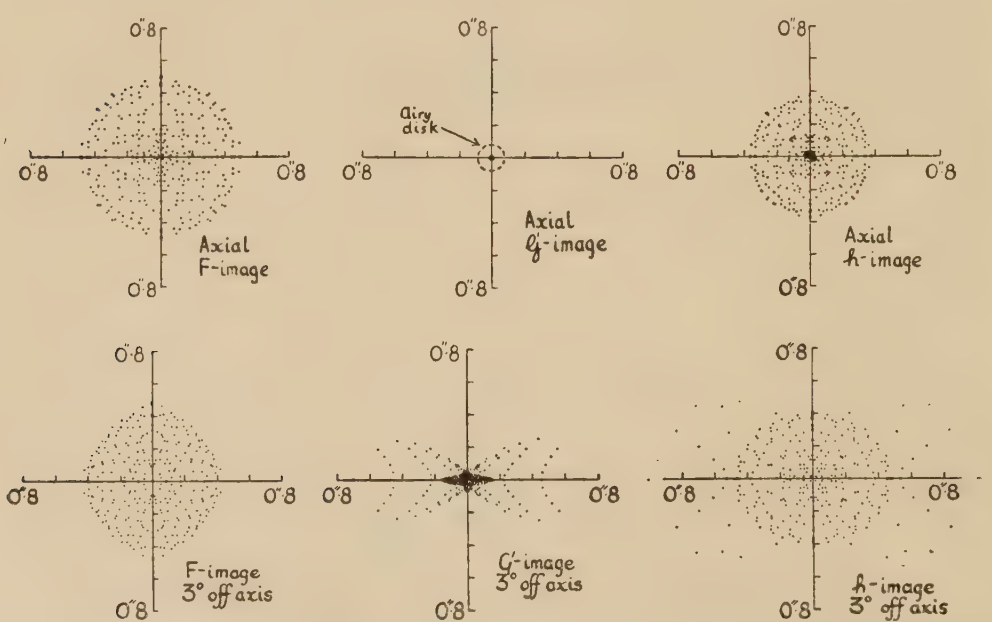

FIG. 8.—*Geometrical images by $f/2{\cdot}5$ Schmidt camera, axially stigmatic in G′-light* ($a = \frac{3}{2}$, $n_{G'} = 1{\cdot}55$, $(n_F - n_{G'})/(n_{G'} - 1) = -0{\cdot}0094$, $(n_h - n_{G'})/(n_{G'} - 1) = 0{\cdot}0070$).

the central obstruction is ignored, as before.* Diagrams for the images at the edge of the field of a classical Schmidt camera of the same size, focal ratio and field-diameter are shown in Fig. 8 for comparison. Fig. 9 shows the manner in which the geometrical images in G′-light are folded over, in the system with aberration function (72), at selected points of the field.

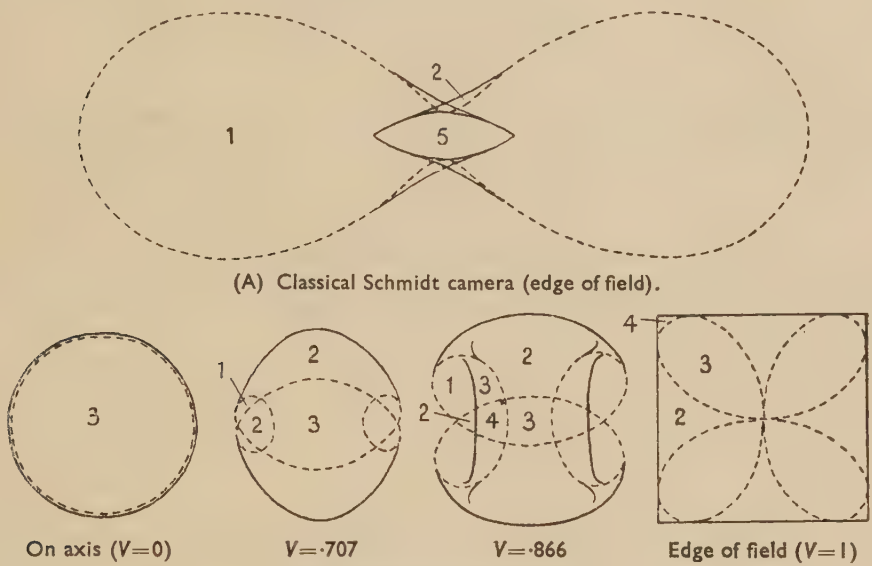

FIG. 9.—*Monochromatic images.* (*Folding and relative sizes of G′-images*: (*A*) *in the classical Schmidt camera of Fig.* 8, 3° *off axis*; (*B*) *in the modified system of Fig.* 7. *The numbers state the degree of many-sheetedness of the image. The dotted lines correspond to the edge of the aperture stop.*)

The Observatory, Cambridge:
1949 *January* 15.

* The Airy disk corresponding to the central obstruction is here comparable in size to the geometrical images given by the full aperture.

THE HYDROGEN SPECTRUM OF THE SUN

R. G. Giovanelli

(Received 1949 February 21*)

Summary

The intensities of the $L\alpha$ and $L\beta$ lines and of the Lyman continuum emitted by the Sun are computed on the assumption of a uniform chromosphere at a kinetic temperature of $2{\cdot}5 \times 10^4$ deg. K. The central intensities of $L\alpha$ and $L\beta$, as derived from a theory assuming coherent scattering, equal those emitted by a black body at $1{\cdot}16 \times 10^4$ deg. K. and are unchanged from centre to limb. The intensity at the beginning of the Lyman continuum is 2×10^4 times as great as if the Sun radiated as a black body at 6000 deg. K., and this ratio increases rapidly with decreasing wave-length. The Lyman continuum should show marked limb brightening.

The central intensity of $H\alpha$ is also computed and found to be 0·19 of that of the surrounding continuum, as compared with Allen's measured value of 0·12.

A short discussion of the radiation from a non-uniform chromosphere is also included.

---

1. *Introduction.*—If the outer layers of the Sun behaved for the emission of radiation as a black body, or as if heated solely by the passage of radiation incident from within the Sun, the solar spectrum in the far ultra-violet would not differ greatly from that of a black body at a temperature of about 6000 deg. K.

It has at times been inferred from ionospheric and other observations (**1, 2**) that the intensity of the far ultra-violet solar radiation, responsible for photo-electric ionization of the Earth's upper atmosphere, greatly exceeds that expected from the Sun if it radiated as a black body at 6000 deg. K. On the other hand, Woolley has shown (**3**) that such conclusions are not inevitable.

Edlén's (**4**) and Redman's (**5**) investigations have shown that the temperatures of the corona and the chromosphere are very much greater than that of the photosphere, so that heating cannot be solely by the radiation passing through them. Consequently the Lyman spectrum of the Sun may depart considerably from that expected on a theory of radiative equilibrium, and perhaps the Lyman lines and continuum may appear in emission rather than in absorption.

If the physical properties of the Sun's atmosphere were sufficiently well known, it would be possible, at least in principle, to deduce the spectral intensity distribution. In fact, however, our knowledge of the chromosphere is very meagre. The temperature has been measured only at one roughly-defined elevation at a single eclipse, but, on the assumption of hydrostatic equilibrium, the mean of the measured gradients of the density in the neighbourhood of this elevation conforms with this temperature. The distribution of temperature with height and over the surface of the Sun is also still unknown.

Despite these uncertainties we can calculate theoretically the profiles and intensities of the hydrogen $L\alpha$, $L\beta$ and $H\alpha$ lines, and, in the case of $H\alpha$, compare the result with the observed value. For simplicity and because of lack of precise

* Revised version received 1949 April 22.

knowledge of the temperature gradient these calculations will be made on the assumption of an isothermal chromosphere superimposed on a region of considerably lower temperature. It will be shown that the Lyman lines and continuum would appear in emission, while the $H\alpha$ line would appear as an absorption line of about the observed intensity.

In the following section we consider the temperature and density of a chromosphere, of uniform temperature throughout, which would best fit eclipse observations. It will become apparent that a chromosphere whose temperature is uniform over the Sun's surface does not agree very well with observation, and in Section 11 we briefly consider a non-uniform chromosphere, deriving an estimate of the error in the calculated intensities introduced by assuming it to be uniform.

2. *Physical properties of the chromosphere*

(*a*) The main evidence for the temperature of the chromosphere is provided by Redman's investigations (**5**) of the widths of chromospheric spectral lines. These he showed to be due to Doppler broadening corresponding to thermal agitation, and he deduced that the temperature at an elevation some 1500 km. above the base of the chromosphere was about $3{\cdot}0 \times 10^4$ deg. K.

The electron gradient in the region 500 to 3000 km. above the base of the chromosphere provides confirmation of such a temperature. The gradient appears to be uniform over this region but estimates of its value as deduced from different observations vary considerably. The mean corresponds to that in a highly ionized hydrogen atmosphere at $2{\cdot}7 \times 10^4$ deg. K., the electron concentration in this region being given approximately by (**6**)

$$N_e = 5 \times 10^{11} \exp(-6 \times 10^{-9} z) \text{ per c.c.}, \qquad (1)$$

where the elevation, z, is measured from a level 500 km. above the base of the chromosphere (this being about the lowest chromospheric level at which such observations have been made).

Between 3000 km. and 20,000 km. the temperature is uncertain. It appears to be about 10^5 deg. K. at 12,000 km., judging from the electron concentration at this level, and about 10^6 deg. K. at 20,000 km. The temperature is also uncertain in the lowest 500 km. of the chromosphere, falling to about 5000 deg. K. in the photosphere.

For the present investigation the temperature in the lower chromosphere is more important than in higher regions. To examine conditions near the base of the chromosphere we shall attempt to relate the known electron concentration (about 5×10^{11} per c.c.) and temperature (apparently still of the order of $2{\cdot}5 \times 10^4$ to 3×10^4 deg. K.) in the region 500 km. above the Sun's visible limb to observations of the sharpness of the limb.

(*b*) The edge of the visible limb of the Sun is very sharp. Kopal has deduced (**7**) that the region where solar brightness drops steeply to zero has a width of the order of $0''{\cdot}1$ or less, i.e. not greater than about 75 km. In Fig. 1, OLA and OCEBD are lines of sight from an observer O tangential to the Sun at two different elevations. If these two lines define the inner and outer limits of the transition region at the visible edge of the Sun's limb, then the visible light along line OCEBD must originate from the region CEB, and the optical thickness of CEB must be of the order of unity. To a rough approximation, the optical thickness is of the order of CE times the absorption coefficient at E. With LE about 75 km., CE is about

10^9 cm., so that the absorption coefficient at E is about 10^{-9} per cm. The absorption of continuous radiation is due to negative hydrogen ions of ionization potential 0·75 electron volts. The concentration of such ions is given closely by Saha's equation

$$\frac{N_-}{N_1 N_e} = \frac{\omega_- h^3 \exp(E_-/k\theta)}{\omega_1 2(2\pi mk\theta)^{\frac{3}{2}}}, \qquad (2)$$

where ω_- and ω_1 are the statistical weights of the negatively ionized and neutral (ground state) hydrogen atoms respectively, h is Planck's constant, k is Boltzmann's constant, m the electron mass and θ the gas temperature. Since $\omega_-/\omega_1 = \frac{1}{2}$,

$$N_- = 1{\cdot}04 \times 10^{-16}\theta^{-\frac{3}{2}} N_1 N_e \exp(8{\cdot}7 \times 10^3/\theta). \qquad (3)$$

As the atomic absorption coefficient per negative hydrogen ion (**8**) is about 3×10^{-17} cm.^{2}, at E

$$N_1 N_e \theta^{-\frac{3}{2}} \exp(8{\cdot}7 \times 10^3/\theta) \approx 3 \times 10^{23}, \qquad (4)$$

so the product $N_1 N_e$ decreases as θ increases; for the lowest possible value of θ, about 5×10^3 deg. K., $N_1 N_e \approx 2 \times 10^{28}$.

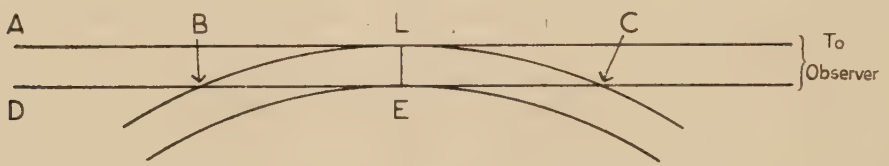

FIG. 1.

This result may be compared with the requirements of hydrostatic equilibrium, taking account of the electron concentration, about 5×10^{11} per c.c., and the gas temperature, about $2{\cdot}5 \times 10^4$ deg. K. at some 5×10^7 cm. above E. The particle concentration increases most rapidly with depth if the temperature at all elevations below 5×10^7 cm. is 5×10^3 deg. K. The atoms are almost all ionized at the higher temperature (**9**). If most of the atoms are neutral at the lower temperature, then $N_1 \approx 5 \times 10^{12}$ per c.c. immediately below 5×10^7 cm. The atom concentration increases to $1{\cdot}3 \times 10^{14}$ per cm. at the base of the chromosphere. Agreement with the product $N_1 N_e$ obtained above can be achieved within tolerable limits of uncertainty only if the electron concentration is of the same order as the neutral atom concentration, a condition which seems rather unlikely and which would denote considerable departure from thermodynamic equilibrium in the highest parts of the photosphere. These are conclusions which have followed from (i) the assumption that the chromosphere is uniform over the Sun's surface and (ii) the inference, from the observed electron concentration gradient, that the temperature at and for some distance above the 500-km. level is of the order of $2{\cdot}5$ to 3×10^4 deg. K.

These difficulties will be shown in Section 11 to disappear with a non-uniform temperature distribution across the Sun's surface, but it is first necessary to examine the emission of radiation from a chromosphere of uniform temperature. The major part of the paper is devoted to this problem.

We shall adopt a model chromosphere in which the temperature is uniform and comparatively high above a given level (defined by the electron concentration) and comparatively low below this level. The temperature of the upper region will be $2{\cdot}5 \times 10^4$ deg. K. and, in numerical examples, the electron concentration at the base of this region will be taken either as 5×10^{11} or $1{\cdot}0 \times 10^{12}$ per c.c.

3. *A survey of the problem of the emission of radiation by the chromosphere.*—In a high temperature chromosphere, excitations from some atomic states to others may be caused to a significant extent by collisions between atoms and electrons. The quantum or quanta of radiation subsequently emitted may be absorbed or scattered or may escape from the chromosphere.

The degree of coherence of the scattered radiation is of importance. Even if the scattered radiation be coherent with respect to the scattering atom, it suffers a frequency change because of the thermal velocity of the atom. The new frequency depends not only on the velocity of the atom but also on the angle of scattering; it is unchanged if re-emitted in the original direction. With an emission line the result of scattering is to transfer radiation from the centre of the line to the wings, where it is less readily absorbed. Hence the contour of the escaping radiation is broader and flatter than when the scattered radiation is coherent.

The difficulties associated with a theory of non-coherent scattering appear to be considerable and it seems that the intensity can be obtained only by iteration. We shall consider only coherent scattering and the solution so obtained is probably not greatly in error.

A computation of the populations of the various excited states, as maintained by the various radiative and collision processes, and an application of the laws of radiation transfer enable the radiation density to be found as a function of optical depth, and the intensity of the emitted radiation to be deduced. It is found that the Lyman continuum should exhibit marked limb brightening and a calculation of the density of the continuous radiation enables the concentration of neutral atoms to be derived. The central intensities and widths of $L\alpha$ and $L\beta$ follow fairly readily. Similarly, the central intensity of $H\alpha$ is calculated and is in satisfactory agreement with observation.

4. *The equations of radiative transfer.*—Consider an atmosphere in which scattering, absorption and emission of radiation may occur.

Let $I_\nu d\nu d\Omega$ be the radiant energy in the frequency interval $d\nu$ and within the solid angle $d\Omega$ which passes perpendicularly through unit surface area per second; let $E_\nu d\nu d\Omega$ be the radiant energy within the same frequency interval emitted or scattered into a solid angle $d\Omega$ from unit volume per second; let α_ν be the absorption coefficient; and let $1-\lambda$ be the fraction of the absorbed radiation which is subsequently scattered, so that λ is the fraction of the absorbed radiation which is "truly" absorbed.

Then the total intensity of radiation J_ν is defined by

$$J_\nu = \int_{4\pi} I_\nu d\Omega; \tag{5}$$

the optical depth τ_ν is defined by

$$d\tau_\nu = -\alpha_\nu dz, \tag{6}$$

where z is the elevation in the atmosphere; and the ergiebigkeit, B_ν, is defined by

$$B_\nu = E_\nu/\alpha_\nu. \tag{7}$$

In a plane parallel atmosphere the intensity I_ν of radiation in a direction ϕ to the normal is given by

$$\frac{\mu dI_\nu}{d\tau_\nu} = I_\nu - B_\nu, \tag{8}$$

where $\mu = \cos\phi$.

If radiation is scattered uniformly with direction, which for simplicity we assume to be the case, this equation may be rewritten *, making use of close approximations introduced by Eddington, in the form

$$\frac{1}{3}\frac{d^2J_\nu}{d\tau_\nu^2} = J_\nu - 4\pi B_\nu. \tag{9}$$

In an atmosphere in local thermodynamic equilibrium (which, however, is not the case in the chromosphere), B_ν is given by the Planckian relation

$$B_\nu = \frac{2h\nu^3}{c^2[\exp(h\nu/k\theta) - 1]}. \tag{10}$$

With coherent scattering, B_ν may be written as

$$4\pi B_\nu = (1-\lambda)J_\nu + 4\pi\epsilon_\nu/\alpha_\nu, \tag{11}$$

where ϵ_ν is the difference between E_ν and the radiation scattered into unit solid angle; ϵ_ν is thus the "true" emission by the medium. Equation (9) then becomes

$$\frac{1}{3\lambda}\frac{d^2J_\nu}{d\tau_\nu^2} = J_\nu - 4\pi\frac{\epsilon_\nu}{\alpha_\nu\lambda}. \tag{12}$$

If λ is uniform and ϵ_ν/α_ν is uniform or varies linearly with optical depth, the solution of this equation takes the form

$$J_\nu = 4\pi\epsilon_\nu/\alpha_\nu\lambda + a\exp(\sqrt{3\lambda}.\tau_\nu) + b\exp(-\sqrt{3\lambda}.\tau_\nu), \tag{13}$$

a and b being integration constants. Consequently at sufficient distance from the boundaries the intensity approaches that in a black body for which $B_\nu = \epsilon_\nu/\alpha_\nu\lambda$; this holds approximately at such optical depths from the boundaries that $\sqrt{3\lambda}.\tau_\nu \geqslant 1$. It also holds well inside a medium in which λ varies only slowly with optical depth.

5. *The absorption and emission coefficients.*—The rates of absorption, emission and scattering depend on the populations of the various atomic states and on the relevant rates of arrival and departure. In this section we discuss the rates of absorption and emission when the populations are known. The calculation of the populations is considered later. There are two special cases of interest, the Lyman continuum and the Lyman line radiation. The first is the simpler, since it is not scattered.

(*a*) *The Lyman continuum.*—The atomic continuous absorption coefficient has been given by Gaunt (**10**) for atoms in highly excited states, and Menzel has shown (**11**) that Gaunt's expression applies also for atoms in the lower and ground states. Gaunt's value for $\alpha(n, \nu)$, the atomic absorption coefficient for atoms in the n-quantum state, is

$$\alpha(n, \nu) = 2^6\pi^4 mZ^4\epsilon^{10}/3\sqrt{3}ch^6\nu^3n^5, \tag{14}$$

where m is the mass of an electron, $Z\epsilon$ is the nuclear charge of the atom (e.s.u.), c the velocity of light and h Planck's constant. For the ground state $n = 1$. Inserting numerical values, we find $\alpha(1, \nu) = 2{\cdot}8 \times 10^{29}\nu^{-3}$ cm.^{2}, so that the absorption coefficient is

$$\alpha_\nu = 2{\cdot}8 \times 10^{29}\nu^{-3}N_1 \text{cm.}^{-1}, \tag{15}$$

where N_1 is the concentration of atoms in the ground state.

In an earlier study (**9**) in which the concentrations of atoms in several of the quantum states were computed for various electron and ion concentrations, gas

* See e.g. S. Rosseland, *Theoretical Astrophysics*, Clarendon Press, Oxford, 1936, p. 112.

temperatures and spectral radiation densities, the results showed that for a gas temperature θ of $2{\cdot}5 \times 10^4$ deg. K. and in the presence of black-body radiation at a temperature T of 5×10^3 deg. K.,

$$N_1 \approx 10^{-3} N_e, \qquad (N_e < 10^{13} \text{ per c.c.}). \tag{16}$$

With these values of N_1 and N_e, the optical depth down to an elevation z is, from equations (1) and (15),

$$\tau_\nu = \int_\infty^z \alpha_\nu dz \approx 2{\cdot}3 \times 10^{46} \nu^{-3} e^{-6 \times 10^{-9} z}. \tag{17}$$

At the series limit, $\nu_0 = 3{\cdot}28 \times 10^{15}$ per sec., and so $\tau \approx 0{\cdot}65 e^{-6 \times 10^{-9} z}$. Hence we see that the optical thickness will not exceed unity at any frequency in the continuum down to levels 500 km. above the base of the chromosphere. When the direct or indirect ionizing effect of the emitted radiation is considered, N_1 may be reduced below the value given by equation (16), as we shall see, so that the optical thickness of the chromosphere will be further reduced.

The rate of spontaneous emission of radiation of frequency ν by recombination is (**12**), since stimulated recombination may be neglected,

$$E_\nu d\nu = \left(\frac{2}{\pi m k \theta}\right)^{\frac{3}{2}} \frac{N_e^2 h^4 \nu^3 \alpha(1, \nu)}{4c^2} \exp\left[(E_1^i - h\nu)/k\theta\right] d\nu \text{ erg per unit volume per unit solid angle per second,} \tag{18}$$

k being Boltzmann's constant and E_1^i the ionization potential of the ground state. This reduces to

$$E_\nu d\nu = 6{\cdot}1 \times 10^{-63} N_e^2 \nu^3 \theta^{-\frac{3}{2}} \alpha(1, \nu) \exp\left[(E_1^i - h\nu)/k\theta\right] d\nu, \tag{19}$$

so that B_ν, which equals E_ν/α_ν, is given by

$$B_\nu = \frac{6{\cdot}1 \times 10^{-63} N_e^2 \nu^3 \exp\left(1{\cdot}58 \times 10^5 \theta^{-1} - 4{\cdot}80 \times 10^{-11} \nu \theta^{-1}\right)}{N_1 \theta^{\frac{3}{2}}}. \tag{20}$$

Thus for $\theta = 2{\cdot}5 \times 10^4$ deg. K.,

$$B_\nu = 3{\cdot}0 \times 10^{-20} \exp\left(-6{\cdot}3\nu/\nu_0\right) . (N_e^2/N_1)(\nu/\nu_0)^3. \tag{21}$$

(*b*) *The Lyman lines.*—The absorption coefficient α_ν varies with $\nu - \nu_0$, where ν_0 is the frequency of the absorption maximum. In the centre of the line the Doppler effect determines the absorption coefficient; in the far wings of the line the influence of the Doppler effect is negligible. The exact expression for α_ν is unwieldy but to a sufficient approximation the absorption is given throughout the chromosphere by considering only the Doppler term. Rosseland, for example, has given an expression (**13**) for α_ν when the frequency lies somewhat beyond the region of Doppler absorption; it takes the form

$$\alpha_\nu = \text{const.}\, N_1 \left(\exp(-\eta^2) + \frac{4D}{\pi \eta^2} \int_0^\eta \zeta^2 e^{-\zeta^2} d\zeta\right), \tag{22}$$

where

$$\eta = \frac{c\Delta\nu}{\nu}\left(\frac{M}{2k\theta}\right)^{\frac{1}{2}}, \qquad D = \frac{Ac}{4\pi\nu_0}\left(\frac{M}{2k\theta}\right)^{\frac{1}{2}},$$

A being the sum of the transition probabilities from the excited state, and M the mass of the atom. The first term inside the brackets gives the absorption coefficient for Doppler absorption, as if the natural line width were infinitely sharp. The Doppler term may be assumed to give the approximate absorption coefficient

until the second term approaches the first in magnitude. For a temperature of $2{\cdot}5 \times 10^4$ deg. K. the two terms are equal in the case of $L\alpha$ when $\eta = 3{\cdot}33$, or when $\Delta\nu$ is $5{\cdot}6 \times 10^{11}$ per sec., and as the absorption coefficient in the region where the Doppler term predominates is given by

$$\alpha_\nu = \frac{N_1 c^3 \omega_j A_{j,1} e^{-\eta^2}}{8\pi\nu^3 \omega_1 (2\pi k\theta/M)^{\frac{1}{2}}}, \tag{23}$$

ω_j and ω_1 being the statistical weights of the upper and ground states respectively, the corresponding value of α_ν as given by the Doppler term alone is found to be $5{\cdot}7 \times 10^{-19} N_1$ per cm. But we know, from equation (16), that N_1 is of the order of $10^{-3} N_e$ or less. From (1) and (16), the optical depth of a region of the chromosphere of elevation z is at this frequency

$$\tau \leqslant 4{\cdot}7 \times 10^{-2} e^{-6 \times 10^{-9} z} \tag{24}$$

(the elevation z is measured from a layer 500 km. above the base of the chromosphere). The optical depth is therefore quite small down to any level to which equation (16) may be reliably extrapolated. Hence for *all* the Lyman lines throughout the region of the Sun's atmosphere with which we are concerned, the absorption coefficients, wherever they are large enough to be significant, are given by a consideration of the Doppler absorption alone.

For $L\alpha$, we thus find

$$\alpha_\nu = 3{\cdot}8 \times 10^{-14} \exp\left[-3{\cdot}55 \times 10^{-23} (\Delta\nu)^2\right] N_1 \text{ per cm.}, \tag{25}$$

when $\theta = 2{\cdot}5 \times 10^4$ deg. K. Similarly, for $L\beta$,

$$\alpha_\nu = 6{\cdot}1 \times 10^{-15} \exp\left[-2{\cdot}54 \times 10^{-23} (\Delta\nu)^2\right] N_1 \text{ per cm.} \tag{26}$$

The total energy emitted per unit volume per second in a Lyman line is $N_j A_{j,1} E_1^j$, where N_j is the concentration of the atoms in the upper state and E_1^j is the energy difference between the states. Of the above emitted energy, some is due to scattering of the incident radiation and some is due to "true" emission by the gas. In accordance with our assumptions in Section 3, the scattered radiation is supposed coherent. Of the "true" emission, a fraction

$$(1/4\pi)(c/\nu_0)(M/2\pi k\theta)^{\frac{1}{2}} \exp(-\eta^2) \cdot d\nu$$

is radiated into unit solid angle within a frequency interval $d\nu$, Doppler broadening alone being taken into account. If n_j is the number of atoms per unit volume whose presence in the j-quantum state is not dependent upon the corresponding incident Lyman radiation line, we thus find

$$\frac{\epsilon_\nu}{\alpha_\nu} = \frac{2\omega_1}{\omega_j N_1} \left(\frac{\nu}{c}\right)^2 [n_j E_1^j]. \tag{27}$$

(*c*) *The Hα line.*—The atomic absorption coefficient for a transition between excited states $l \to j$ is

$$(\alpha_\nu)_{l,j} = \frac{c^3}{8\pi\nu^3} \left(\frac{M}{2\pi k\theta}\right)^{\frac{1}{2}} \exp\left[-\left(\frac{\Delta\nu}{\nu}\right)^2 \frac{Mc^2}{2k\theta}\right] \cdot \frac{\omega_j}{\omega_l} A_{j,l}, \tag{28}$$

and the absorption coefficient for the $H\alpha$ line, for $\theta = 2{\cdot}5 \times 10^4$ deg. K., is

$$\alpha_\nu = 3{\cdot}1 \times 10^{-21} \exp\left[-1{\cdot}04 \times 10^{-21} (\Delta\nu)^2\right] (6{\cdot}8 \times 10^7 N_{2S} + 1{\cdot}1 \times 10^8 N_{2P}). \tag{29}$$

The emission of $H\alpha$ radiation is $h\nu \Sigma A_{j,1} \cdot N_j$ erg per unit volume per second. Of this, there is an amount

$$(\Sigma N_j A_{j,1}) hc (M/2\pi k\theta)^{\frac{1}{2}} \exp\left[-\left(\frac{\Delta\nu}{\nu}\right)^2 \frac{Mc^2}{2k\theta}\right] d\nu$$

in a frequency interval $d\nu$. Hence

$$\frac{\epsilon_\nu}{\alpha_\nu} = \frac{2h\nu^3}{c^2} \frac{\Sigma(N_j A_{j,l})}{\Sigma(N_l A_{j,l}\omega_j/\omega_l)}. \tag{30}$$

6. *The populations of the various quantum states.*—The populations of the different atomic substates may be computed from a set of simultaneous equations, each of which expresses the condition that the rate at which atoms arrive in a substate equals that at which they depart. Arrivals in any substate may be due to spontaneous or induced transitions from higher levels, absorption of radiation in a lower level, 2- or 3-body recombination, or transitions caused by inelastic or super-elastic electron collisions. As shown in a previous investigation (**9**), the populations of substates of principal quantum number 1, 2 or 3 can be computed to within a factor of the order of two even when transitions to or from higher quantized states are neglected, a simplification adopted below.

One of the factors which limit the accuracy of the present investigation is lack of knowledge of the cross-section for different types of collision. We adopt here the cross-sections used in the work referred to above, where they were considered in detail. Briefly, the cross-section for excitation by electron collision is assumed to vary as $W^{-\frac{1}{2}}$, where W, the energy of the colliding electrons, exceeds the excitation potential. This assumption gives close agreement with the computed cross-sections of Massey and Mohr (**14**) for excitation from the ground to the 2S and 2P states, these being used to provide an absolute value for the cross-section. Moreover, for transitions involving other states, the excitation cross-section for electrons whose energy just exceeds the excitation potential is assumed proportional to the corresponding B_{nr}, the Einstein coefficient for transition under the influence of radiation from a state of principal quantum number n to one of principal quantum number r. Of such transitions a fraction $1/r$ is assumed to occur to each of the r substates of principal quantum number r. Absolute values are then obtained by comparison with the known cross-sections for $1 \rightarrow 2$ transitions. Elastic collisions causing transitions $2S \rightleftarrows 2P$, $3S \rightleftarrows 3P$, etc. are neglected. The cross-sections adopted for ionization by collision are those given by Fowler ((**12**), p. 431). The rates of excitation and ionization by collision are obtained by combining the above cross-sections with a Maxwellian distribution of electron energies.

When photoelectric ionization and excitation by the absorption of radiation, at a rate $\int (J_\nu \alpha_\nu / h\nu)\, d\nu$ per unit volume per second, are taken into account, equations for the populations of the lower atomic states may be obtained, as below. In these, the temperature of the chromosphere is taken to be $2{\cdot}5 \times 10^4$ deg. K., and the Balmer and Paschen continua are assumed to equal 6×10^3 deg. K. black-body radiation diluted by a factor of $\frac{1}{2}$. Reference should be made to the earlier work (**9**) for further details.

The ionized state:

$$1{\cdot}25 \times 10^{-10} N_e N_1 \quad \text{Collision ionization from the ground state}$$

$$+1{\cdot}95 \times 10^{-6} N_e (N_{3S} + N_{3P} + N_{3D}) \quad \text{collision ionization from 3S, 3P and 3D}$$

$$+2{\cdot}57 \times 10^{4} (N_{2S} + N_{2P}) \quad \text{photoelectric ionization from 2S and 2P}$$

$$= 1{\cdot}99 \times 10^{-13} N_e^2 \quad \text{spontaneous recombination}$$

$$+2{\cdot}29 \times 10^{-7} N_e (N_{2S} + N_{2P}) \quad \text{collision ionization from 2S and 2P}$$

$$+4{\cdot}26 \times 10^{55} N_1 \int_{Lc} (J_\nu / \nu^4)\, d\nu \quad \text{photoelectric ionization from 1S}$$

$$+2{\cdot}32 \times 10^{5} (N_{3S} + N_{3P} + N_{3D}) \quad \text{photoelectric ionization from 3S, 3P and 3D}$$

$$+3{\cdot}57 \times 10^{-27} N_e^3 \quad \text{3-body recombination} \tag{31}$$

2P

$2{\cdot}33\times10^{-3}N_1\int_{L\alpha}J_\nu\exp[-3{\cdot}55\times10^{-23}(\Delta\nu)^2]\,.\,d\nu$ $+6{\cdot}32\times10^{6}N_{3S}+6{\cdot}47\times10^{7}N_{3D}$
radiative excitation from 1S — spontaneous transition from 3S and 3D

$+3{\cdot}21\times10^{-7}N_e(N_{3S}+\frac{1}{3}N_{3P}+\frac{1}{5}N_{3D})$ $+6{\cdot}42\times10^{-10}N_eN_1$
super-elastic collision from 3S, 3P and 3D — collision excitation from 1S

$+3{\cdot}36\times10^{-14}N_e^2$
spontaneous recombination

$=6{\cdot}32\times10^{8}N_{2P}$ $+1{\cdot}13\times10^{-1}N_{2P}\int_{H\alpha}J_\nu\exp[-1{\cdot}04\times10^{-22}(\Delta\nu)^2]\,d\nu$
spontaneous transition to 1S — radiative excitation to 3S and 3D

$+1{\cdot}07\times10^{-7}N_eN_{2P}$ $+2{\cdot}57\times10^{4}N_{2P}$
collision excitation to 3S, 3P and 3D — photoelectric ionization

$+2{\cdot}29\times10^{-7}N_eN_{2P}$ (32)
collision ionization

2S

$6{\cdot}42\times10^{-10}N_eN_1$ $+1{\cdot}64\times10^{-14}N_e^2$
collision excitation from 1S — spontaneous recombination

$+2{\cdot}26\times10^{7}N_{3P}$ $+1{\cdot}07\times10^{-7}N_e(N_{3S}+\frac{1}{3}N_{3P}+\frac{1}{5}N_{3D})$
spontaneous transition from 3P — super-elastic collision from 3S, 3P and 3D

$=2{\cdot}57\times10^{4}N_{2S}$ $+2{\cdot}29\times10^{-7}N_eN_{2S}$
photoelectric ionization — collision ionization

$+6{\cdot}97\times10^{-2}N_{2S}\int_{H\alpha}J_\nu\exp[-1{\cdot}04\times10^{-22}(\Delta\nu)^2]\,.\,d\nu$
radiative excitation to 3P

$+1{\cdot}07\times10^{-7}N_eN_{2S}$ $+7{\cdot}34\times10^{-8}N_eN_{2S}$ (33)
collision excitation to 3S, 3P and 3D — super-elastic collision to 1S

3S

$3{\cdot}39\times10^{-11}N_eN_1$ $+3{\cdot}56\times10^{-8}N_e(N_{2S}+N_{2P})$
collision excitation from 1S — collision excitation from 2S and 2P

$+2{\cdot}17\times10^{-3}N_{2P}\int_{H\alpha}J_\nu\exp[-1{\cdot}04\times10^{-22}(\Delta\nu)^2]\,.\,d\nu$ $+2{\cdot}57\times10^{-15}N_e^2$
radiative excitation from 2P — spontaneous recombination

$+3{\cdot}97\times10^{-28}N_e^3$
3-body recombination

$=2{\cdot}32\times10^{5}N_{3S}$ $+1{\cdot}95\times10^{-6}N_eN_{3S}$
photoelectric ionization — collision ionization

$+6{\cdot}32\times10^{6}N_{3S}$ $+4{\cdot}28\times10^{-7}N_eN_{3S}$ (34)
spontaneous transition to 2P — super-elastic collision to 2S and 2P

3P

$3{\cdot}39\times10^{-11}N_eN_1$ $+3{\cdot}56\times10^{-8}N_e(N_{2S}+N_{2P})$
collision excitation from 1S — collision excitation from 2S and 2P

$+3{\cdot}15\times10^{-4}N_1\int_{L\beta}J_\nu\exp[-2{\cdot}54\times10^{-23}(\Delta\nu)^2]\,.\,d\nu$
radiative excitation from 1S

$$+6{\cdot}97\times10^{-2}N_{2S}\int_{H\alpha}J_\nu\exp\left[-1{\cdot}04\times10^{-22}(\Delta\nu)^2\right].d\nu \qquad +7{\cdot}70\times10^{-15}N_e^2$$

radiative excitation from 2S — spontaneous recombination

$$+1{\cdot}19\times10^{-27}N_e^3$$

3-body recombination

$$=2{\cdot}32\times10^{5}N_{3P} \qquad +1{\cdot}95\times10^{-6}N_eN_{3P}$$

photoelectric ionization — collision ionization

$$+1{\cdot}92\times10^{8}N_{3P} \qquad +1{\cdot}43\times10^{-7}N_eN_{3P} \qquad (35)$$

spontaneous transition to 2S and 1S — super-elastic collision to 2S and 2P

3D

$$3{\cdot}39\times10^{-11}N_eN_1 \qquad +3{\cdot}56\times10^{-8}N_e(N_{2S}+N_{2P})$$

collision excitation from 1S — collision excitation from 2S and 2P

$$+1{\cdot}11\times10^{-1}N_{2P}\int_{H\alpha}J_\nu\exp\left[-1{\cdot}04\times10^{-22}(\Delta\nu)^2\right].d\nu \qquad +1{\cdot}28\times10^{-14}N_e^2$$

radiative excitation from 2P — spontaneous recombination

$$+1{\cdot}99\times10^{-27}N_e^3$$

3-body recombination

$$=2{\cdot}32\times10^{5}N_{3D} \qquad +1{\cdot}95\times10^{-6}N_eN_{3D}$$

photoelectric ionization — collision ionization

$$+6{\cdot}47\times10^{7}N_{3D} \qquad +8{\cdot}57\times10^{-8}N_eN_{3D} \qquad (36)$$

spontaneous transition to 2P — super-elastic collision to 2S and 2P

7. *The approximate ionization equation.*—The above equations may in principle be solved in terms of J_ν and N_e for the populations of the various substates 1S, 2S, 2P, 3S, 3P and 3D, but they are cumbersome in their present form and a solution of adequate accuracy may be obtained by neglecting unimportant terms. We first find an approximate relationship between the concentrations of ions and ground-state neutral atoms.

For this, we can make use of the relative rates of ionization, from the various substates, by photoelectric absorption and by electron collision for a gas in equilibrium at a kinetic temperature of $2{\cdot}5\times10^4$ deg. K. in the presence of 5000 deg. K. black-body radiation. These have been computed from previous results (**9**) and are shown in Table I. It is clear that under these temperature conditions ionizations occur mainly by collision from the 1S or metastable 2S state. As the latter state is metastable, spontaneous transitions cannot take place from it, and the population of the 2S state and consequently the rate of ionization from it may be greatly enhanced.

We must consider also the effect of the Lyman radiation emitted by the chromosphere on the populations of the various substates and the rates of ionization from them; for this purpose we can neglect the rates at which atoms are brought into a substate other than directly or indirectly through the action of $L\alpha$ or $L\beta$ radiation. The populations of the 2P, 3P and 2S states are the most affected by such radiation. Since, as will be shown later, this radiation is almost entirely scattered, we can put

$$A_{2P,1S}N'_{2P}=\Lambda_\alpha N_1 \qquad (37)$$

and

$$A_{3P,1S}N'_{3P}=\Lambda_\beta N_1, \qquad (38)$$

where N'_{2P} and N'_{3P} are the populations of the 2P and 3P states as maintained solely by the absorption of resonance radiation, and $\Lambda_\alpha N_1$ and $\Lambda_\beta N_1$ are the numbers of such absorptions from the ground state per unit volume per second.

TABLE I

Rates of ionization by various processes. Gas temperature $2{\cdot}5\times10^4$ deg. *K.* ; *black-body radiation at* 5×10^3 deg. *K.*

N_e per c.c.	Photoelectric Ionization from			
	1S	2S	2P	3S+3P+3D
10^{12}	$3{\cdot}4\times10^3$	$4{\cdot}7\times10^9$	$1{\cdot}0\times10^7$	$1{\cdot}7\times10^9$
10^{11}	$6{\cdot}1\times10^2$	$1{\cdot}1\times10^8$	$1{\cdot}7\times10^6$	$2{\cdot}9\times10^7$
10^{10}	$6{\cdot}6\times10$	$1{\cdot}4\times10^6$	$2{\cdot}0\times10^4$	$3{\cdot}2\times10^5$
N_e per c.c.	Collision Ionization from			
	1S	2S	2P	3S+3P+3D
10^{12}	$8{\cdot}9\times10^{10}$	$9{\cdot}4\times10^{10}$	$2{\cdot}1\times10^8$	$1{\cdot}4\times10^{10}$
10^{11}	$1{\cdot}6\times10^9$	$2{\cdot}3\times10^8$	$3{\cdot}4\times10^5$	$2{\cdot}5\times10^7$
10^{10}	$1{\cdot}7\times10^7$	$2{\cdot}7\times10^5$	$3{\cdot}9\times10^2$	$2{\cdot}8\times10^4$

From our previous investigations, we can easily verify that in the presence of 5000 deg. K. black-body radiation, and for electron concentrations such as occur in the chromosphere, 90 per cent or more of the arrivals in the 2S state are due to electron impact with atoms in the ground state. Hence allowing for the possible influence of arrivals in the 2S state from the 3P state, the 2S population is given approximately by

$$6{\cdot}42\times10^{-10}N_eN_1+2{\cdot}26\times10^7N'_{3P}=2{\cdot}57\times10^4N_{2S}+2{\cdot}29\times10^{-7}N_eN_{2S}$$
$$+8{\cdot}39\times10^5N_{2S}+1{\cdot}07\times10^{-7}N_eN_{2S}+7{\cdot}34\times10^{-8}N_eN_{2S}$$

or

$$N_{2S}=\frac{6{\cdot}42\times10^{-10}N_eN_1+1{\cdot}34\times10^{-1}\Lambda_\beta N_1}{8{\cdot}65\times10^5+4{\cdot}09\times10^{-7}N_e}, \qquad (39)$$

the intensity of $H\alpha$ being taken to correspond to the radiation in a black body at 5000 deg. K.

Taking into account photoelectric and collision ionizations from the 1S, 2S, 2P and 3P states, the ionization equation becomes

$$(1{\cdot}25\times10^{-10}N_e+\Lambda_c)N_1+(2{\cdot}29\times10^{-7}N_e+2{\cdot}57\times10^4)$$
$$\times\left(1{\cdot}58\times10^{-9}\Lambda_\alpha N_1+\frac{6{\cdot}42\times10^{-10}N_eN_1+1{\cdot}34\times10^{-1}\Lambda_\beta N_1}{8{\cdot}65\times10^5+4{\cdot}09\times10^{-7}N_e}\right)$$
$$+(1{\cdot}95\times10^{-6}N_e+2{\cdot}32\times10^5)(5{\cdot}9\times10^{-9}\Lambda_\beta N_1)$$
$$=1{\cdot}99\times10^{-13}N_e^2+3{\cdot}57\times10^{-27}N_e^3, \qquad (40)$$

where Λ_cN_1 is the rate of photoelectric ionization from the ground state. Since $N_e<10^{12}$ per c.c. everywhere, $4{\cdot}09\times10^{-7}N_e$ will be neglected in comparison with

$8{\cdot}65 \times 10^5$, and $3{\cdot}57 \times 10^{-27} N_e^3$ will be neglected in comparison with $1{\cdot}99 \times 10^{-13} N_e^2$, so that the equation becomes

$$N_1 = \frac{1{\cdot}99 \times 10^{-13} N_e^2}{\Lambda_c + 1{\cdot}44 \times 10^{-10} N_e + 1{\cdot}70 \times 10^{-22} N_e^2 + (3{\cdot}61 \times 10^{-16} N_e + 4{\cdot}07 \times 10^{-5})\Lambda_\alpha + (4{\cdot}70 \times 10^{-14} N_e + 5{\cdot}37 \times 10^{-3})\Lambda_\beta}. \quad (41)$$

Little significant error is introduced by neglecting the term in N_e^2 in the denominator. It may be noted (i) that N_1 cannot exceed $1{\cdot}38 \times 10^{-3} N_e$, and may be very much less, and (ii) that at sufficient altitudes, where N_e is small enough, ionization results predominantly either directly or indirectly from the absorption of Lyman radiation.

8. *The emission and scattering equations.*—The rate of emission of Lyman line radiation depends explicitly on the populations of the P substates. While an exact solution of the population equations can be obtained, it is far more convenient to consider approximate solutions, and to use separate methods for estimating the scattering and the true emission. For the purposes of this section it may be assumed that the intensity of $H\alpha$ equals that in a black body at 5000 deg. K.

(*a*) *Scattering of* $L\alpha$.—To estimate the fraction of absorbed $L\alpha$ quanta which are subsequently re-emitted, we follow the various transitions which the excited atom may undergo until it is finally ionized or finally returns to the ground state. Most of the atoms which arrive in the 2P state do, in fact, return directly to the ground state. The fraction which do not may be obtained from the transition probabilities appearing in equations (31) to (36). Below are listed the important transitions, together with the relative numbers of atoms making such transitions. It should be noted that an atom arriving in the 3S or 3D state may be ionized or may return spontaneously to the 2P state. An atom arriving in the 3P state has a relatively small chance, however, of returning to the 2P state.

Transitions	*Number per second per excited atom*
P.E. ionization	$2{\cdot}57 \times 10^4$
collision ionization	$2{\cdot}29 \times 10^{-7} N_e$
2P→3D→ionization $H\alpha$	$\dfrac{1{\cdot}33 \times 10^6 (2{\cdot}32 \times 10^5 + 1{\cdot}95 \times 10^{-6} N_e)}{6{\cdot}47 \times 10^7 + 1{\cdot}95 \times 10^{-6} N_e}$
2P→3S→ionization $H\alpha$	$\dfrac{2{\cdot}61 \times 10^4 (2{\cdot}32 \times 10^5 + 1{\cdot}95 \times 10^{-6} N_e)}{6{\cdot}55 \times 10^6 + 1{\cdot}95 \times 10^{-6} N_e}$
2P→3D→ionization collision	$\dfrac{3{\cdot}6 \times 10^{-8} N_e (2{\cdot}32 \times 10^5 + 1{\cdot}95 \times 10^{-6} N_e)}{6{\cdot}47 \times 10^7 + 1{\cdot}95 \times 10^{-6} N_e}$
2P→3P collision	$3{\cdot}6 \times 10^{-8} N_e$
2P→3S→ionization collision	$\dfrac{3{\cdot}6 \times 10^{-8} N_e (2{\cdot}32 \times 10^5 + 1{\cdot}95 \times 10^{-6} N_e)}{6{\cdot}55 \times 10^6 + 1{\cdot}95 \times 10^{-6} N_e}$
2P→1S collision	$2{\cdot}45 \times 10^{-8} N_e$

The ratio of the number of true absorptions to the number of scattered $L\alpha$ quanta is almost identical with λ, so

$$\lambda=(6{\cdot}32\times10^{-8})^{-1}\left[2{\cdot}29\times10^{-7}N_e+2{\cdot}57\times10^{4}+3{\cdot}6\times10^{-8}N_e+2{\cdot}45\times10^{-8}N_e\right.$$
$$+(1{\cdot}33\times10^{6}+\{3{\cdot}6\times10^{-8}N_e\})\left(\frac{2{\cdot}32\times10^{5}+1{\cdot}95\times10^{-6}N_e}{6{\cdot}47\times10^{7}+\{1{\cdot}95\times10^{-6}N_e\}}\right)$$
$$\left.+(2{\cdot}61\times10^{4}+3{\cdot}6\times10^{-8}N_e)\left(\frac{2{\cdot}32\times10^{5}+1{\cdot}95\times10^{-6}N_e}{6{\cdot}55\times10^{6}+\{1{\cdot}95\times10^{-6}N_e\}}\right)\right]. \quad (42)$$

Since the electron concentrations do not exceed 10^{12} per c.c., the expressions in {} brackets may be neglected, whence

$$\lambda=4{\cdot}97\times10^{-5}+5{\cdot}33\times10^{-16}N_e+1{\cdot}70\times10^{-29}N_e^2. \quad (43)$$

Further, the last term may be neglected, giving the final value

$$\lambda=5{\cdot}0\times10^{-5}(1+1{\cdot}07\times10^{-11}N_e). \quad (44)$$

(*b*) *Scattering of* $L\beta$.—$L\beta$ absorptions may be treated similarly.

Transitions	*Number per second per excited atom*
P.E. ionization	$2{\cdot}32\times10^{5}$
collision ionization	$1{\cdot}95\times10^{-6}N_e$
$3P\rightarrow2P$ super-elastic collision	$1{\cdot}07\times10^{-7}N_e$

Spontaneous $3P\rightarrow2S$ transitions must also be considered. The relative rate is $2{\cdot}26\times10^{7}$. For atoms in the 2S state, the possible transitions are:—

Transitions	*Number per second per excited atom*
P.E. and collision ionizations	$2{\cdot}57\times10^{4}+2{\cdot}29\times10^{-7}N_e$
$2S\rightarrow1S$ super-elastic collision	$7{\cdot}34\times10^{-8}N_e$
$2S\rightarrow3S$ and 3D collision	$7{\cdot}1\times10^{-8}N_e$
$2S\rightarrow3P$ $H\alpha$ absorption and collision	$8{\cdot}39\times10^{5}+3{\cdot}6\times10^{-8}N_e$

Consequently the fraction β of these atoms which do not return to the 3P state after $3P\rightarrow2S$ transitions is

$$\beta=\frac{2{\cdot}57\times10^{4}+3{\cdot}73\times10^{-7}N_e}{8{\cdot}65\times10^{5}+4{\cdot}09\times10^{-7}N_e}. \quad (45)$$

Denoting by α the fraction of atoms in the 3P state which leave by $3P\rightarrow1S$ transitions, and by γ the fraction which leave other than by $3P\rightarrow1S$ or $3P\rightarrow2S$ transitions, we see that the fraction of the absorbed $L\beta$ quanta which eventually result in scattered $L\beta$ quanta is

$$\alpha+\alpha(1-\alpha-\gamma)(1-\beta)+\alpha(1-\alpha-\gamma)^2(1-\beta)^2+\ldots$$
$$=\alpha[1-(1-\alpha-\gamma)(1-\beta)]^{-1}. \quad (46)$$

Noting that β and γ are small compared with α, we may write this as

$$1-\left[\frac{\beta+\gamma}{\alpha}-\frac{\beta}{\alpha}(\alpha+\gamma)\right].$$

Consequently λ, the fraction truly absorbed, is given by

$$\alpha^{-1}[\gamma+\beta(1-\alpha-\gamma)].$$

Since $\alpha=0{\cdot}88$,

$$\lambda=(0{\cdot}88)^{-1}\left[\frac{2{\cdot}32\times10^{5}+2{\cdot}06\times10^{-6}N_e}{1{\cdot}92\times10^{8}+2{\cdot}10\times10^{-6}N_e}\right.$$
$$\left.+\frac{2{\cdot}57\times10^{4}+3{\cdot}73\times10^{-7}N_e}{8{\cdot}65\times10^{5}+4{\cdot}09\times10^{-7}N_e}\left(1-0{\cdot}88-\frac{2{\cdot}3\times10^{5}+2{\cdot}06\times10^{-6}N_e}{1{\cdot}92\times10^{8}+2{\cdot}10\times10^{-6}N_e}\right)\right]$$
$$=1{\cdot}38\times10^{-3}+1{\cdot}22\times10^{-14}N_e$$
$$+\frac{2{\cdot}57\times10^{4}+3{\cdot}73\times10^{-7}N_e}{8{\cdot}65\times10^{5}+4{\cdot}09\times10^{-7}N_e}(0{\cdot}135-1{\cdot}2\times10^{-14}N_e). \qquad (47)$$

It will be noted that λ is very small for both $L\alpha$ and $L\beta$, so that the absorbed $L\alpha$ and $L\beta$ radiation is almost entirely scattered: this is the justification for approximations adopted in Section 7.

(*c*) *The emission of Lα radiation.*—From the population equations the population of the 2P state can be derived when the approximate ionization equation and equation (39) for N_{2S} are taken into account. Substitution of the populations of the 3S, 3P and 3D states from equations (34), (35) and (36) into equation (32) for the 2P state leads to the result, using (37) and (38),

$$6{\cdot}32\times10^{8}N_{2P}=\Lambda_\alpha N_1+N_eN_1[7{\cdot}09\times10^{-10}+5{\cdot}60\times10^{-16}\Lambda_\beta]$$
$$+N_eN_1\left[\frac{6{\cdot}42\times10^{-10}N_e+1{\cdot}34\times10^{-1}\Lambda_\beta}{8{\cdot}65\times10^{5}+4{\cdot}09\times10^{-7}N_e}\right][7{\cdot}06\times10^{-8}+1{\cdot}80\times10^{-21}N_e]$$
$$+4{\cdot}89\times10^{-14}N_e^2, \qquad (48)$$

when the $H\alpha$ intensity is taken equal to that in a black body at 5000 deg. K., and terms of negligible significance for $N_e\leqslant10^{12}$ per c.c. are omitted. It will be noted that, in the presence of $L\beta$ radiation, collisions between electrons and excited atoms increase the population of the 2P state. Neglecting the effect of $L\beta$ radiation, we find from equation (27)

$$\frac{\epsilon}{\alpha}=1{\cdot}16\times10^{-10}\left\{7{\cdot}09\times10^{-10}N_e+\frac{6{\cdot}42\times10^{-10}N_e^2(7{\cdot}06\times10^{-8}+1{\cdot}80\times10^{-21}N_e)}{8{\cdot}65\times10^{5}+4{\cdot}09\times10^{-7}N_e}\right.$$
$$\left.+4{\cdot}89\times10^{-14}N_e^2/N_1\right\}. \qquad (49)$$

Even for $N_e=10^{12}$ per c.c., the second term inside the brackets is no greater than one-twentieth of the first, so to good approximation

$$\frac{\epsilon}{\alpha}=1{\cdot}16\times10^{-10}\{7{\cdot}09\times10^{-10}N_e+4{\cdot}89\times10^{-14}N_e^2/N_1\}. \qquad (50)$$

(*d*) *The emission of Lβ radiation.*—Proceeding in a similar manner, we find, on rejecting a few obviously negligible terms, that

$$1{\cdot}92\times10^{8}N_{3P}=3{\cdot}39\times10^{-11}N_eN_1+\left(\frac{5{\cdot}4\times10^{-4}N_e+1{\cdot}12\times10^{5}\Lambda_\beta}{8{\cdot}65\times10^{5}+4{\cdot}09\times10^{-7}N_e}\right)N_1$$
$$+5{\cdot}61\times10^{-17}N_eN_1\Lambda_\alpha+3{\cdot}15\times10^{-32}N_e^2N_1\Lambda_\beta$$
$$+\Lambda_\beta N_1+7{\cdot}70\times10^{-15}N_e^2. \qquad (51)$$

Neglecting the terms involving Λ_α and Λ_β, we find

$$1{\cdot}92\times10^{8}N_{3P}=3{\cdot}39\times10^{-11}N_eN_1+\frac{5{\cdot}4\times10^{-4}N_eN_1}{8{\cdot}65\times10^{5}+4{\cdot}09\times10^{-7}N_e}+7{\cdot}70\times10^{-15}N_e^2. \tag{52}$$

Consequently,

$$\frac{\epsilon}{\alpha}=6{\cdot}40\times10^{-10}\left\{3{\cdot}39\times10^{-11}N_e+\frac{5{\cdot}4\times10^{-4}N_e}{8{\cdot}65\times10^{5}+4{\cdot}09\times10^{-7}N_e}+7{\cdot}70\times10^{-15}N_e^2/N_1\right\}. \tag{53}$$

9. *Application of the emission and scattering formulae to the ionization equation.*— From equations (12) and (13), we may deduce that, in a medium where the emission, absorption and scattering coefficients do not change too rapidly with optical depth, the total intensity J_ν approximates to $4\pi\epsilon_\nu/\alpha_\nu\lambda$. At optical depths given by $\sqrt{3\lambda}\tau\geqslant1$, the chromosphere behaves as such a medium, as we shall subsequently confirm for wave-lengths near the centres of $L\alpha$ and $L\beta$. We therefore take the $L\alpha$ and $L\beta$ intensities *inside* the chromosphere to be given by

$$J=4\pi\epsilon/\alpha\lambda. \tag{54}$$

From this relation, it is now possible to estimate Λ_α and Λ_β.

For $L\alpha$ we find from equations (44) and (50) that

$$\frac{\epsilon}{\alpha\lambda}=\frac{1{\cdot}16\times10^{-10}\{7{\cdot}09\times10^{-10}N_e+4{\cdot}89\times10^{-14}N_e^2N_1^{-1}\}}{5{\cdot}0\times10^{-5}(1+1{\cdot}07\times10^{-11}N_e)}. \tag{55}$$

The approximate number of $L\alpha$ absorptions per unit volume per second is most readily found by noting that in a black body at temperature T

$$B=\frac{2h\nu^3}{c^2[\exp(h\nu/kT)-1]}, \tag{56}$$

while in such a case the number of $L\alpha$ quanta absorbed per second is

$$\frac{N_1\omega_{2P}A_{2P,\,1S}}{\omega_1[\exp(h\nu/kT)-1]}=\frac{N_1\omega_{2P}A_{2P,\,1S}c^2B}{2\omega_1h\nu^3}.$$

Consequently it follows that

$$\Lambda_\alpha=\frac{\omega_{2P}A_{2P,\,1S}c^2\epsilon}{2\omega_1h\nu^3\alpha\lambda}=\frac{8{\cdot}5\times10^{9}\epsilon}{\alpha\lambda}. \tag{57}$$

Hence

$$\Lambda_\alpha=(1{\cdot}40\times10^{-5}N_e+9{\cdot}68\times10^{-10}N_e^2N_1^{-1})(1+1{\cdot}07\times10^{-11}N_e)^{-1}. \tag{58}$$

In a similar manner, we find from equations (47) and (53) that for $L\beta$

$$\frac{\epsilon}{\alpha\lambda}=\frac{6{\cdot}40\times10^{-10}\left\{3{\cdot}39\times10^{-11}N_e+\dfrac{5{\cdot}4\times10^{-4}N_e}{8{\cdot}65\times10^{5}+4{\cdot}09\times10^{-7}N_e}+7{\cdot}7\times10^{-15}N_e^2N_1^{-1}\right\}}{1{\cdot}38\times10^{-3}+1{\cdot}22\times10^{-14}N_e+\dfrac{2{\cdot}57\times10^{4}+3{\cdot}73\times10^{-7}N_e}{8{\cdot}65\times10^{5}+4{\cdot}09\times10^{-7}N_e}(0{\cdot}135-1{\cdot}22\times10^{-14}N_e)} \tag{59}$$

and

$$\Lambda_\beta=\frac{1{\cdot}37\times10^{9}\epsilon}{\alpha\lambda}. \tag{60}$$

After some reduction and rejection of terms which are obviously negligible for $N_e \leqslant 10^{12}$ per c.c., it is found that

$$\Lambda_\beta = \frac{5{\cdot}0 \times 10^{-4} N_e + 5{\cdot}82 \times 10^{-9} N_e^2 (1 + 4{\cdot}7 \times 10^{-13} N_e) N_1^{-1}}{4{\cdot}66 \times 10^3 + 6{\cdot}10 \times 10^{-8} N_e}. \tag{61}$$

The above values of Λ_α and Λ_β may now be substituted in equation (41) to enable the concentration of ground-state neutral hydrogen atoms to be obtained. After some rearrangement N_1 is found to be equal to an expression whose numerator is

$$1{\cdot}99 \times 10^{-13} N_e^2 [1 - (1{\cdot}76 \times 10^{-12} N_e + 1{\cdot}98 \times 10^{-1})(1 + 1{\cdot}07 \times 10^{-11} N_e)^{-1}$$
$$- (1 + 4{\cdot}7 \times 10^{-13} N_e)(1{\cdot}38 \times 10^{-9} N_e + 1{\cdot}58 \times 10^2)(4{\cdot}66 \times 10^3 + 6{\cdot}10 \times 10^{-8} N_e)^{-1}]$$

and whose denominator is

$$\Lambda_c + 1{\cdot}44 \times 10^{-10} N_e + 1{\cdot}70 \times 10^{-22} N_e^2 + (5{\cdot}08 \times 10^{-21} N_e^2 + 5{\cdot}70 \times 10^{-10} N_e)$$
$$\times [1 + 1{\cdot}07 \times 10^{-11} N_e]^{-1} + (4{\cdot}83 \times 10^{-21} N_e^2 + 5{\cdot}74 \times 10^{-10} N_e)[1 + 1{\cdot}31 \times 10^{-11} N_e]^{-1}. \tag{62}$$

The numerator and the denominator of this expression are given below for various values of N_e:

N_e (per c.c.)	Numerator $\times 10^{13} N_e^{-2}$	Denominator
10^{12}	1·59	$\Lambda_c + 1{\cdot}19 \times 10^{-9} N_e$
10^{11}	1·58	$\Lambda_c + 1{\cdot}15 \times 10^{-9} N_e$
10^{10}	1·54	$\Lambda_c + 1{\cdot}26 \times 10^{-9} N_e$
10^9	1·52	$\Lambda_c + 1{\cdot}29 \times 10^{-9} N_e$

It is thus a very good approximation to put

$$N_1 = \frac{1{\cdot}55 \times 10^{-13} N_e^2}{\Lambda_c + 1{\cdot}22 \times 10^{-9} N_e}. \tag{63}$$

For large enough electron concentrations, $\Lambda_c \ll 1{\cdot}22 \times 10^{-9} N_e$, and hence

$$N_1 = 1{\cdot}27 \times 10^{-4} N_e. \tag{64}$$

We shall find that equation (64) applies over a considerable region of our model chromosphere. By comparison with previous results for cases where ionization from the 2P and 3P states was negligible (**9**), and where N_1 was about $10^{-3} N_e$, we see that in this chromosphere ionization following the absorption of $L\alpha$ and $L\beta$ radiation is about 10 times as important as ionization from the 1S and 2S states. The reason for this is evident. For example, the cross-section for collision excitation to the 2P state is about five times that for collision ionization from the ground state, and as ionizations occur much more frequently from the 2P state than do super-elastic collisions, the end result of the processes of emission and absorption initiated by an excitation or recombination to the 2P state is likely to be an ionization. The end result of an excitation or recombination to a 3-quantum state is likely also to be an ionization. This will not occur, however, if the optical thickness of the gas is small enough to allow most of the emitted $L\alpha$ and $L\beta$ quanta to escape.

We may now verify that $\epsilon/\alpha\lambda$ is uniform for $L\alpha$ and $L\beta$. Putting $N_1 = 1{\cdot}27 \times 10^{-4} N_e$,

$$\frac{\epsilon}{\alpha\lambda} = \frac{2{\cdot}54 \times 10^{-15} N_e}{1 + 1{\cdot}07 \times 10^{-11} N_e} \tag{65}$$

for $L\alpha$, and this has a constant value when N_e much exceeds 10^{11} per c.c. For $L\beta$, we find approximately,

$$\frac{\epsilon}{\alpha\lambda} = \frac{8{\cdot}52 \times 10^{-17} N_e}{1 + 1{\cdot}28 \times 10^{-11} N_e}, \tag{66}$$

which is also constant for similar values of N_e. These results justify our assumption at the beginning of this section that equation (54) holds near the centres of $L\alpha$ and $L\beta$.

10. *Intensities in the Sun's hydrogen spectrum*

The intensity of the Lyman continuum: (*a*) *Centre of the disk.*—We saw in Section 5 (*a*) that with the assumption $N_1 \approx 10^{-3} N_e$, the optical thickness of the chromosphere down to $N_e = 5 \times 10^{11}$ per c.c. was 0·65 at the Lyman series limit. As we have now seen, $N_1 \leqslant 1{\cdot}27 \times 10^{-4} N_e$ (depending on the value of Λ_c), so the corresponding optical thickness is not more than 0·08; and if N_e is 10^{12} per c.c. at the base of the high-temperature region, this figure will only be doubled. The chromosphere is thus effectively transparent to the Lyman continuum at the centre of the disk. At the edge, however, the optical thickness will be much greater, and marked limb brightening will occur.

The base of the chromosphere has interesting reflecting properties for Lyman radiation. Lyman continuous radiation from the chromosphere entering the low-temperature region will be rapidly absorbed because of the high neutral atom concentration. The recombination which will eventually occur between electrons and ions so formed may be a 2-body or a 3-body process. The rate of 2-body recombination is about $2 \times 10^{-11} N_e N_+ \theta^{-\frac{1}{2}}$ per c.c. per sec., or $3 \times 10^{-13} N_e^2$ at a temperature of 5000 deg. K. The rate of 3-body recombination when the third body is an electron is about $1{\cdot}3 \times 10^{-22} N_e^2 N_+ \theta^{-1}$ per c.c. per sec. or $2{\cdot}6 \times 10^{-26} N_e^3$ at 5000 deg. K. Thus such 3-body recombinations are more frequent than 2-body recombinations when N_e much exceeds 10^{13} per c.c. Three-body recombinations involving a neutral hydrogen atom will not occur nearly as rapidly as those involving an electron, unless the concentration of neutral atoms is large compared with that of the electrons. This is probably so just below the base of the chromosphere, but, owing to the necessity for continuity of pressure, it does not seem that, on our assumption of a sudden temperature change at the base of the chromosphere, the particle concentration can exceed 10^{13} per c.c. there. It appears likely that in these regions recombinations are largely two-body; and thus that this medium acts as a good scatterer, and consequently a good reflector, for the Lyman continuum. In such a case the intensity of the radiation escaping normal to the Sun's surface would be about doubled.

From equation (19), the intensity of radiation emitted per c.c. per second into unit solid angle is

$$E_\nu d\nu = 4{\cdot}35 \times 10^{-40} N_e^2 \exp\left[(E_1^i - h\nu)/k\theta\right] . d\nu. \tag{67}$$

Neglecting self-absorption, as we have shown to be justifiable, and omitting any reflection at the base, the total emission per unit solid angle normal to the Sun's surface is thus

$$\int_0^\infty E_\nu d\nu\, dz = 3{\cdot}6 \times 10^{-32} N_0^2 \exp\left[(E_1^i - h\nu)/k\theta\right] . d\nu \text{ erg/cm.}^2\text{/sec.}, \tag{68}$$

where N_0 is the electron concentration at the base of the chromosphere. With $N_0 = 10^{12}$ per c.c., the intensity is $3{\cdot}6 \times 10^{-8}$ erg/cm.^{2}/sec. per unit frequency

interval per unit solid angle at the series limit. The corresponding emission from a black body at temperature T is

$$\frac{2h\nu^3\,d\nu}{c^2(\exp h\nu/kT-1)}\ \text{erg/cm.}^2\text{/sec./unit solid angle,}$$

or $5{\cdot}2\times10^{-1}[\exp(1{\cdot}58\times10^5/T)-1]^{-1}$ at the series limit. Equating, we find that the intensity of the Lyman continuum at the series limit, wave-length 912 A., at the centre of the disk equals that from a black body at 9600 deg. K., about 2×10^4 times that from a black body at 6000 deg. K. Reasonable changes in N_0 and allowance for reflection of radiation at the base of the chromosphere would not change this effective temperature greatly.

The total spectral emission per unit area of Sun's surface is readily obtained, since the optical thickness of the chromosphere is small. Neglecting reflection at the base, one-half of the quanta emitted by recombination to the ground state escape outwards. Hence the total emission is

$$2\pi\int_0^\infty E_\nu\,d\nu\,dz$$

or $2{\cdot}3\times10^{-7}$ erg/cm.^{2}/sec./unit frequency interval at the series limit if N_0 is 10^{12} per c.c.

It may be noted that at the centre of the disk the energy falls off with decreasing wave-length much less rapidly than in a black body at 9600 deg. K. At a wave-length of 456 A., the intensity is about 10^{12} times as great as black-body radiation at 6000 deg. K.

(*b*) *Variation from centre to limb.*—In so far as the chromosphere can be regarded as a uniform plane parallel atmosphere, it is possible to examine the variation in brightness from centre to limb. Moreover, a knowledge of this brightness leads by integration to an approximate value for Λ_c.

At the top of the atmosphere the intensity of radiation in solid angle $d\Omega$ at an angle ϕ to the normal is given by

$$I_\nu\,d\nu\,d\Omega=\int_0^\infty E_\nu\,d\nu\,d\Omega\exp\left(-\int_z^\infty\alpha_\nu\sec\phi\,dz\right).\sec\phi\,dz. \tag{69}$$

From equations (15), (19) and (64), this may be written as

$$I_\nu\,d\nu\,d\Omega=G\sec\phi\,d\nu\,d\Omega\int_0^\infty N_e^2\exp\left(-H\sec\phi\int_z^\infty N_e\,dz\right).dz, \tag{70}$$

where $G=1{\cdot}72\times10^{-33}\theta^{-\frac{3}{2}}\exp\{(E_1^4-h\nu)/k\theta\}$ and $H=3{\cdot}59\times10^{25}\nu^{-3}$.

Since $N_e=N_0\exp(-\beta z)$, this may be rewritten

$$\begin{aligned}I_\nu\,d\nu\,d\Omega&=G\sec\phi\,.\,\beta^{-1}\,d\nu\,d\Omega\int_0^{N_0}N_e\exp(-H\sec\phi\,.\,\beta^{-1}N_e).\,dN_e\\&=G\beta H^{-2}\cos\phi\,d\nu\,d\Omega[1-(1+N_0H\sec\phi\,.\,\beta^{-1})\exp(-N_0H\sec\phi\,.\,\beta^{-1})]\\&=1{\cdot}39\times10^{-3}\cos\phi\left(\frac{\nu}{\nu_0}\right)^6\exp\left(-6{\cdot}3\,\frac{\nu}{\nu_0}\right)d\nu\,d\Omega\\&\times\left[1-\left\{1+1{\cdot}69\times10^{-13}\left(\frac{\nu_0}{\nu}\right)^3N_0\sec\phi\right\}\exp\left\{-1{\cdot}69\times10^{-13}\left(\frac{\nu_0}{\nu}\right)^3N_0\sec\phi\right\}\right]\end{aligned} \tag{71}$$

for $\beta=6\times10^{-9}$ per cm. and $\theta=2{\cdot}5\times10^4$ deg. K.

Neglect of the finite value of Λ_c, and the extrapolation of equation (63) to the upper chromosphere, have not produced any significant errors in the above results.

The variation in brightness with angle to the normal, as given by equation (71), is plotted in Fig. 2.

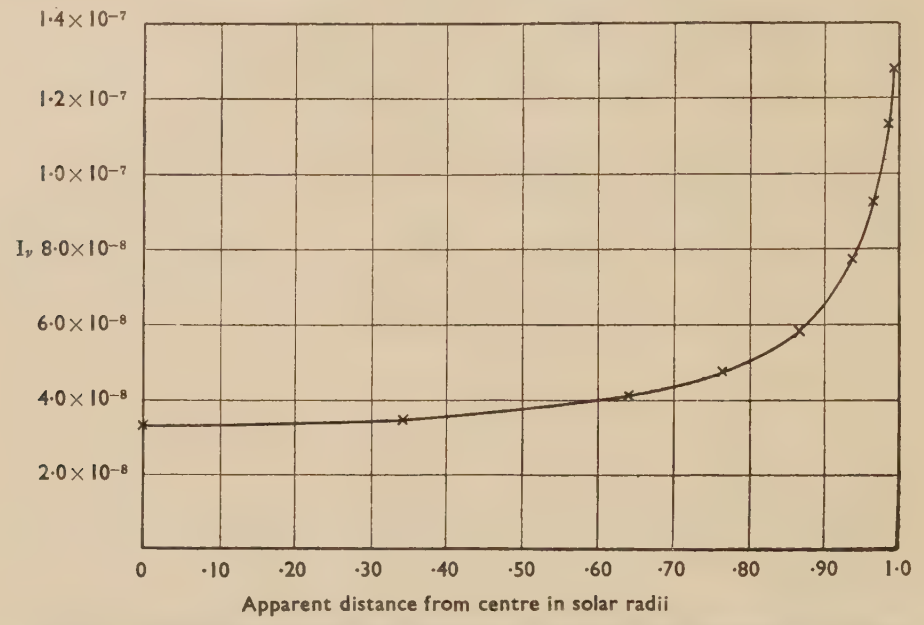

FIG. 2.—*Variation in brightness from the centre to the limb at the beginning of the Lyman continuum. The chromosphere is supposed uniform across the surface of the Sun; the temperature is assumed to be* $2{\cdot}5\times10^4$ *deg. K. at all heights above that for which* $N_e=10^{12}$ *per c.c., and to be small for lower heights.*

From the total intensity $J_\nu d\nu$, Λ_c may be deduced; for, integrating $I_\nu d\nu$ over a hemisphere,

$$J_\nu=\pi G\beta H^{-2}\int_0^{\pi/2}[\sin 2\phi-(\sin 2\phi+2N_0H\beta^{-1}\sin\phi)\exp(-N_0H\beta^{-1}\sec\phi)]\,d\phi, \quad (72)$$

and if $x=a\sec\phi$, where $a=N_0H\beta^{-1}$, this takes the form

$$\begin{aligned}J_\nu&=\pi G\beta H^{-2}\left[1-2a^2\int_a^\infty\frac{\exp(-x)}{x^3}dx-2a^2\int_a^\infty\frac{\exp(-x)}{x^2}dx\right]\\&=\pi G\beta H^{-2}[1-(1+a)\exp(-a)-a^2Ei(-a)],\end{aligned} \quad (73)$$

where $-Ei(-a)=\int_a^\infty\frac{\exp(-x)}{x}dx$. Consequently

$$\begin{aligned}J_\nu=4{\cdot}36\times10^{-3}\left(\frac{\nu}{\nu_0}\right)^6\exp\left(-6{\cdot}3\frac{\nu}{\nu_0}\right)\Bigg[1-\left\{1+1{\cdot}69\times10^{-13}\left(\frac{\nu_0}{\nu}\right)^3N_0\right\}\\\times\exp\left\{-1{\cdot}69\times10^{-13}\left(\frac{\nu_0}{\nu}\right)^3N_0\right\}\\-2{\cdot}85\times10^{-26}\left(\frac{\nu_0}{\nu}\right)^6N_0Ei\left\{-1{\cdot}69\times10^{-13}\left(\frac{\nu_0}{\nu}\right)^3N_0\right\}\Bigg].\end{aligned} \quad (74)$$

Since $1{\cdot}69\times10^{-13}(\nu_0/\nu)^3N_0$ is always very small compared with unity, this simplifies to

$$J_\nu=6{\cdot}2\times10^{-29}N_0^2\exp(-6{\cdot}3\nu/\nu_0)[1-2Ei\{-1{\cdot}69\times10^{-13}(\nu_0/\nu)^3N_0\}]. \quad (75)$$

Values of J_ν obtained from this formula are given in Table II. Because of the small optical thickness, J_ν will not vary greatly throughout the chromosphere.

TABLE II

Frequency ν/ν_0	J_ν erg/cm.²/sec./unit frequency interval
1·0	$4{\cdot}3\times10^{-7}$
1·1	$2{\cdot}6\times10^{-7}$
1·2	$1{\cdot}6\times10^{-7}$
1·3	$9{\cdot}2\times10^{-8}$
1·4	$5{\cdot}1\times10^{-8}$
1·5	$3{\cdot}0\times10^{-8}$
1·7	$1{\cdot}0\times10^{-8}$
2·0	$1{\cdot}6\times10^{-9}$
2·5	$7{\cdot}7\times10^{-11}$
3·0	$5{\cdot}5\times10^{-12}$

Values of total intensity, J_ν, in the Lyman continuum at the top of the chromosphere. These values should apply approximately throughout the chromosphere. Reflection at the base of the chromosphere is neglected; the electron concentration there is taken to be 10^{12} per c.c. ν_0 is the frequency of the Lyman series limit.

The number of photoelectric ionizations per unit volume per second is given by

$$\Lambda_c N_1 = \int_{\nu_0}^{\infty} (J_\nu \alpha_\nu / h\nu)\, d\nu. \tag{76}$$

But in the range of values listed in Table II, J_ν varies approximately as $(\nu/\nu_0)^{-6}$. Hence

$$\begin{aligned}\Lambda_c &= \frac{2{\cdot}82\times10^{29} J_0 \nu_0^6}{h}\int_{\nu_0}^{\infty}\frac{d\nu}{\nu^{10}}\\ &= 1{\cdot}34\times10^{8} J_0\\ &= 58\ \text{sec.}^{-1},\end{aligned} \tag{77}$$

if we take the electron concentration to be 10^{12} per c.c. at the base of the chromosphere.

Photoelectric ionizations from the ground state would be more frequent than other kinds for $N_e < 4{\cdot}8\times10^{10}$ per c.c., i. e. for $z > 3{\cdot}9\times10^{3}$ km., provided equation (63) held at this height. In the next section we shall find the height to which equation (63) remains valid.

The intensity of Lα.—The total intensity of the $L\alpha$ radiation at optical depths which are not too small is given by equation (54) which, from (55) and (64), becomes

$$J = 4\pi\left(\frac{2{\cdot}54\times10^{-15}N_e}{1+1{\cdot}07\times10^{-11}N_e}\right). \tag{78}$$

This is the same as in a black body whose temperature, T, is defined by

$$\frac{2{\cdot}54\times10^{-15}N_e}{1+1{\cdot}07\times10^{-11}N_e} = \frac{2h\nu^3}{c^2[\exp(h\nu/kT)-1]}. \tag{79}$$

For $N_e > 10^{11}$, J has the approximately constant value of $4\pi(2{\cdot}37\times10^{-4})$, and the corresponding value of T is found from equation (79) to be $1{\cdot}72\times10^{4}$ deg. K.

The approximate values of J given by equation (78) are valid at depths such that $\sqrt{3\lambda}\tau > 1$ or, at the centre of the line, for $N_e > 7{\cdot}5 \times 10^{10}$ per c.c., but are too great at higher elevations. Hence the inference of the preceding section concerning the relative importance of photoelectric ionization from the ground state in the upper chromosphere is reasonable.

A detailed discussion of the intensity and contour of the emitted $L\alpha$ line seems as yet impracticable, but approximate deductions of the magnitude and contour can be obtained simply from equation (13) by considering an atmosphere of uniform electron concentration, for which ϵ_ν, α_ν and λ will be the same everywhere. To evaluate the arbitrary constants a and b, we note that at the outer boundary to the chromosphere, $J = \frac{2}{3}(dJ/d\tau)$, and at the inner boundary, where the reflection coefficient must approach unity, $dJ/d\tau = 0$. Consequently a and b are given by

$$\frac{4\pi\epsilon_\nu}{\alpha_\nu\lambda} + a + b = 2(\lambda/3)^{\frac{1}{2}}(a-b) \tag{80}$$

and

$$a\exp(\sqrt{3\lambda}\tau_1) = b\exp(-\sqrt{3\lambda}\tau_1), \tag{81}$$

where τ_1 is the optical thickness of the chromosphere. Hence

$$b = -\frac{4\pi\epsilon_\nu}{\alpha_\nu\lambda}\left[1 + 2\sqrt{\frac{\lambda}{3}} + \left(1 - 2\sqrt{\frac{\lambda}{3}}\right)\exp(-2\tau_1\sqrt{3\lambda})\right]^{-1}. \tag{82}$$

The real atmosphere may be replaced by a uniform density atmosphere having the same electron concentration N_0 at the base. Allocating a thickness given by the scale height, β^{-1}, or $1{\cdot}67 \times 10^8$ cm., and using equation (64),

$$\tau_1 = 4{\cdot}8 \times 10^{-18} N_0 \beta^{-1} \exp[-3{\cdot}55 \times 10^{-23}(\Delta\nu)^2]. \tag{83}$$

Inserting numerical data for the centre of the line, and putting $N_0 = 5 \times 10^{11}$ per c.c.,

$$\tau_1 = 4{\cdot}0 \times 10^2,$$

while from equation (44)

$$\sqrt{3\lambda} = 3{\cdot}08 \times 10^{-2},$$

so $a = b\exp(-25)$ and is negligible. The boundary value of J is

$$J_0 = \frac{4\pi\epsilon}{\alpha\lambda} \cdot 2\sqrt{\frac{\lambda}{3}} = 14{\cdot}5\epsilon/\alpha\sqrt{\lambda}$$
$$= 5{\cdot}2 \times 10^{-5} \text{ c.g.s. units.} \tag{84}$$

This is the total intensity immediately above a black body of temperature $1{\cdot}16 \times 10^4$ deg. K., which is therefore an approximation to the apparent temperature for the centre of $L\alpha$. This is about $1{\cdot}5 \times 10^4$ times as great as black-body radiation at 6000 deg. K. Owing to the high scattering, the escaping radiation should be of uniform brightness across the disk.

The exact solution of equations (80) and (81) yields the result that at the outer boundary

$$J = \frac{4\pi\epsilon}{\alpha\lambda}\left\{1 - [1 + \exp(-2\tau_1\sqrt{3\lambda})]\left[1 + 2\sqrt{\frac{\lambda}{3}} + \left(1 - 2\sqrt{\frac{\lambda}{3}}\right)\exp(-2\tau_1\sqrt{3\lambda})\right]^{-1}\right\}. \tag{85}$$

With the above numerical data, the values of the term in {} brackets may be obtained as functions of τ_1 and so of $\Delta\nu$, the frequency interval from the centre of

the line. These values are given in Table III. Roughly, the intensity has fallen to about one-half maximum for $\Delta\nu = \pm 2{\cdot}9 \times 10^{11}$ per sec., or $\Delta\lambda = \pm 0{\cdot}14$ A.

TABLE III

The Lα contour. $N_0 = 5 \times 10^{11}$ *per c.c.*

Frequency interval from centre of line, $\Delta\nu$	$\Delta\lambda$ in A.	τ_1	$J_\nu\{4\pi\epsilon/a\lambda\}^{-1}$
0	0·000	$4{\cdot}02 \times 10^2$	$2{\cdot}1 \times 10^{-2}$
$1{\cdot}0 \times 10^{11}$	0·050	$2{\cdot}82 \times 10^2$	$2{\cdot}1 \times 10^{-2}$
$2{\cdot}0 \times 10^{11}$	0·099	$9{\cdot}72 \times 10$	$2{\cdot}0 \times 10^{-2}$
$2{\cdot}5 \times 10^{11}$	0·124	$4{\cdot}37 \times 10$	$1{\cdot}8 \times 10^{-2}$
$2{\cdot}7 \times 10^{11}$	0·134	$3{\cdot}02 \times 10$	$1{\cdot}5 \times 10^{-2}$
$2{\cdot}8 \times 10^{11}$	0·138	$2{\cdot}49 \times 10$	$1{\cdot}3 \times 10^{-2}$
$2{\cdot}9 \times 10^{11}$	0·144	$2{\cdot}03 \times 10$	$1{\cdot}1 \times 10^{-2}$

Far enough away from the centre of the line, scattering may be appreciable but true absorption negligible so, with perfect reflection at the base, all the radiation originally emitted in a frequency interval $d\nu$ escapes from the chromosphere. For this to be so, it is sufficient that, say, $\sqrt{3\lambda}\tau_1 \leqslant 0{\cdot}15$. With $N_1 \simeq 1{\cdot}27 \times 10^{-4} N_e$ and $N_0 = 10^{12}$ per c.c., it readily follows that this holds for $\Delta\nu \geqslant 3{\cdot}8 \times 10^{11}$ per sec. and that the hemispherical emission is

$$1{\cdot}3 \times 10^{-3} \exp\{-3{\cdot}55 \times 10^{-23}(\Delta\nu)^2\} . d\nu \text{ erg/cm.}^2\text{/sec.}$$

The emission is given in Table IV for a few values of $\Delta\nu$, N_0 being taken as 5×10^{11} per c.c. For comparison we may note that the hemispherical emission, πB, from a black body at temperature 6000 deg. K. is $1{\cdot}7 \times 10^{-9}$ erg/cm.^{2}/sec./unit frequency interval.

TABLE IV

Intensities in the wings of Lα ($N_0 = 5 \times 10^{11}$ *per c.c.*)

Frequency interval from centre of $L\alpha$ per sec.	$\Delta\lambda$ (in A.)	Energy (in ergs) in unit frequency interval crossing one square cm. per second at the top of the chromosphere. Photospheric radiation is not included.
$3{\cdot}8 \times 10^{11}$	0·188	$1{\cdot}9 \times 10^{-6}$
$4{\cdot}0 \times 10^{11}$	0·198	$1{\cdot}0 \times 10^{-6}$
$4{\cdot}5 \times 10^{11}$	0·222	$2{\cdot}3 \times 10^{-7}$
$5{\cdot}0 \times 10^{11}$	0·247	$4{\cdot}3 \times 10^{-8}$
$6{\cdot}0 \times 10^{11}$	0·296	$8{\cdot}4 \times 10^{-10}$

The intensity of Lβ.—In a similar manner, we find from (54), (60), (61) and (64) that the total intensity of $L\beta$ radiation at optical depths which are not too small is given by

$$J = 4\pi . \frac{5{\cdot}46 \times 10^{-4} N_e + 2{\cdot}15 \times 10^{-17} N_e^2}{6{\cdot}40 \times 10^{12} + 8{\cdot}35 \times 10 N_e} . \qquad (86)$$

With $N_e \sim 5 \times 10^{11}$, this is approximately independent of N_e, and reduces to

$$J \simeq 8{\cdot}2 \times 10^{-5}, \qquad (87)$$

which is the same as in a black body at a temperature of $1{\cdot}28 \times 10^4$ deg. K.

Replacing the real atmosphere by an atmosphere having a uniform electron concentration of $N_e = 5 \times 10^{11}$ per c.c. and thickness β^{-1}, the boundary value of J at the centre of the line is

$$J_0 = 0{\cdot}174 \times \frac{4\pi\epsilon}{\alpha\lambda} = 1{\cdot}3 \times 10^{-5} \text{ c.g.s. units,} \qquad (88)$$

and the apparent temperature corresponding to the centre of the escaping $L\beta$ line is $1{\cdot}16 \times 10^4$ deg. K., which happens to be the same as for $L\alpha$. This is 8×10^4 times as great as radiation from a black body at 6000 deg. K.

From equation (85), with appropriate constants, it appears that the width of the line where the intensity equals about one-half its maximum value is $\Delta\nu = \pm 3{\cdot}8 \times 10^{11}$ per sec., or $\Delta\lambda = \pm 0{\cdot}13$ A.

In the wings of $L\beta$ the intensity may be computed as for $L\alpha$, the base of the chromosphere again being a perfect reflector. The hemispherical emission from unit surface area of the chromosphere is given in Table V for $N_0 = 5 \times 10^{11}$ per c.c. For comparison, it may be noted that the corresponding hemispherical emission from a black body at 6000 deg. K. is $8{\cdot}7 \times 10^{-11}$ erg/cm.^{2}/sec./unit frequency interval.

TABLE V

Intensities in the wings of $L\beta$ ($N_0 = 5 \times 10^{11}$ per c.c.)

Frequency interval from centre of $L\beta$ per sec.	$\Delta\lambda$ (in A.)	Energy (in ergs) in unit frequency interval crossing one square cm. per second at the top of the chromosphere. Photospheric radiation is not included.
$4{\cdot}5 \times 10^{11}$	0·158	$8{\cdot}4 \times 10^{-7}$
$5{\cdot}0 \times 10^{11}$	0·176	$2{\cdot}5 \times 10^{-7}$
$5{\cdot}5 \times 10^{11}$	0·193	$6{\cdot}5 \times 10^{-8}$
$6{\cdot}0 \times 10^{11}$	0·210	$1{\cdot}5 \times 10^{-8}$
$7{\cdot}0 \times 10^{11}$	0·245	$5{\cdot}6 \times 10^{-10}$
$8{\cdot}0 \times 10^{11}$	0·280	$1{\cdot}3 \times 10^{-11}$

The intensity of $H\alpha$.—The observed intensity of the $H\alpha$ line provides the only direct check on the present theory.

To compute the central intensity of $H\alpha$, the populations of the N_{2S}, N_{2P}, N_{3S}, N_{3P} and N_{3D} states, required for equation (30), may be derived from equations (39), (32), (34), (35) and (36) respectively, omitting terms in the last three equations which depend on the $H\alpha$ intensity, and writing $\Lambda_{2S,\,3P}N_{2S}$ for the rate of transition from 2S to 3P in equation (39). From equations (58), (61) and (64), these populations may be expressed in terms of the electron concentration. The scattering, absorption and emission properties of the chromosphere may then be computed, with the following results.

The value of λ is found to be 0·363 for $N_e = 10^{12}$ per c.c. and 0·343 for $N_e = 10^{11}$ per c.c., and so has a mean value about 0·35.

The term $\Sigma N_l A_{j,l}\omega_j/\omega_l$, which appears in equations (29) and (30), has a value

$$\frac{1{\cdot}5 \times 10^{19}}{\Lambda_{2S,\,3P} + 4{\cdot}3 \times 10^5} + 4{\cdot}1 \times 10^{13}$$

for $N_e = 10^{12}$ per c.c. and

$$\frac{6{\cdot}4 \times 10^{17}}{\Lambda_{2S,\,3P} + 6{\cdot}7 \times 10^4} + 2{\cdot}3 \times 10^{12}$$

for $N_e = 10^{11}$ per c.c.

Very approximately, it may be written as

$$\frac{10^7 N_e}{\Lambda_{2S,3P}} + 30 N_e.$$

The order of magnitude, which is all that is needed, is obtained by putting $\Lambda_{2S,3P} \approx 8 \times 10^4$. Hence from (29)

$$\alpha_\nu \approx 1{\cdot}3 \times 10^{-19} N_e \exp\left[-1{\cdot}04 \times 10^{-21} (\Delta\nu)^2\right], \tag{89}$$

and the optical depth of the chromosphere at the centre of $H\alpha$ is

$$\tau_1 \approx 1{\cdot}3 \times 10^{-19} N_0 \beta^{-1}; \tag{90}$$

so, with $\beta = 6 \times 10^{-9}$ per cm., $\tau_1 \approx 2{\cdot}2 \times 10^{-11} N_0$. The optical depth is about unity for $N_e \approx 5 \times 10^{10}$ per c.c., and the optical thickness of the chromosphere is about 11 if $N_0 = 5 \times 10^{11}$ per c.c. at the base.

Because λ is large and $\tau_1 \gg 1$, the radiation escaping at the centre of $H\alpha$ is quite independent of the $H\alpha$ radiation incident upon the chromosphere from the photosphere, and may be estimated from data appropriate to the chromosphere at about optical depth unity. For this purpose we evaluate ϵ/α, which does not vary rapidly with electron concentration, for $N_e = 10^{11}$ per c.c. The result is, using equation (30),

$$\frac{c^2}{2h\nu^3} \cdot \frac{\epsilon}{\alpha} = \frac{5{\cdot}94 \times 10^{14} + 7{\cdot}93 \times 10^9 \Lambda_{2S,3P}}{7{\cdot}94 \times 10^{17} + 2{\cdot}30 \times 10^{12} \Lambda_{2S,3P}}, \tag{91}$$

which we shall denote by R.

From equation (85), the total intensity of the escaping radiation is, for $2\tau_1\sqrt{3\lambda} \gg 1$ (as here),

$$J = \frac{4\pi\epsilon}{\alpha\lambda}\left\{1 - \frac{1}{1 + 2\sqrt{\lambda/3}}\right\}$$
$$= 0{\cdot}40\left(\frac{4\pi\epsilon}{\alpha\lambda}\right). \tag{92}$$

At optical depth unity the value of J is about double this, or $0{\cdot}80(4\pi\epsilon/\alpha\lambda)$. But it is easy to show that with this value of J

$$\Lambda_{2S,3P} = \frac{3A_{3P,2S}Jc^2}{8\pi h\nu^3} = 1{\cdot}6 \times 10^8 R. \tag{93}$$

By substitution in equation (91), we find that $R = 2{\cdot}1 \times 10^{-3}$. It readily follows that the intensity of the escaping radiation equals the hemispherical emission from a black body at 4200 deg. K., and that the central intensity of the $H\alpha$ line is 0·19 of that of the surrounding continuum, which corresponds to that of a black body at a temperature of 6150 deg. K. This is in very satisfactory agreement with Allen's measured central intensity (**15**) of 0·12.

11. *Emission from a non-uniform chromosphere.*—One of the principal assumptions in the whole of the above discussion of the hydrogen spectrum of the Sun is that of an isothermal chromosphere. We shall now discuss the modifications required by one model of a non-uniform chromosphere.

(*a*) If the temperature of the chromosphere is uniform, there seems to be no doubt that this temperature is about 30,000 deg. K., for both the line contours and the density gradient require such a temperature. The mottled appearance of the chromosphere in spectroheliograms, and the irregularities at the limb in eclipse photographs are strong evidence, however, that the chromosphere is by no means

uniform in temperature. As a second approximation to a model more consistent with all the observational data, we shall briefly consider a chromosphere in which the temperature is uniform radially, but is non-uniform across the Sun's surface. For simplicity, we consider columns at only two temperatures, θ_1 and θ_2, where $\theta_1 > \theta_2$, the areas of surface at these temperatures being S_1 and S_2 respectively.

Because of the difference in temperature the density gradient will be greater over S_2 than over S_1: so that, if there be hydrostatic equilibrium at the photosphere, the density will be greater over S_1 than over S_2 at an elevation depending on θ_1 and θ_2, but probably of the order of 1000 km. or less.

The hydrogen lines used in obtaining the density gradient are high members of the Balmer series; the emission of these is proportional to N_e^2, and so the observed density gradient will tend to be that of the higher temperature regions. Similarly, Redman's measurements of line contours 1500 km. above the base of the chromosphere would have corresponded to the regions of maximum density, i. e. maximum temperature. Hence these would be measurements of θ_1.

There does not seem to have been any optical measurement of the temperature of the lower temperature regions, but recent radio observations, kindly made available by Dr J. H. Piddington, prior to publication, indicate that the *mean* temperature of the chromosphere is about 10,000 deg. K. or a little less. The elevation to which these results apply is at present uncertain but would appear to be somewhere in the middle chromosphere. Assuming chromospheric columns of two temperatures only, these results indicate that

$$\frac{\theta_1 S_1 + \theta_2 S_2}{S_1 + S_2} = 10^4 \text{ deg. K.} \tag{94}$$

Arbitrarily putting $\theta_1 = 2{\cdot}5 \times 10^4$ deg. K., $\theta_2 = 5 \times 10^3$ deg. K., we find that the higher temperature region occupies about one-quarter of the Sun's surface. If this interpretation be valid, the total emission from the Sun as estimated in this paper is too great by a factor of about four. Moreover, limb brightening computations become of doubtful significance.

In Section 2 (*b*) we found difficulty in reconciling the estimated concentrations of negative hydrogen ions in the upper photosphere and of electrons in the chromosphere. These difficulties do not arise in an atmosphere consisting of adjacent hot and cold columns. On the one hand, the limb of the Sun occurs where the rate of formation and the concentration of negative hydrogen ions become significant. But a reduction in temperature from 25,000 deg. K. by, say, a factor of 3 or 5 gives rise to a great increase in the rate of formation and the concentration of negative hydrogen ions if the gas pressure be kept constant. Hence we should expect the emissivity of a given thickness of gas to be much greater for a cool column at a comparable pressure, and the Sun's limb should correspond to the highest elevation at which significant emission takes place in the cool columns; significant emission would only occur in a hot column at a rather lower elevation. On the other hand, the observed chromospheric electron concentration would correspond to that of the hotter columns, as explained above. Hence the estimated concentrations of hydrogen ions in the upper photosphere and of electrons in the lower chromosphere would not be directly comparable.

The electron concentration in the hotter columns, as deduced from eclipse observations, would not exceed that for an isothermal chromosphere by a factor greater than two, but the concentration at the base of these columns might be more

than 10^{12} per c.c. This would partly compensate for the reduction in estimated Lyman emission due to the non-uniform temperature.

(*b*) It is of interest to compare the emission of the Lyman continuum from an isothermal chromosphere at $2{\cdot}5 \times 10^4$ deg. K. with that of the corona, the latter having been discussed in recent papers by Kiepenheuer (**16**) and by Woolley and Allen (**17**).

Suppose the corona to be pure hydrogen, and isothermal at $\theta_1 = 10^6$ deg. K., the electron concentration at the base being 4×10^8 per c.c. and the electron gradient $1{\cdot}63 \times 10^{-10}$ per cm. (the gradient corresponding to hydrostatic equilibrium). Neglecting self-absorption and reflection from the base of the chromosphere, the radiation which escapes from a radial column of the corona above one square centimetre of the Sun's surface is found to be

$$5{\cdot}76 \times 10^{-15} \exp\left[(E_1^i - h\nu)/k\theta_2\right] \text{ erg/cm.}^2\text{/sec./unit interval frequency.}$$

This may be compared with the corresponding chromospheric emission, Section 10 (*a*), viz.

$$2{\cdot}27 \times 10^{-7} \exp\left[(E_1^i - h\nu)/k\theta_1\right] \text{ erg/cm.}^2\text{/sec./unit frequency interval,}$$

where θ_1 is the chromospheric temperature of $2{\cdot}5 \times 10^4$ deg. K. Chromospheric emission greatly exceeds that of the corona down to very short wave-lengths, and is of the same order of magnitude at about 240A.

12. *Acknowledgment.*—The work in this paper has been carried out as part of the programme of the Commonwealth Council for Scientific and Industrial Research.

Division of Physics,
Council for Scientific and Industrial Research,
Sydney :
1949 *February* 10.

References

(1) M. N. Saha, *Proc. Roy. Soc.*, A., **160,** 155, 1937.
(2) A. Hunter, *Phys. Soc. Reports*, **9,** 5, 1943. (Summarizes these deductions.)
(3) R. v. d. R. Woolley, *Proc. Roy. Soc.*, A., **187,** 403, 1946.
(4) B. Edlén, *Z. Astrophys.*, **22,** 30, 1942.
(5) R. O. Redman, *M.N.*, **102,** 140, 1942.
(6) R. G. Giovanelli, *Aust. J. Sci. Res.*, **1,** 360, 1948.
(7) Z. Kopal, *Ap. J.*, **104,** 60, 1946.
(8) G. Münch, *Ap. J.*, **106,** 217, 1947.
(9) R. G. Giovanelli, *Aust. J. Sci. Res.*, **1,** 289, 1948.
(10) J. A. Gaunt, *Phil. Trans. Roy. Soc.*, A., **229,** 163, 1930.
(11) D. H. Menzel, *Lick Observatory Publications*, **17,** 1931.
(12) R. H. Fowler, *Statistical Mechanics*, Cambridge, 1929, p. 428.
(13) S. Rosseland, *Theoretical Astrophysics*, Oxford, 1936, p. 101.
(14) H. S. W. Massey and C. B. O. Mohr, *Proc. Roy. Soc.*, A., **132,** 605, 1931.
(15) C. W. Allen, *Memoirs of the Commonwealth Solar Observatory*, **1,** No. 5, 1934.
(16) K. O. Kiepenheuer, *M.N.*, **106,** 515, 1946.
(17) R. v. d. R. Woolley and C. W. Allen, *M.N.*, **108,** 292, 1948.

AN INVESTIGATION INTO THE POSSIBILITY OF OBSERVING STREAMS OF CORPUSCLES EMITTED BY SOLAR FLARES

F. D. Kahn *

(Communicated by Professor S. Chapman, F.R.S.)

(Received 1948 December 10)

Summary

This paper discusses Chapman's suggestion that a stream of corpuscles, emitted from the Sun by a flare, should be spectroscopically detectable before and during the magnetic storm which it is thought to cause. After an investigation of the mode of expansion and the state of ionization of such a stream, it is estimated that the particles in it may cause abnormal absorption near the H and K lines of calcium which is detectable soon after the end of the flare. Should this absorption not be observable, however, the failure will not necessarily disprove the corpuscular theory of magnetic storms, as the depth of absorption may lie below the observational limit.

1. *Introduction*

1.1. It has long been known that magnetic storms are more frequent at periods of sunspot maxima than at sunspot minima and this has led to the conclusion that the Sun is somehow responsible for these terrestrial phenomena. A closer analysis of their times of occurrence reveals that the storms can be divided into two classes, one class being relatively weak and showing a tendency to recur at 27 days interval, i. e. the period of the Sun's rotation, while storms of the other class are more intense and occur quite irregularly. This paper is concerned with the latter type of storm.

1.2. *Solar flares and magnetic storms.*—Carrington (**1**), in 1859, was the first to suggest that a connection existed between intense solar flares and the irregular magnetic storms and this hypothesis has been amply confirmed by the work of Newton (**2, 3**) and others, though some large flares, generally near the edge of the Sun's disk, do not give rise to storms. The average interval between the occurrence of the flare and the commencement of the associated storm is about 26 hours and the storm may last for anything between half a day and two or three days.

1.3. *The corpuscular theory of magnetic storms.*—Chapman and Ferraro have worked out a theory indicating how magnetic storms can be produced whenever a cloud of ionized solar corpuscles impinges on the Earth. In the case of the irregularly occurring magnetic storms these particles may be supposed expelled from the Sun by the action of the flare. The theory is described by Chapman and Bartels in their book *Geomagnetism* (**4**). This theory works well—there are mechanisms available which explain why flares should expel .corpuscles and many terrestrial effects observed during magnetic storms can be explained on it, but no one has ever demonstrated the actual existence of the clouds of corpuscles.

* Skynner Senior Student in Astronomy, Balliol.College, Oxford.

1.4. *Spectroscopic verification of the theory.*—In 1929 Chapman (**5**) suggested that the clouds of particles might be spectroscopically detectable in the following way. Let us assume such a cloud to be travelling with a velocity v away from the Sun along the line of sight from the Earth. We take it that the cloud contains some *Ca* II ions, which normally absorb light of wave-length $\lambda_0 \approx 3960$ A. Owing to the Doppler effect light from the Sun of wave-length λ will have a wave-length $\lambda(1+v/c)$ relative to the ions in the cloud, and will be absorbed if

$$\lambda_0 = \lambda(1+v/c)$$

$$\text{or } \lambda = \lambda_0(1-v/c) \text{ to the first order.}$$

Thus the travelling ions will cause a displaced absorption line to appear in the solar spectrum, the displacement being to the violet if the ions are travelling towards the Earth. The aim of this paper is to estimate the density of *Ca* II ions in the cloud, to ascertain whether this suffices to make the absorption detectable. Elements other than *Ca* II may also cause anomalous absorption.

As there is likely to be a range of velocities in the cloud we should expect to find a band of absorption, rather than a sharp line. Richardson in California, and Brück and Rutllant in Cambridge (**6, 7**) have published tentative observations of such absorption bands near the H and K lines of *Ca* II made during certain magnetic storms.

2. *A Possible Mode of Emission of the Particles*

2.1. *Lα radiation pressure as the cause of the emission.*—The observations of solar flares made by Waldmeier (**8, 9**), Giovanelli (**10**) and Ellison (**11, 12**) all record that hydrogen lines, particularly *Hα*, are very prominent in their emission spectra. The observed emission of *Hα* in strength and in great width implies the subsequent emission of *Lα* ($\lambda = 1215$ A.), which may be expected to be very wide also. This strongly suggests that hydrogen atoms near the flare will be repelled by the radiation pressure on them of *Lα*, their resonance line. Now according to Unsöld (**13**), and according to later estimates by Strömgren (**14**), hydrogen is by far the most abundant element in the solar atmosphere (*cf.* Table I in Section 4.1 below). So, if the hydrogen atoms are repelled by the radiation from the flare, they may be expected to drag along also the atoms intermingled with them. This theory was suggested by Kiepenheuer in 1937 (**15**).

2.2. *The line width and intensity of Lα.*—The *Lα* emission line must be very wide to be able to cause the expulsion of atoms with speeds of up to 1600 km./sec., as inferred from the average length (26 hours) of the interval between the flare and the onset of the magnetic storm. To expel atoms with such a speed the *Lα* line needs a half-width of at least 6 A., and also a considerable intensity. We expect fairly high ionization of the hydrogen near the flare, say 90 per cent, so that only 10 per cent of the hydrogen can respond to the radiation pressure of *Lα*, and these non-ionized atoms will have to drag along with them the rest of the particles nearby. Under these conditions the intensity at the centre of the *Lα* line is required to be about 10^7 times that of the continuum near 1215 A. of a black body at 6000 deg. K. Since the *Lα* emission must be rather stronger than that of *Hα*, this seems attainable, and Giovanelli's recent theoretical work (**16**) suggests an *Lα* intensity during a flare of about one-quarter this estimate. However, we should do well to wait on detailed results of the recent observations made by

Richardson, who, according to the 1947 Mt. Wilson Report (**17**), has measured the intensities and widths of the Balmer lines down to H_{21} which occur in a flare. From a consideration of these results it should be possible to infer the nature of the $L\alpha$ emission.

2.3. *Discussion.*—According to Ellison (**11, 12**) the intensities and widths of emission lines in a flare decrease after its peak. If this holds also for $L\alpha$ the particles expelled early during the flare would be given higher speeds than those emitted later on. Thus the cloud should lengthen as it advances, owing to this differential velocity and so magnetic storms should last much longer than flares. This accords with observation.

The apparent red-shift of the $H\alpha$ emission line in a flare, also noted by Ellison, can be explained as well. Ellison attributes this to an excess absorption of light to the violet of $H\alpha$ by a cloud of gas travelling away from the flare. If the cloud is being expelled by $L\alpha$ radiation there must, at any instant, be many H-atoms in it in the second quantum state, having just absorbed an $L\alpha$ photon. In this state they will absorb $H\alpha$ light and the Doppler effect will shift this absorption to the violet side of the line centre.

Kiepenheuer's theory is attractive, because of its simplicity; it explains much about intense flares and the expulsion of corpuscles by them, and can doubtless be adapted to explain also the prominence surges observed at times of smaller flares. But until we know more about the $L\alpha$ radiation of a flare, it must remain uncertain whether or not this mechanism is the correct one.

3. *The Expansion of the Cloud*

3.1. *A model of a flare.*—To facilitate the calculation of how the cloud of particles may be expected to expand, the following simple model of a flare is assumed. Let the surface of the flare be spherical, of radius b, and suppose that particles, i.e. atoms and ions, are emitted from it within a solid angle Ω during the interval $t=0$ until $t=\tau_1$, at right angles to the surface. Let the emission at the instant $t=\tau$ be at the rate $N(\tau)$ particles per second per unit area, with a velocity $v(\tau)$ cm./sec.; $v(\tau)$, the speed at emission of any particle, will be supposed to remain unaltered throughout its time of flight.

$$\text{Let} \quad v(0)=v_0,$$
$$v(\tau_1)=v_1$$

and, to simplify calculations, assume a linear law of variation for $v(\tau)$, so that

$$v(\tau)=\{v_0(\tau_1-\tau)+v_1\tau\}/\tau_1. \qquad (1)$$

Thus, if R is the Earth's distance from the Sun, a magnetic storm sets in at a time R/v_0 after the beginning of a flare, and ends at a time $R/v_1+\tau_1$; τ_1 is small compared with R/v_0 and R/v_1.

Adopting typical values for the interval between the flare and the onset of the storm, and for the duration of the storm,

$$R/v_0=26 \text{ hours},$$
$$R/v_1-R/v_0=18 \text{ hours (duration of the storm)},$$

so that with $R=1{\cdot}5\times10^{13}$ cm.,

$$v_0=1{\cdot}6\times10^{8} \text{ cm./sec.},$$
$$v_1=\quad 10^{8} \text{ cm./sec. approx.}$$

Flares have an area of the order of 10^{-3} of the Sun's disk, so that b, their hypothetical radius, may be put equal to 2×10^9 cm.

3.2. *Particle density in the cloud.*—Consider the particles emitted between the times τ and $\tau+\Delta\tau$. At time t they will occupy part of a spherical shell concentric with the flare, and subtending a solid angle Ω at the flare centre. This shell has the radius

$$r = b + v(\tau)(t-\tau) \tag{2}$$

and thickness

$$\begin{aligned}\Delta r &= v(\tau)(t-\tau) - v(\tau+\Delta\tau)(t-\tau-\Delta\tau) \\ &= v(\tau)\Delta\tau - \frac{dv}{d\tau}(t-\tau)\Delta\tau. \end{aligned} \tag{3}$$

With formula (1) for $v(\tau)$, (3) becomes

$$\Delta r = \frac{\Delta\tau}{\tau_1}[v_0(t+\tau_1-2\tau) - v_1(t-2\tau)]. \tag{4}$$

The number of particles emitted between the times τ and $\tau+\Delta\tau$ is

$$\Omega b^2 N(\tau)\Delta\tau.$$

At a time t these particles occupy a volume

$$\Omega r^2 \Delta r,$$

so that the corresponding particle density at a distance r from the centre of the flare is

$$n(r, t) = \frac{\Omega b^2 N(\tau)\Delta\tau}{\Omega r^2 \Delta r}$$

$$\text{or } n(r, t) = N(\tau)\frac{b^2\tau_1}{r^2[v_0(t+\tau_1-2\tau) - v_1(t-2\tau)]}. \tag{5}$$

Note that r, t and τ are conected by the formula (2) which becomes

$$r - b = \frac{v_0(\tau_1-\tau) + v_1\tau}{\tau_1}(t-\tau).$$

3.31. *The early stages of the cloud's existence.*—Early in the cloud's existence the value of $t-\tau$ will be small, and

$$v_0(t+\tau_1-2\tau) - v_1(t-2\tau) \approx v_0(\tau_1-\tau) + v_1\tau = v(\tau).$$

Hence

$$n(r, t) \approx \frac{b^2 N(\tau)}{r^2 v(\tau)}. \tag{6}$$

This inverse square law will hold approximately while the flare is still in progress.

3.32. *The later stages.*—For values of t large compared with τ and τ_1,

$$n(r, t) = \frac{b^2 N(\tau)\tau_1}{r^2(v_0-v_1)t}. \tag{7}$$

Here the longitudinal expansion has become important, as is shown by the presence in the denominator of $(v_0-v_1)t$, which is absent from (6). In particular, for the front of the cloud, where $r = v_0 t$ and for which $\tau = 0$,

$$\begin{aligned} n(r, t) \equiv n_0(t) &= \frac{b^2 N(0)\tau_1}{v_0^2 t^2 (v_0-v_1)t} \\ &= \frac{b^2 N(0)\tau_1}{v_0^2(v_0-v_1)} \cdot \frac{1}{t^3}. \end{aligned} \tag{8}$$

We now estimate the density of atoms and ions at the front of the cloud, and assume that the values elsewhere are similar. By (6) the density at the front on emission is $N(0)/v_0$, and this is taken to be of the same order as the density of the Sun's atmosphere near the flare, so that $N(0)/v_0 = 10^k$, where $10 \leqslant k \leqslant 14$.

Adopting the values of Section 3.1 for b, v_0 and v_1, and assuming $\tau_1 = 10^3$ secs., or about a quarter of an hour, we find

$$n_0(t) = 4 \times 10^{k+5}/t^3. \tag{9}$$

A very tentative estimate of the momentum density of the cloud when near the Earth has been made by Chapman and Ferraro in their magnetic storm theory; for a speed of $1{\cdot}6 \times 10^8$ cm./sec. it corresponds to a density of 100 H atoms per c.c. The estimated average atomic weight of the solar atmosphere, and therefore of the cloud, is from 1·5 to 2·5 {*cf.* (**13**), (**18**)}, which gives 40–60 particles per c.c. as the corresponding density near the Earth. The cloud reaches the Earth when $t \approx 10^5$ secs., so that

$$n_0(t) = 4 \times 10^{k-10} = 40 \text{ for } k = 11.$$

The density may, however, be larger than that given by this value of k.

4. *Ionization in the Cloud. Which Elements can we Expect to Observe?*

4.1. *Constitution of the cloud.*—Table I below gives a list of the elements expected to be present in the cloud, their ionization potentials and the approximate quantum weights of their ionized states. Composition A is given by Unsöld (**13**), and B by Strömgren (**14, 18**). The other data are taken from Unsöld.

TABLE I

Composition of the solar atmosphere

Element	Propn. by number of atoms		At. No.	At. Wt.	g_0	χ_0	g_1	χ_1	g_2	χ_2	g_3
	A (Unsöld)	B (Strömgren)									
H	$9{\cdot}3 \times 10^{-1}$	≈ 1	1	1	2	13·53	...	...	...	...	...
O	$3{\cdot}5 \times 10^{-2}$		8	16	9	13·55	4	34·93	9	54·87	6
Fe	$1{\cdot}3 \times 10^{-2}$		26	56	25	7·83	30	16·5	?	?	?
Si	$1{\cdot}0 \times 10^{-2}$		14	28	9	8·12	6	16·27	1	33·53	2
Mg	$5{\cdot}2 \times 10^{-3}$	$3{\cdot}8 \times 10^{-5}$	12	24	1	7·61	2	14·96	1	80	?
Ni	$1{\cdot}0 \times 10^{-3}$		28	59	21	7·61	10	18·2	?	?	?
Al	$2{\cdot}1 \times 10^{-3}$		13	27	6	5·96	1	18·74	2	28·31	1
Ca	$1{\cdot}5 \times 10^{-3}$	$1{\cdot}6 \times 10^{-6}$	20	40	1	6·09	2	11·82	1	51·0	6
Na	$7{\cdot}0 \times 10^{-4}$	$8{\cdot}7 \times 10^{-7}$	11	23	2	5·12	1	47·0	6	?	?

In this table

g_r = approximate quantum weight of rth ionized state,

χ_r = ionization potential of the rth ionized state, measured in electron volts.

Composition B contains, of course, elements other than those indicated: the table gives only the amounts of the most important elements present, from our point of view. It will be noted that the hydrogen : metal ratio is much higher in B than in A.

4.12. *Physical conditions in the cloud.*—The cloud is taken to remain at 6000 deg. K, though a certain amount of heating may take place during its expulsion and, as the flare is not known to emit photons with more than 22 e.V. energy, no element in the cloud will be expected to be more than doubly ionized. The work of Lindemann (**19**) and Chapman and Ferraro (**20**) has shown that the cloud will remain electrically neutral: this is an essential condition for it not to disperse. So, as most of the electrons will come from the hydrogen, the electron density will approximately equal that of the hydrogen ions.

4.13. *Possible absorption lines.*—A good absorption line can be obtained only from the resonance line of any constituent of the cloud, with the possible exception of *H*. For this absorption to be observable the resonance line must lie in a part of the spectrum that is not completely absorbed in the Earth's atmosphere, i. e. its wave-length λ must exceed 2930 A. Among the elements concerned, or their ionized states, only *Ca* II and *Na* satisfy this condition.

4.2. *Early ionization in the cloud.*—It can readily be shown that in the early stages of the cloud's existence, while the flare is still in progress, both *Ca* II and *Na* are too rare to give detectable absorption. The flare strongly emits *L*α radiation whose photons have 10·15 e.V. energy. This will ionize almost all the *Na* to *Na* II, which affords no visible resonance lines.

Calcium, also, will be almost completely ionized from *Ca* II to *Ca* III, for the emission of *H*α [$H_{3\to2}$] by the flare implies the simultaneous emission of the Lyman line $\lambda = 1026$ A., corresponding to the transition $H_{3\to1}$. The transition probability of $H_{3\to1}$ is $0{\cdot}55\times10^8$ per sec., which exceeds that of $H_{3\to2}$ ($0{\cdot}43\times10^8$). Since χ_2 for calcium is 11·8 e.V., these photons of wave-length 1026 A., which have an energy of 12 e.V., are able to ionize *Ca* II to *Ca* III, which has no suitable resonance lines.

The remaining hope for visible absorption during the early stages of the cloud's existence is hydrogen. Indeed, *H*α absorption is quite possible, and the apparent red-shift of the *H*α emission line in a flare, reported by Ellison and discussed in Section 2.3, is probably due to this cause.

4.3. *The later stages of the cloud's existence.*—While the flare is still in progress its radiation will play the major part in the ionization of the cloud, but once it has died down the radiation of the Sun as a whole becomes important. The Sun is taken to be a black body at 6000 deg. K., the temperature of the cloud being the same.

4.31. *Possible modes of ionization and recombination.*—The following processes tend to ionize the constituents of the cloud: (*a*) photo-ionization, and (*b*) thermal ionization.

(*a*) Photo-ionization takes place whenever a photon interacts with an atom *X*, in its ground state or in an excited state, and raises its energy above its ionization potential χ. Consider a gas, in thermodynamical equilibrium at temperature *T*, which contains n_0 non-ionized atoms of *X* per unit volume. Let the fraction of *X* atoms in the *r*th quantum state be $p_r(T)$, so that $\sum_{r=1}^{\infty} p_r(T) = 1$. Then the number of photo-ionizations from the *r*th quantum state per unit volume per unit time may be written $n_0 p_r(T)\gamma_r(T)$, and the total rate of photo-ionization per unit volume will be $n_0 \sum_{r=1}^{\infty} p_r(t)\gamma_r(t)$. In a field of black-body radiation diluted by a factor β, the fraction of *X* atoms excited to the *r*th state ($r \geqslant 2$) is less than $\beta p_r(T)$,

say $\beta_r p_r(T)$, and when β is small, as in the cloud, almost all the atoms will be in the ground state ($r=1$). The rate of formation of X^+ ions is then $\beta n_0 \gamma_1(T)\left[1-\sum_{r=2}^{\infty}\beta_r p_r(T)\right]+\sum_{r=2}^{\infty}\beta\beta_r n_0\gamma_r(T)p_r(T)$. Since β, β_r are small, this is effectively $\beta\gamma_1(T)n_0$.

(*b*) For ionization of X by collision with a particle Y, written $X+Y=X^++Y+e$, the number of reactions per unit volume per unit time is $\rho(T)n_0N$, where n_0, N, denote the densities by numbers of X and Y. This reaction plays only a minor part in the ionization of the cloud.

There are several processes of recombination which tend to balance (*a*) and (*b*).

(*a*) Recombination of an ion and electron with the emission of a photon, $X^++e=X+h\nu$, is the reverse of photo-ionization. The resulting X atom may be excited or in its ground state; if it is excited, it will almost immediately fall to the ground state. If n_+, n_e are the densities of X^+ ions and electrons respectively, the rate of recombination to the rth quantum state of X may be written $\delta_r(T)n_+n_e$, and the total rate of recombination will be $\sum_{r=1}^{\infty}\delta_r(T)n_+n_e=\Delta(T)n_+n_e$, where $\sum_{r=1}^{\infty}\delta_r(T)=\Delta(T)$.

(*a'*) There is also stimulated recombination, written $X^++e+h\nu_1=X+h\nu_2$ which is, however, very infrequent compared with recombination (*a*).

(*b*) Recombination by three-body collision, written $X^++Y+e=X+Y$, is the inverse of thermal ionization; the rate of this reaction may be written σn_+n_eN.

4.32. *The special case of thermodynamical equilibrium.*—These reactions take place in any gas exposed to a field of radiation, but we shall first treat the case of thermodynamical equilibrium. Once more, let the temperature be T, and let n_0, n_+ and n_e be the densities of X atoms, X^+ ions and electrons respectively. As shown by Fowler (**21**) the principle of detailed balancing must hold in thermodynamical equilibrium, that is to say, the rate of decrease in the density of X atoms in the rth quantum state by ionization must equal exactly the rate of recombination of X^+ ions to that state; symbolically,

$$n_0\gamma_r(T)p_r(T)=\delta_r(T)n_+n_e \quad \text{for all } r$$

or

$$\frac{n_+n_e}{n_0}=\frac{\gamma_r(T)p_r(T)}{\delta_r(T)} \quad \text{for all } r.$$

In the case of thermal ionization we find similarly that

$$\frac{n_+n_e}{n_0}=\frac{\rho}{\sigma}.$$

The common value of all these fractions was first found by Saha (**22**), who gave a formula equivalent to

$$\frac{n_+n_e}{n_0}=2W\frac{(2\pi kmT)^{\frac{3}{2}}}{h^3}e^{-\chi/kT},$$

where

W = a weight function for the element X,

m = electronic mass,

k = Boltzmann's constant,

h = Planck's constant.

The values of the $\delta_r(T)$ coefficients have been worked out by means of wave-mechanics by Bates, Massey, Buckingham and Unwin (**23**). An extrapolation of their results gives, for H at 6000 deg. K., that $\delta_1(T)=2{\cdot}4\times10^{-13}$ cm.^{3} and $\Delta(T)=\sum_{r=1}^{\infty}\delta_r(T)=7\times10^{-13}$ cm.^{3}. To find $\gamma_1(T)$, the only one of the γ coefficients which interests us, we note that

$$\frac{n_+n_e}{n_0}=\frac{\gamma_1(T)p_1(T)}{\delta_1(T)}.$$

For $T=6000$ deg. K., $p_1(T)\approx1$, and by using Saha's formula we find that $\gamma_1(T)=1{\cdot}2\times10^{-3}$. $\gamma_1(T)$ and $\Delta(T)$ may also be evaluated for *Na* and *Ca* II. The cross-section at the spectral head has been given by Rudkjøbing (**24**) for the *Na* atom, and by Bates and Massey (**25**) for the *Ca* II ion. By means of the results found by these authors $\gamma_1(T)$ has been calculated in these two cases. $\Delta(T)$ has also been worked out on the assumption that the excited states of both *Na* and *Ca* II are hydrogen-like; in neither case is recombination to the ground state important. The values of $\gamma_1(T)$ and $\Delta(T)$ for $T=6000$ deg. K. are given in Table II.

TABLE II

Ionization and Recombination Coefficients for a Temperature $T=6000$ deg. K.

	Ionization coeff. from *ground* state	Total recombination coefficient	Ratio
	γ_1	Δ (cm.^{3})	γ_1/Δ (cm.$^{-3}$)
H	$1{\cdot}2\times10^{-3}$	7×10^{-13}	$1{\cdot}7\times10^{9}$
Na	$3{\cdot}7\times10$	3×10^{-13}	$1{\cdot}2\times10^{14}$
Ca II	$7{\cdot}4\times10^{-4}$	2×10^{-13}	$3{\cdot}7\times10^{9}$

4·33. *Application to the cloud.*—Although the cloud of corpuscles is far removed from thermodynamical equilibrium, this theory can be applied to it in a modified form. Here photo-ionization is predominant owing to the very low particle densities involved.

Consider a particular group of particles in the cloud, supposed to consist of an element X with only one ionized state, say hydrogen. Let $nx, n(1-x)$ be the densities of X^+ ions and X atoms respectively. If the cloud is electrically neutral, $n_e=nx$. The group is subject to dilute radiation from the Sun, and its equations of ionization are

$$\frac{d}{dt}(nx)=\beta\gamma_1n(1-x)-\Delta n^2x^2-\frac{nx}{V}\frac{dV}{dt}, \tag{1}$$

$$\frac{d}{dt}[n(1-x)]=-\beta\gamma_1n(1-x)+\Delta n^2x^2-\frac{n(1-x)}{V}\frac{dV}{dt}. \tag{2}$$

Here (1) gives the rate of increase of X^+, (2) the rate of increase of X. The terms $\frac{nx}{V}\frac{dV}{dt}$ and $\frac{n(1-x)}{V}\frac{dV}{dt}$ denote the rates of decrease of ion and atom density owing to the cloud's expansion. (1) and (2) may be written

$$x\frac{dn}{dt}+n\frac{dx}{dt}=\beta\gamma_1n(1-x)-\Delta n^2x^2-\frac{nx}{V}\frac{dV}{dt}, \tag{3}$$

$$(1-x)\frac{dn}{dt}-n\frac{dx}{dt}=-\beta\gamma_1n(1-x)+\Delta n^2x^2-\frac{n(1-x)}{V}\frac{dV}{dt}. \tag{4}$$

Multiplication of (3) by $(1-x)$ and (4) by x gives, on subtraction and division by n,

$$\frac{dx}{dt} = \beta\gamma_1(1-x) - \Delta n x^2 . \qquad (5)$$

The treatment is entirely similar when there is a mixture of elements present, each with several possible states of ionization. In this case equation (5) must be written

$$\frac{dx'}{dt} = \beta\gamma_1'(1-x') - \Delta' n_e x' \qquad (6)$$

for every ionized state of each element. Here x', γ_1' and Δ' refer to the element which is being ionized, and each element contributes to n_e, the electron density. In the cloud of corpuscles hydrogen effectively determines n_e, the value of which may hence be found by solving equation (5) on the assumption that the cloud is pure hydrogen. We may then put $n_e = nx$ in (6).

We have now all the data necessary to investigate the ionization of the cloud: the values of γ_1 and Δ are known (Section 4.32), and a very tentative estimate has been adopted for the particle density in the front of the cloud (Section 3.32). We can now determine the progress of the ionization there by solving the equations (5) and (6) and assume similar values to hold elsewhere in the cloud; here an approximate method will be used to find a solution.

To fix the boundary conditions of the problem we note that the initial ionization of the hydrogen is likely to be high, say between 90 per cent and 99 per cent; this will be so because the observed helium emission line of the flare, $\lambda = 6678$ A. ($3^1D \rightarrow 2^1P$), will be succeeded by $\lambda = 584$ A. ($2^1P - 1^1S$), which can ionize hydrogen. According to Ellison $\lambda = 6678$ A. is not at all comparable in strength with $H\alpha$, so that $\lambda = 584$ A. will not be comparable in strength with $L\alpha$, but it will nevertheless cause strong ionization. *Na* and *Ca* II are also known to be ionized to *Na* II and *Ca* III, and we must find out how quickly these elements will recombine in order to ascertain whether the spectral absorption will be observable.

The rate of recombination, $\Delta n x^2$, is proportional to the density of the cloud, so that a dense cloud will recombine more quickly than a tenuous one. Our method will be to find the rate of recombination of the hydrogen, and also its rate of ionization by solar black-body radiation.

The intensity of ionization of the other elements present is then estimated as follows. By equation (6) the ionization of each element tends, at any stage, to the equilibrium given by $n_e x'/(1-x') = \beta\gamma_1'/\Delta'$. This holds also for the hydrogen present, and so

$$\frac{x'}{1-x'} \Big/ \frac{x}{1-x} = \frac{\gamma_1'}{\Delta'} \Big/ \frac{\gamma_1}{\Delta}, \qquad (7)$$

giving x' for the element X.

In a cloud for which the flare's duration, τ_1, is 10^3 secs., or a quarter of an hour (*cf.* Section 3.32), and for which $v_0 = 1{\cdot}6 \times 10^8$ cm./sec., $n_0(t)$, the particle density at the front, is given by $4 \times 10^{k+5}/t^3$, so that the equation of recombination becomes

$$\frac{dx}{dt} = -\Delta n x^2 = -\frac{7 \times 10^{-13} \times 4 \times 10^{k+5}}{t^3} x^2$$

or

$$\frac{dx}{x^2} = -\frac{2{\cdot}8 \times 10^{k-7}}{t^3} dt.$$

On integration we find

$$\frac{1}{x} - \frac{1}{x_1} = 1{\cdot}4 \times 10^{k-7}\left(\frac{1}{\tau_1^2} - \frac{1}{t^2}\right), \tag{8}$$

where x_1, τ_1 refer to the time when the flare ends.

When $t \gg \tau_1$,

$$\frac{1}{x} - \frac{1}{x_1} = \frac{1{\cdot}4 \times 10^{k-7}}{\tau_1^2} = 1{\cdot}4 \times 10^{k-13},$$

since $\tau_1 = 10^3$ secs. For $k = 11$, which corresponds to our estimate of the cloud's density, $\frac{1}{x} - \frac{1}{x_1} \leqslant 1{\cdot}4 \times 10^{-2}$. If $x_1 = 0{\cdot}9$ (90 per cent ionization of H at $t = \tau_1$), $x \geqslant 0{\cdot}89$; if $x_1 = 0{\cdot}99$ (99 per cent ionization), $x \geqslant 0{\cdot}98$. In this case recombination is negligible.

In fact the cloud can never completely recombine, and this sets a lower limit to the ionization of the hydrogen. This limit will, however, be exceeded owing to photo-ionization by solar radiation. The equation of ionization is

$$\frac{dx}{dt} = \beta\gamma_1(1-x) - \Delta n x^2,$$

and as long as the cloud is so highly ionized (i. e. by the flare) that $\Delta n x^2 > \beta\gamma_1(1-x)$ by an appreciable amount, recombination will take place. This will soon cease and the $\beta\gamma_1(1-x)$ term will become important, so that the cloud will tend to reach the state of ionization given by

$$x^2 n/(1-x) = \beta\gamma_1/\Delta. \tag{9}$$

Table III gives the intensity of ionization of the hydrogen at two typical times for clouds of various densities. The initial ionization, x_1, is taken to be 0·9 (assumption I) and 0·99 (assumption II). In every case here given the ionization will be greater at $t = 10^5$ secs. than we should have deduced from the rate of recombination, had we ignored ionization by the Sun as a whole.

TABLE III

Initial ionization assumed	Time after flare (secs.)	Distance from Sun (cm.)	Percentage ionization of hydrogen for $k=11$	$k=12$	$k=13$
I: $x_1=0{\cdot}9$	2×10^3	$3{\cdot}2\times10^{11}$	89·0	80·0	40·0
	$\approx10^5$	$1{\cdot}5\times10^{13}$	99·5	96·0	70·0
II: $x_1=0{\cdot}99$	2×10^3	$3{\cdot}2\times10^{11}$	98·0	87·0	42·0
	$\approx10^5$	$1{\cdot}5\times10^{13}$	99·5	96·0	70·0

The ionization of the sodium and the calcium present in the cloud may now be discussed. For sodium we find

$$\frac{x'}{1-x'} \Big/ \frac{x}{1-x} = \frac{\gamma_1'}{\Delta'} \Big/ \frac{\gamma_1}{\Delta} = 7 \times 10^4 \text{ by Table II.}$$

Even in the rather extreme case of $k = 13$, which is hardly likely to occur, $x \geqslant 0{\cdot}4$ for hydrogen, so that $x/(1-x) \geqslant 0{\cdot}67$ and $x'/(1-x') \geqslant 4{\cdot}7 \times 10^4$, which gives

$1-x' \leqslant 2{\cdot}1 \times 10^{-5}$. Such a high degree of ionization would certainly not leave sufficient sodium in the form of *Na* I to cause any observable anomalous absorption.

Only an inappreciable amount of calcium will be present as *Ca* I, and for the ratio of *Ca* III : *Ca* II we have that $\frac{x'}{1-x'} \Big/ \frac{x}{1-x} = 2{\cdot}2$, by the results of Table II. Table IV gives the percentage of calcium present as *Ca* II.

TABLE IV

Initial ionization of *H* assumed	Time after flare (secs.)	Distance from Sun (cm.)	Percentage of calcium in *Ca* II form $k=11$	$k=12$	$k=13$
I : $x_1=0{\cdot}9$	2×10^3	$3{\cdot}2\times10^{11}$	5·5	10·2	40·7
	$\approx10^5$	$1{\cdot}5\times10^{13}$	0·2	1·9	16·3
II : $x_1=0{\cdot}99$	2×10^3	$3{\cdot}2\times10^{11}$	0·9	6·4	38·7
	$\approx10^5$	$1{\cdot}5\times10^{13}$	0·2	1·9	16·3

4.4. *Which absorption lines are observable?*—Sodium atoms cannot cause detectable absorption after the end of the flare, and the Balmer spectrum of hydrogen may also be rejected. Only hydrogen atoms in the second quantum state can absorb in any Balmer line and, in a gas at 6000 deg. K., 2×10^{-9} of the *H* atoms are in this state, or even less, in the cloud, which is subject merely to dilute solar radiation. This leaves the one possibility of detectable absorption near the H and K lines of *Ca* II.

To be observable the absorption has to be at least 1 per cent deep, and the formulae of Unsöld (**26**) show that this requires 10^{11} *Ca* II ions in a column of one square centimetre cross-section between the Earth and the Sun, capable of absorbing light within one angstrom width. These ions must all lie in a part of the cloud in which the fastest atoms travel $7{\cdot}5\times10^6$ cm./sec. faster than the slowest, since a group of particles with this differential velocity causes an absorption of width $\lambda\times\frac{7{\cdot}5\times10^6}{3\times10^{10}}$ A. = 1 A. for H or K light. When the cloud reaches the Earth, 10^5 secs., after the flare, such a group of particles will have a length of $7{\cdot}5\times10^{11}$ cm., so that a mean density of $1{\cdot}3\times10^{-1}$ *Ca* II ions per c.c. is needed in the stream of particles for detectable absorption during a magnetic storm. Soon after the end of the flare, at $t=2\times10^3$ secs., a band of 1 A. width will be caused by a group of particles $1{\cdot}5\times10^{10}$ cm. long, so that 6·7 *Ca* II ions per c.c. is the density required for 1 per cent depth of absorption then.

Bearing in mind the law of variation of the particle density and using the data in Tables I and IV, we find the densities of *Ca* II ions listed in Table V. These results have been worked out for both Unsöld's (A) and for Strömgren's (B) composition of the solar atmosphere.

TABLE V

Initial ionization of *H* assumed	Time after flare (secs.)	Distance from Sun (cm.)	Density of *Ca* II ions in the cloud (cm.$^{-3}$) Unsöld's composition (A) $k=11$	$k=12$	$k=13$	Strömgren's composition (B) $k=11$	$k=12$	$k=13$
I : $x_1=0{\cdot}9$	2×10^3	$3{\cdot}2\times10^{11}$	$4{\cdot}1\times10^2$	$7{\cdot}7\times10^3$	3×10^5	$4{\cdot}4\times10^{-1}$	8·2	$3{\cdot}2\times10^2$
	10^5	$1{\cdot}5\times10^{13}$	$1{\cdot}2\times10^{-4}$	$1{\cdot}1\times10^{-2}$	$9{\cdot}7\times10^{-1}$	—	—	$1{\cdot}0\times10^{-3}$
II : $x_1=0{\cdot}99$	2×10^3	$3{\cdot}2\times10^{11}$	$7{\cdot}0\times10$	$4{\cdot}9\times10^3$	$2{\cdot}9\times10^5$	$7{\cdot}3\times10^{-2}$	5·0	$3{\cdot}0\times10^2$
	10^5	$1{\cdot}5\times10^{13}$	$1{\cdot}2\times10^{-4}$	$1{\cdot}1\times10^{-2}$	$9{\cdot}7\times10^{-1}$	—	—	$1{\cdot}0\times10^{-3}$

Table VI lists the intensities of absorption which correspond to the densities given in Table V. Values of less than 1 per cent are denoted by a dash.

TABLE VI

Initial ionization of H assumed	Time after flare (secs.)	Distance from Sun (cm.)	Percentage intensity of absorption: Unsöld's composition (A) $k=11$	$k=12$	$k=13$	Strömgren's composition (B) $k=11$	$k=12$	$k=13$
I: $x_1=0{\cdot}9$	2×10^3	$3{\cdot}2\times10^{11}$	46	99+	99+	—	1·2	38
	10^5	$1{\cdot}5\times10^{13}$	—	—	7·5	—	—	—
II: $x_1=0{\cdot}99$	2×10^3	$3{\cdot}2\times10^{11}$	10	99+	99+	—	—	36
	10^5	$1{\cdot}5\times10^{13}$	—	—	7·5	—	—	—

Table VI shows that if Unsöld's composition of the solar atmosphere is correct, then we may expect to find quite definite anomalous absorption in the solar spectrum soon after the end of a flare. Clouds for which $k \geqslant 12$ would absorb so intensely as almost to blot out the region to the violet of the H and K lines. The absorption would rapidly diminish and only remain detectable for very dense clouds ($k \geqslant 13$) on reaching the Earth.

On the other hand, if Strömgren's composition is the right one, and modern astrophysical opinion tends to favour this view, then the anomalous absorption would be detectable early on only for dense clouds, in which $k \geqslant 12$, and would fade out long before the particles reached the Earth.

To obtain 1 per cent absorption due to the cloud during a magnetic storm, as announced (provisionally) by Richardson (**6**) and Brück and Rutllant (**7**), we need a stream whose particle density near the Earth is $1{\cdot}5\times10^3$ per c.c. ($k=12{\cdot}6$) on composition A (Unsöld), or 5×10^5 per c.c. ($k=15{\cdot}1$) on composition B (Strömgren). These values are 40 times and $1{\cdot}3\times10^4$ times the estimate derived from the theory of Chapman and Ferraro. Such dense streams can hardly exist, since they would cause almost complete absorption to the violet of the H and K lines soon after the end of the flare. This has never been observed. Another reason for treating these observations with caution is that both Richardson and Brück and Rutllant found greater average absorption near the H than near the K line; one would expect the opposite, for the K line has twice the oscillator strength of the H line.

5. *Discussion.*—It has been shown that streams of solar corpuscles, thought to be emitted by flares, will cause bands of anomalous absorption to appear in the solar spectrum. In general these bands will lie in an unsuitable part of the spectrum or be too weak to be detectable, but near the H and K lines of *Ca* II there may be observable absorption soon after the end of the flare. The intensity of absorption caused by a cloud of given density will depend on whether the solar atmosphere, and the corpuscular cloud, are constituted according to Unsöld's or to Strömgren's composition. In either case magnetic storms may be produced by streams so tenuous as to escape spectroscopic detection, so that if the anomalous absorption cannot be found, the corpuscular theory will not be disproved. An attempt at observing the streams would, nevertheless, be interesting, since there is a chance of its being successful.

More measurements are also needed of the various Balmer lines of hydrogen in a flare. These, if made simultaneously, would allow the deduction of more details about the unobservable $L\alpha$ emission, a knowledge of which could decide the correctness of Kiepenheuer's expulsion theory, and would be most useful in a study of the behaviour, at the time of a flare, of the Earth's upper atmosphere.

Acknowledgments

I wish to thank Professor S. Chapman for suggesting this problem to me and for much helpful advice, and also Professor H. H. Plaskett and Dr M. A. Ellison, with both of whom I have had most instructive discussions bearing on this paper. I am also indebted to the referees for making a number of most valuable comments.

Balliol College,
Oxford:
1948 *December* 6.
Revised 1949 *February* 25.

References

(1) R. C. Carrington, *M.N.*, **20,** 13, 1859.
(2) H. W. Newton, *M.N.*, **103,** 244, 1943.
(3) H. W. Newton, *M.N.*, **104,** 4, 1944.
(4) S. Chapman and J. Bartels, *Geomagnetism*, Vol. II, Oxford, 1940, Chaps. 24 and 25.
(5) S. Chapman, *M.N.*, **89,** 456, 1929.
(6) R. S. Richardson, *Trans. Amer. Geophys. Union*, p. 558, 1944.
(7) H. A. Brück and F. Rutllant, *M.N.*, **106,** 130, 1946.
(8) M. Waldmeier, *Z. f. Ap.*, **16,** 277, 1938.
(9) M. Waldmeier, *Z. f. Ap.*, **20,** 46, 1940.
(10) R. G. Giovanelli, *Ap. J.*, **91,** 334, 1940.
(11) M. A. Ellison, *M.N.*, **103,** 3, 1943.
(12) M. A. Ellison, *M.N.*, **106,** 500, 1946.
(13) A. Unsöld, *Physik der Sternatmosphären*, Berlin, 1938, p. 82.
(14) B. Strömgren, Festschrift für E. Strömgren, Copenhagen, 1940.
(15) K. O. Kiepenheuer, *Z. f. Ap.*, **15,** 53, 1937.
(16) R. G. Giovanelli, *M.N.*, **108,** 163, 1948.
(17) Report of the Mt. Wilson Observatory, 1947.
(18) A. Unsöld, *Z. f. Ap.*, **24,** 306, 1948.
(19) F. A. Lindemann, *Phil. Mag.*, **38,** 669, 1919.
(20) S. Chapman and V. C. A. Ferraro, *M.N.*, **89,** 470, 1929.
(21) R. H. Fowler, *Statistical Mechanics*, 2nd edition, Cambridge, 1936, Chap. 17.
(22) See A. Unsöld, *Physik der Sternatmosphären*, p. 64.
(23) D. R. Bates, H. S. W. Massey and others, *Proc. Roy. Soc.* A, **170,** 322, 1939.
(24) M. Rudkjøbing, *Meddelølser, København Observatorium*, **18,** 1, 1940.
(25) D. R. Bates and H. S. W. Massey, *Proc. Roy. Soc.* A, **177,** 329, 1941.
(26) A. Unsöld, *Physik der Sternatmosphären*, Chaps. 8 and 9.

THE EMISSION OF RADIATION FROM FLARES

R. G. Giovanelli

(Received 1948 October 18*)

Summary

An extension of recent theories of the emission and absorption of radiation indicates that the temperature in a typical flare is less than 2×10^5 deg. K. and the electron concentration is less than 10^{13} per c.c.

---

1. *Introduction.*—The results of recent investigations (**1, 2, 3**) of the emission and absorption of radiation by hydrogen when the physical conditions depart markedly from those of thermodynamic equilibrium may be applied to the calculation of upper limits to the temperature and electron concentration in a typical chromospheric flare.

The theory that flares are due to electric fields set up by the variation in magnetic flux through a sunspot (**4**) has been developed so far only for a chromosphere in which a considerable fraction of the hydrogen is neutral, so that soon after they acquire sufficient energy, electrons excite neutral atoms by collision. At the same time such collisions would prevent the conductivity for strong electric fields from increasing by a factor of more than three or four over that for a weak electric field. It now seems to be established, however, that the ionization of hydrogen atoms is almost complete in the normal chromosphere (**5**), and in such a case it is relevant to consider (1) how the electron energy varies with the rate of sunspot growth, taking into account the increase of conductivity with electron energy, and (2) whether an increase in electron temperature produces an increase in $H\alpha$ emission; in other words, does the electromagnetic theory of flares remain valid for an almost completely ionized chromosphere? We show here that this is so, although it appears from the discussion that it will eventually be necessary to take into account the Lyman radiation densities within the flare in order to describe the phenomena adequately. In the meantime it is possible to derive upper limits to the temperature and electron concentration in a typical flare.

2. *The Dependence of Electron Energy on the Induced E.M.F.*—Suppose the total e.m.f. around a current-carrying circuit, such as discussed previously, to be V, the resistance of the circuit being divided into a steady part R_1 and the much smaller resistance of the flare R_2. Then the e.m.f. across R_2 is VR_2/R_1. But when collisions occur mainly with protons, the resistivity in the direction of the magnetic field (i.e. along one of the permissible current paths) is proportional to $\theta^{-\frac{3}{2}}$, where θ is the electron temperature (**6**), i.e. to $W^{-\frac{3}{2}}$, where W is the electron energy. Hence the electric field strength, E_2, in the flare may be written as

$$E_2 = E_0(W_0/W)^{\frac{3}{2}}, \qquad (1)$$

where E_0 would be the corresponding field strength if the electron energy remained unchanged by the application of the field and W_0 is the electron energy in the normal chromosphere. E_0 is thus the field expected on the assumption of constant conductivity, as discussed previously (**7**).

* Amended version received 1949 May 14.

The equilibrium electron energy is difficult to compute. Since electrons gain energy from the field more rapidly than do ions, the electron energy will exceed that of the ions. In the case of an almost completely ionized gas, the most important way in which electrons lose energy is probably elastic collision with positive ions. The rate of such loss depends on the ratio of the mean kinetic energy of the ions to the energy of the electrons, and to estimate the electron energy we assume in the following discussion that the energy of the ions remains unchanged. This assumption cannot be strictly valid, but it results in a lower estimate of the electron energy than would any attempt to allow for the increase in ion energy.

The rate of gain of energy by electrons under such conditions is described by equation (2) of an earlier paper (**8**). Making appropriate substitutions, this equation becomes

$$\frac{dW}{dt} = \frac{2^{\frac{3}{2}}E_0^2\epsilon^2 W_0^3}{\pi\beta^2 m^{\frac{3}{2}} N_+ W^{\frac{3}{2}}} - \frac{\pi\beta^2 m^{\frac{3}{2}} N_+}{2^{\frac{1}{2}} M W^{\frac{1}{2}}}\left(1 - \frac{W_+}{W}\right), \tag{2}$$

where ϵ is the electronic charge in e.m.u., m and M are the masses of an electron and a proton respectively, N_+ is the positive ion concentration (and equals N_e, the electron concentration), W_+ is the mean energy of a positive ion (and by assumption equals W_0) and β is a constant equal to $1{\cdot}57 \times 10^9$ cm.^{3} sec.$^{-2}$. After some reduction, the equilibrium energy (obtained by putting $dW/dt = 0$) is found to be given by

$$\frac{W - W_0}{W_0} = \frac{4}{27}\frac{E_0^2}{E_c^2}, \tag{3}$$

where

$$E_c = \frac{\sqrt{3}}{9} \cdot \frac{\pi\beta^2 m^{\frac{3}{2}} N_+}{W_0 \epsilon M^{\frac{1}{2}}}, \tag{4}$$

or $E_c = 2{\cdot}9 \times 10^{-7} N_+$ e.m.u. if W_0 corresponds to a temperature of 3×10^4 deg. K.

The equilibrium energy increases rapidly with E_0 for $E_0 > E_c$. It is clear that even when other energy losses are taken into account, the electron energy is much greater than normal when E_0 much exceeds E_c. Since for $N_+ = 10^{12}$ per c.c., E_c is about 3×10^5 e.m.u., E_0 considerably exceeds E_c during the growth of many spot groups. The condition we have found here for a considerable rise in electron energy is much the same as the condition previously adopted (**4**) for a flare, viz. $E_0 > E_c$.

3. *The Emission of Radiation from a Heated Region of the Chromosphere.*—We now consider the radiation emitted by a region of the chromosphere which is hotter than normal. Suppose we have an ionized hydrogen gas in local thermodynamic equilibrium, so that the distributions of electron and atom kinetic energies are Maxwellian at temperature θ; this will be called the kinetic or gas temperature. As has been shown elsewhere (**3**) the energy radiated per unit area per second into a solid angle $d\Omega$, in a frequency range $d\nu$ near an emission line, from a uniform gas of thickness y may be expressed in the form

$$R_\nu d\nu\, d\Omega = d\nu\, d\Omega P_{\nu,\zeta}[1 - \exp(-\alpha_\nu y)] \tag{5}$$

provided $h\nu/k\zeta \gg 1$, α_ν being the absorption coefficient at a frequency ν and $P_{\nu,\zeta}$ the Planckian function at a temperature, ζ, defined by

$$\exp(-h\nu/k\zeta) = \frac{\sum_j N_j A_{j,l}}{\sum_l (\omega_j N_l A_{j,l}/\omega_l)}. \tag{6}$$

Here N_j is the concentration of atoms in the (upper) j state, $A_{j,l}$ is the Einstein coefficient for spontaneous transition from the j to the (lower) l state and ω_j the statistical weight of the j state, the sums being taken over all states and substates which can contribute to the formation of the line. The temperature, ζ, depends through N_j and N_l on the electron concentration, N_e, the gas temperature and the density of radiant energy. As, however, there is little information about the spectral radiation densities with a flare, and particularly those in the neighbourhood of the Lyman lines, we shall here assume irradiation by 5000 deg. K. black-body radiation and discuss the intensity of $H\alpha$ in flares using effective temperatures as computed elsewhere (**3**) for such conditions; some of these are shown in Fig. 1.

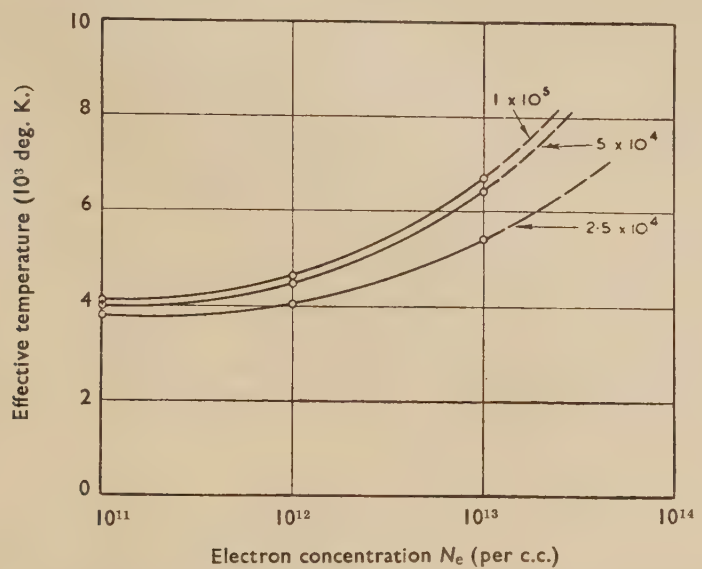

FIG. 1.—*Variation with electron concentration of the effective temperature of hydrogen for the emission of Hα radiation. The three curves are for temperatures as indicated, the gas in all cases being assumed irradiated with 5000 deg. K. black-body radiation.*

An inspection of absorption coefficients at the centre of the $H\alpha$ line, as computed (**3**) for the same conditions of irradiation, indicates that to a rough approximation

$$\alpha \approx 5 \times 10^{-15} N_e^{1\cdot5}/\theta^{2\cdot5} \qquad (7)$$

for the range $10^{11} \leqslant N_e \leqslant 10^{13}$ per c.c., $2\cdot5 \times 10^4 \leqslant \theta \leqslant 1\cdot0 \times 10^5$ deg. K.

A recent discussion (**5**) of all relevant observations has indicated that the electron concentration in the lower chromosphere is given approximately by

$$N_e = 5 \times 10^{11} \exp(-6 \times 10^{-9} z) \text{ per c.c.}, \qquad (8)$$

where z is the height in cm., measured from a level 500 km. above the base of the chromosphere. This equation holds for $0 < z < 2500$ km. There are no observations from which details of the variation of N_e with height in the lowest 500 km. may be deduced, but it is known that N_e is of the order of 10^{13} per c.c. at the base of the chromosphere, so that the mean gradient considerably exceeds 6×10^{-9} per cm. in the lowest 500 km.

From equations (7) and (8)

$$\alpha \gtrsim 1{\cdot}8 \times 10^{3}\theta^{-2{\cdot}5} \exp(-9 \times 10^{-9} z). \qquad (9)$$

Since the kinetic temperature within a flare is considerably greater than that of the normal chromosphere, according to the electromagnetic theory, the pressure is, at least in the initial stages, higher inside than outside the flare. Whether or not the particle concentration is significantly increased within the flare in the initial stages depends on whether the concentration of neutral atoms in the normal chromosphere is comparable with that of the ions. At heights greater than 500 km. above the base of the chromosphere neutral atoms are few. Thus at these elevations the electron concentration remains unchanged during the early stages of a flare, and the initial pressure is proportional to the kinetic temperature.

Suppose a flare involves a sudden increase in kinetic temperature in some region. The sudden increase in pressure produces expansion waves which are propagated along lines of magnetic force at or somewhat faster than the velocity of sound, about $1{\cdot}65 \times 10^{4}\sqrt{\theta}$ cm. per sec. in a completely ionized hydrogen gas. For $\theta = 2{\cdot}5 \times 10^{4}$ deg. K., this velocity is $2{\cdot}6 \times 10^{6}$ cm. per sec. If a flare has linear dimensions of 3×10^{9} cm., then the pressure is reduced to normal in a time of the order of a quarter of an hour, and so for at least a period of some minutes we may assume the density of a flare to remain unchanged.

Suppose the gas temperature θ throughout all the emitting and absorbing regions in and above a flare to be constant, and α to be given by equation (9). Then for the normal electron concentration as given by equation (8), the optical depth at z_1 is

$$\int_{z_1}^{\infty} \alpha \, dz = 2 \times 10^{11}\theta^{-2{\cdot}5} \exp(-9 \times 10^{-9} z_1), \qquad (10)$$

so that the optical depth of a given elevation z_1 decreases as the gas temperature increases. Fig. 1 indicates that the effective temperature for the emission of $H\alpha$ radiation increases with electron concentration, i.e. with depth. To a first approximation the flare radiation at the centre of $H\alpha$ may be assumed to equal that from a black body whose temperature is the effective temperature of the gas at optical depth unity. Table I shows the way in which the electron concentration at optical depth unity (obtained where necessary by extrapolation of equation (8))

TABLE I

Chromosphere Assumed Irradiated by Black Body at Temperature 5×10^{3} *deg. K.*

Gas temperature (deg. K.)	$2{\cdot}5 \times 10^{4}$	$5{\cdot}0 \times 10^{4}$	$1{\cdot}0 \times 10^{5}$	$3{\cdot}0 \times 10^{5}$
Electron concentration at optical depth unity (per c.c.)	$3{\cdot}2 \times 10^{11}$	$1{\cdot}0 \times 10^{12}$	$3{\cdot}2 \times 10^{12}$	$2{\cdot}0 \times 10^{13}$
Effective temperature for the emission of $H\alpha$ (deg. K.)	$3{\cdot}8 \times 10^{3}$	$4{\cdot}5 \times 10^{3}$	$5{\cdot}5 \times 10^{3}$	$7{\cdot}4 \times 10^{3}$

and effective temperature ζ vary with the flare kinetic temperature θ. Since from observation the effective temperature of a typical flare is about 6000 deg. K., we deduce that the kinetic temperature of a typical flare is of the order of 2×10^5 deg. K., and that the flare radiation comes from depths where $N_e \approx 10^{13}$ per c.c., i. e. from the bottom of the chromosphere. Consideration of the greater concentration gradient near the bottom of the chromosphere would have led to increased values of N_e and ζ corresponding to a given θ, so that the estimated kinetic temperature of the flare, for which ζ is known from observation, would be lowered.

We have neglected the effect of irradiation by the radiation (particularly Lyman radiation) emitted by the flare and by the intense Lyman radiation of the normal chromosphere, which increases the $H\alpha$ absorption coefficient and effective temperature of the gas. That this is of importance may be inferred from consideration of those flares which are on occasions seen in prominences; for if the prominence electron concentration were even as high as 10^{11} per c.c., the effective temperature when irradiated by a black body at 5×10^3 deg. K. would be only of the order of those given in line 1, Table II. These effective temperatures

TABLE II

Effective Temperature for the Emission of Hα.
$N_e = 10^{11}$ per c.c.

Irradiation	Gas Temperature (deg. K.) $2{\cdot}5 \times 10^4$	$5{\cdot}0 \times 10^4$	$1{\cdot}0 \times 10^5$
	Effective Temperature		
Black body at 5×10^3 deg. K.	$3{\cdot}8 \times 10^3$	$4{\cdot}0 \times 10^3$	$4{\cdot}1 \times 10^3$
Lα and Lβ corresponding to black body at 10^4 deg. K., together with black-body radiation at 5×10^3 deg. K.	$4{\cdot}7 \times 10^3$		

are much lower than those deduced from observations of flares, so it appears that some other factor must be taken into account. We know, however, that Lyman radiation must be emitted in large quantities by flares, and that the effective temperature for the emission of $H\alpha$ increases with the density of Lyman radiation (see Table II). It is clear that the presence of high-intensity Lyman radiation should be taken into account in attempting to explain the presence of flares, not only in prominences but also in the middle regions of the chromosphere where most flares probably occur.

At this stage we have no quantitative knowledge of the Lyman radiation densities in flares, or even in the normal chromosphere, so that a direct test between theory and observation is not possible. It seems quite likely, however, that satisfactory agreement will be achieved when such information becomes available. In the meantime, the arguments given above on the assumption of irradiation by a black body at 5000 deg. K. have enabled a lower limit to be obtained for the elevation of a typical flare, and upper limits to be put upon the gas temperature and electron concentration.

The work described in this paper was carried out as part of the research programme of the Division of Physics, Council for Scientific and Industrial Research.

Council for Scientific and Industrial Research,
National Standards Laboratory,
Chippendale, Sydney, N.S.W.:
1948 *October* 7.

References

(1) *Aust. J .Sci. Res.*, **1**, 275, 1948.
(2) *Aust. J. Sci. Res.*, **1**, 289, 1948.
(3) *Aust. J. Sci. Res.*, **1**, 305, 1948.
(4) *M.N.*, **108**, 163, 1948.
(5) *Aust. J. Sci. Res.*, **1**, 360, 1948.
(6) T. G. Cowling, *Proc. Roy. Soc.* A, **183**, 453, 1945.
(7) *M.N.*, **107**, 338, 1947.
(8) *Phil. Mag.*, **40**, 206, 1949.

CENTRE-LIMB VARIATIONS OF FRAUNHOFER LINE-BREADTHS AND INTENSITIES

C. W. Allen

(Communicated by the Commonwealth Astronomer)

(Received 1949 January 3)

Summary

Measurements have been made of the breadths, equivalent breadths and central intensities of twenty rather faint blue and violet Fraunhofer lines at various positions on the Sun's disk. The breadths of all fainter lines increase as one approaches the limb. The manner of this variation shows the Sun's reversing layer to be in a state of non-isotropic large-scale turbulence with a vertical velocity of 1·74 km./sec. and a horizontal velocity of 2·79 km./sec.

Measurements show that the equivalent breadths of the faintest lines increase steadily from centre to limb while central intensities are approximately constant. No variation between equatorial limb and polar limb intensities or breadths could be detected.

The breadth of faint Fraunhofer lines is usually ascribed to Doppler broadening associated with thermal and turbulent motions (**1, 2**). Attention has been given mainly to lines at the centre of the solar disk, but if the explanation is to be maintained consistently it must also account for the increase of breadth towards the Sun's limb. The chief aim of the present work was to make an observational study of this point. Observations of equivalent breadths and central intensities are also included.

1. *Observations.*—A step slit method of photometry described elsewhere (**3**) has been employed with the solar tower telescope and three-prism spectrograph of the Commonwealth Observatory. The dispersion was 2·1 mm. per A. at 4200 A. and 1·5 mm. per A. at 4600 A., while the linear magnification of the microphotometer was 6·8. The measurements made on each line were (*a*) Δ_m, the measured whole breadth of the line at half its uncorrected maximum depth, and (*b*) r_m, the uncorrected central intensity relative to the continuum. From Δ_m and r_m we derive the corrected breadth Δ_c and corrected central intensity r_c by applying an instrumental correction, and the equivalent breadth W from the relation $W = p\Delta_m(1 - r_m)$, where p is a constant between 1·06 and 1·57.

Freedom from blending was the main consideration in choosing the lines which are in two groups near 4200 A. and 4600 A. Very faint lines would be preferred for our purpose, but in order to maintain reasonable accuracy most of the lines chosen are about 0 on the Rowland scale. Some stronger lines are measured for comparison.

The observations were completed in 1940 but have been analysed more recently.

2. *Determination of Δ_c, W and r_c.*—In the present work we are more interested in the changes of breadths and equivalent breadths across the Sun's disk than in their absolute values. Consequently we have avoided the elaborate technique

of determining the instrumental profile directly. Instead we chose an instrumental profile to fit earlier observations as well as possible, and then used this to determine the true variations from the apparent variations.

Van de Hulst's method of expressing each broadening factor as a Voigt profile (**4**) is very well suited to our purpose. He shows that if the broadening factors contain components g of the Gaussian type (no wings) then the total broadening of this type is represented by $G=(g^2+\dots)^{\frac{1}{2}}$, while if they contain components d of the dispersion type (extended wings) the total broadening of this type is $D=(d+\dots)$. Another relation that appears in his paper is also well worth using, although it introduces inaccuracies of the order of 1 per cent. In his Fig. 1 it is noticed that the curves of constant width are nearly linear. Approximating them to a linear relation, we have

$$\left.\begin{aligned} \frac{2{\cdot}80G^2}{B^2}+\frac{2D}{B}&=1 \\ \text{or}\qquad B^2&=2BD+2{\cdot}80G^2, \end{aligned}\right\} \qquad (1)$$

where B is the whole breadth. It is easily seen that for a purely dispersion type of broadening $B=2D$, and for a purely Gaussian type $B=1{\cdot}67G=2(ln2)^{\frac{1}{2}}G$. This defines D and G in the usual way. In our case Δ_m gives a measure of B, thermal and turbulent Doppler broadenings give factors of the Gaussian type and the instrumental broadening and the Fraunhofer abundance broadening can be represented by mixed Voigt profiles. The instrumental profile can be taken as the remainder, after Doppler broadenings for the narrowest faint lines have been subtracted from the measured broadening in accordance with van de Hulst's ideas.

To determine equivalent breadths W, we use the relation $W=p\Delta_m(1-r_m)$, where p varies from 1·06 for a Gaussian profile to 1·57 for a dispersion profile. The values of p for other Voigt profiles depend on D/G and can be found from the tabulations (**5**). For stronger lines, p may be measured directly and, for this spectrograph, in the violet (**3**) is 1·15. This value has been used for the determination of W.

The corrected central intensity r_c can be determined from the measured value r_m by the use of an instrumental correction curve (**1**) relating $(1-r_m)/(1-r_c)$ to Δ_m. The curves actually used had been prepared earlier (**3**). However, we have approximately

$$W=p\Delta_m(1-r_m)=p\Delta_c(1-r_c)$$

and

$$(1-r_m)/(1-r_c)=\Delta_c/\Delta_m. \qquad (2)$$

This relation used with the Δ_c and Δ_m of the next section also defines a correction curve which agrees satisfactorily with the one actually used.

3. *Centre-Limb Variations of Breadth.*—For all observed lines there is an increase of measured breadth Δ_m with distance from the Sun's centre, and with the exception of the strongest line 4210·37 A. the increase continues to the limit of the observations at $\cos\theta=0{\cdot}13$ (θ is the angle between the Sun's radius and the line of sight). An increase of breadth from centre to limb can be seen also in the results published by ten Bruggencate and Houtgast (**6**) and by Adam (**7**), and without doubt these results are typical of all fainter Fraunhofer lines.

A corresponding variation must occur in the true breadth Δ_c. To apply the corrections outlined in Section 2 we need to know both Δ_c and Δ_m for some lines and also d/g for the instrumental profile. We then have enough factors to solve

(1). Fortunately our results are not at all sensitive to the choice of d/g which defines the precise shape of the instrumental profile and is not strictly known. We have used $d/g = 0{\cdot}6$ which is the practical instrumental value in van de Hulst's paper (**4**). Δ_c will be defined by Doppler effect alone for the narrowest faint lines, then

$$\Delta_c = \frac{1{\cdot}67\lambda}{c}\left(\frac{2RT}{M} + v_t^2\right)^{\frac{1}{2}} = 1{\cdot}67\lambda v_d/c. \qquad (3)$$

Here Δ_c is in wave-length units, λ is the wave-length, $2RT/M$ the usual expression for thermal motion, c the velocity of light, v_t the most probable turbulent velocity and v_d the most probable velocity due to both turbulent and thermal motion. Four independent values obtained for v_t are 1·0 to 1·5 km./sec. (Redman (**8**)), 1·5 to 1·8 km./sec. (Allen (**1**)), 1·8 km./sec. (ten Bruggencate (**2**)), and 1·74 km./sec. (van de Hulst (**4**)). We use 1·74 km./sec. for this value and 1·41 km./sec. for $(2RT/M)^{\frac{1}{2}}$. With these data for narrow faint lines we can solve (1) to obtain d and g for the instrumental contour, and the results may then be used in (1) again for correcting other lines and other positions in the Sun's disk. We need to know the character of the true Fraunhofer profiles, but these are essentially Gaussian for all but the strongest line measured. No important error is introduced by regarding them all as Gaussian.

The values of Δ_c for the stronger lines are found to increase towards the limb in a manner that is approximately linear in $\cos\theta$ in the range 1·0 to 0·3. The values at the centre ($\cos\theta = 1{\cdot}0$) and the limb ($\cos\theta = 0{\cdot}3$) have been extracted from graphs and are given in Table I. The values of Δ_c continue to increase linearly beyond $\cos\theta = 0{\cdot}3$ to $\cos\theta = 0{\cdot}13$ for all lines except 4210·37 A., in which case there is a maximum Δ_c at $\cos\theta = 0{\cdot}3$.

TABLE I

Breadths (Δ_c), equivalent breadths (W), and central intensities (r_c) at the centre and limb of the Sun

Wave-length	El.	E.P.	Centre Δ_c mA.	Centre $10^6 W/\lambda$	Centre r_c per cent	Limb Δ_c mA.	Limb $10^6 W/\lambda$	Limb r_c per cent	Limb / Centre W
4159·648	Ti	2·1	68	3·5	81	82	4·4	81	1·26
4179·819	Zr^+	1·7	48	3·2	78	70	4·5	76	1·40
4202·762	Fe		65	13·7	28	99	17·4	35	1·27
4207·135	Fe	2·8	79	19·6	13	102	22·7	21	1·16
4207·409	CN		106	15·3	47	121	17·4	47	1·14
4207·825			58	5·8	67	73	7·1	67	1·22
4208·987	Zr^+	0·7	57	10·5	39	79	12·8	44	1·22
4210·37	Fe	2·5	166	43·0	4	186	45·5	9	1·06
4210·970	CH		130	24·8	31	158	27·3	38	1·10
4220·053	V^+	1·7	72	10·9	49	90	12·6	52	1·16
4220·349	Fe		78	19·5	15	99	22·0	23	1·13
4578·562	Ca	2·5	90	17·7	17	111	19·1	27	1·08
4579·340	Fe	2·8	58	5·3	64	82	7·2	64	1·36
4583·417	—Ti^+	1·2	59	6·3	58	80	7·8	59	1·24
4585·348			59	3·7	75	77	4·6	76	1·24
4588·206	Cr^+	4·0	82	15·3	24	100	15·5	36	1·02
4588·687	Co ?	0·4	69	3·1	82	89	4·1	81	1·32
4589·955	Ti^+	1·2	85	17·6	15	108	19·3	26	1·10
4593·184			64	1·8	89	77	2·5	87	1·39
4593·535			55	5·3	63	78	6·8	65	1·26

Particular interest is centred in the variation of Δ_c for faint lines, since in this case the breadth change must be due to an effective change in v_d. To increase accuracy, four faint violet lines and six faint blue lines have been grouped together, and the mean values have been reduced slightly in order to represent the breadth of the narrowest lines. The measurements have been converted into terms of v_d by (3) and are plotted against $\cos\theta$ in Fig. 1.

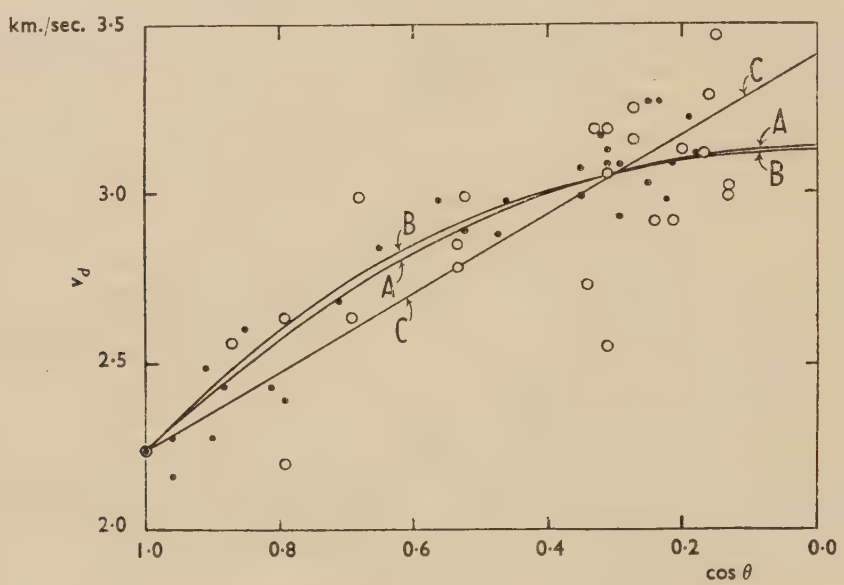

FIG. 1.—*Relation between Doppler broadening velocity and position on Sun's disk.*
○ *Violet lines.* ● *Blue lines.*
Empirical curves (*A*) $v_d = 3{\cdot}14 - 0{\cdot}90\cos^2\theta$ *km./sec.*
(*B*) $v_d^2 = 9{\cdot}8 - 4{\cdot}8\cos^2\theta$ „ „
(*C*) $v_d = 3{\cdot}40 - 1{\cdot}16\cos\theta$ „ „

They are fitted empirically to the expressions

$$v_d = 3{\cdot}14 - 0{\cdot}90\cos^2\theta \text{ km./sec.}, \qquad (4A)$$

$$v_d^2 = 9{\cdot}8 - 4{\cdot}8\cos^2\theta \text{ km./sec.} \qquad (4B)$$

and

$$v_d = 3{\cdot}40 - 1{\cdot}16\cos\theta \text{ km./sec.} \qquad (4C)$$

but do not fit the linear relation (4C) as well as (4A) and (4B).

4. *Variation of Turbulence with* θ.—We have now to determine whether this result is in agreement with any reasonable hypothesis concerning the nature of the Sun's turbulence. There are two possibilities to be examined: (*a*) the reversing layer turbulence is non-isotropic with a horizontal velocity greater than the vertical, and (*b*) the velocity of the turbulence increases with height in the solar atmosphere.

Consider first the case of non-isotropic turbulence. Let the probability that the components of the turbulent velocity lie between u and $u+du$, v and $v+dv$ and w and $w+dw$ (where u and v represent the horizontal components and w the vertical component) be

$$\frac{1}{m^2 n \pi^{\frac{3}{2}}} \exp\left[-\left(\frac{u^2}{m^2} + \frac{v^2}{m^2} + \frac{w^2}{n^2}\right)\right],$$

where the root mean square of the horizontal and vertical velocity components are $m/\sqrt{2}$ and $n/\sqrt{2}$ respectively. Any non-isotropic turbulence found in practice is not likely to deviate seriously from this form. In order to compute the form of a spectrum line viewed at an angle θ from the axis of w it is necessary to determine the probabilities of the various velocities in that direction. Transforming to the coordinates x, y and z, where

$$\begin{aligned} x &= \quad w\cos\theta + u\sin\theta, \\ y &= -w\sin\theta + u\cos\theta, \\ z &= \quad v, \end{aligned}$$

we find the probability of a velocity with components between x and $x+dx$, y and $y+dy$ and z and $z+dz$ is

$$\frac{1}{m^2 n\pi^{\frac{3}{2}}} \exp\left[-\left(\frac{x\sin\theta + y\cos\theta}{m}\right)^2 - \frac{z^2}{m^2} - \left(\frac{x\cos\theta - y\sin\theta}{n}\right)^2\right].$$

Integrating over y and z one finds the total probability of a velocity within the range x to $x+dx$ is

$$\pi^{-\frac{1}{2}}(n^2\cos^2\theta + m^2\sin^2\theta)^{-\frac{1}{2}} \exp\left[-\frac{x^2}{n^2\cos^2\theta + m^2\sin^2\theta}\right],$$

which is a Gaussian distribution again with a velocity of $(n^2\cos^2\theta + m^2\sin^2\theta)^{\frac{1}{2}}$ replacing m and n. Combining this with the thermal velocity we get a Doppler broadening velocity

$$\begin{aligned} v_d &= (2RT/M + n^2\cos^2\theta + m^2\sin^2\theta)^{\frac{1}{2}} \\ &= (2RT/M + m^2 - (m^2 - n^2)\cos^2\theta)^{\frac{1}{2}}. \end{aligned}$$

This agrees with the empirical curve (4B) when

$$\begin{aligned} (2RT/M)^{\frac{1}{2}} &= 1{\cdot}41 \text{ km./sec.}, \\ m &= 2{\cdot}79 \text{ km./sec.}, \\ n &= 1{\cdot}74 \text{ km./sec.} \end{aligned}$$

The observations are therefore in good agreement with the requirements of non-isotropic turbulence with a horizontal velocity of 2·79 km./sec. and a vertical velocity of 1·74 km./sec.

Consider next the case when the extra broadening towards the limb is due to increase of Doppler velocity with height in the Sun's atmosphere. Suppose the Doppler broadening (combined thermal and turbulent) were related to the optical depth τ by the expression

$$v_d = (2RT/M + v_t)^{\frac{1}{2}} = a + b\tau^q, \tag{5}$$

where a would be the value at the limb. A Fraunhofer line can be considered as being formed at an optical depth $\cos\theta$, and the observed Fraunhofer line-breadths would fit the relation

$$v_d = a + b(\cos\theta)^q. \tag{6}$$

Comparing this with the observed empirical expression (4A) we obtain $a = 3{\cdot}14$ km./sec., $q = 2$ and $b = -0{\cdot}90$ km./sec. The relation between Doppler velocity and depth becomes

$$v_d = 3{\cdot}14 - 0{\cdot}90\tau^2.$$

This represents a most improbable relation between v_d and depth. It implies constancy of turbulence in the chromosphere and higher reversing layer and a rapid downwards decrease in the lower reversing layer. The first is violated

by the high turbulence of the chromosphere and the second by the existence of a layer of instability not far below the reversing layer. Any other empirical expression for v_d such as $v_d = 1/(a + b\tau)$, when fitted to Fig. 1, leads to a similar improbable result. Furthermore, if the contributions from the different depths of the reversing layer are averaged from a weighting function of exponential form $g = \exp(-\tau/0{\cdot}7 \cos\theta)$ (after the manner of the analyses of Unsöld (**9**) and Minnaert (**10**)) the result from (5) with $q = 2$ reproduces (6) again and we see that the simplification of the argument has not affected the result. Change of turbulence with depth is thus unlikely to be a major factor in explaining the observed breadth variation.

We therefore conclude that the Sun's atmosphere is in a state of non-isotropic turbulence with greater horizontal than vertical velocity. This conclusion is supported by Evershed's observation (**11**) that small Fraunhofer line displacements could be detected on the Sun's disk away from the centre but not at the centre of the Sun.

On the other hand, ten Bruggencate and Houtgast have found that the turbulence derived from the curve of growth is isotropic (**6**). The two results, however, are not contradictory if the turbulence causing the line broadening is of a large-scale character (**1, 12**). In that case the lines are displaced by Doppler movements without influencing the equivalent breadths. There is good reason for supposing the turbulence to be associated with the granulation cells which are larger than the depth of the reversing layer. The large-scale character of the turbulence is thus supported from several points of view.

5. *Centre-Limb Variation of Equivalent Breadths.*—The centre-limb variations of equivalent breadth are plotted in Fig. 2, where we have used the convenient unit $10^6 W/\lambda$ (W is in wave-length units and λ is the wave-length). For faint lines there is an increase of equivalent breadth towards the limb which appears to be approximately linear in $\cos\theta$ over the range of the observations. For stronger lines ($10 < 10^6 W/\lambda < 30$) there is a maximum at $\cos\theta = 0{\cdot}3$ and the variation is linear in the range $\cos\theta = 1{\cdot}0$ to $0{\cdot}3$. For still stronger lines (**13**) (only one measured here) the maximum may fall earlier, or there may be a decrease of W over the whole range of θ.

The sharp decrease of W close to the limb makes the extreme limb unsuitable for centre-limb comparison. Consequently the limb distance represented by $\cos\theta = 0{\cdot}3$ is selected for this purpose. The values of $10^6 W/\lambda$ at the centre of the Sun and the limb at $\cos\theta = 0{\cdot}3$ are given in Table I, which also contains the limb/centre ratio of the equivalent breadths. The limb/centre ratio has been plotted against the central value of $10^6 W/\lambda$ in Fig. 3.

Fig. 3 contains also some measurements of the limb/centre ratio made by Adam (**7**) and Nicholson (**14**). All agree in showing the faint line limb values to be some 40 per cent greater than the central values. In the violet and blue regions the high limb-centre ratio extends to greater values of W (or W/λ) than in the green and yellow. The observations and those of Adam and Nicholson in the green and yellow have been averaged into the curves which are shown and which are in good agreement with one another. The values at 4100 A. taken from Adam's paper refer to the actual measurements of equivalent breadths, since her values, taken from the measurements of central intensity alone, do not allow for the observable increase of breadth from centre to limb. The blue and violet observations of Adam and myself are also in reasonably good agreement, and give together

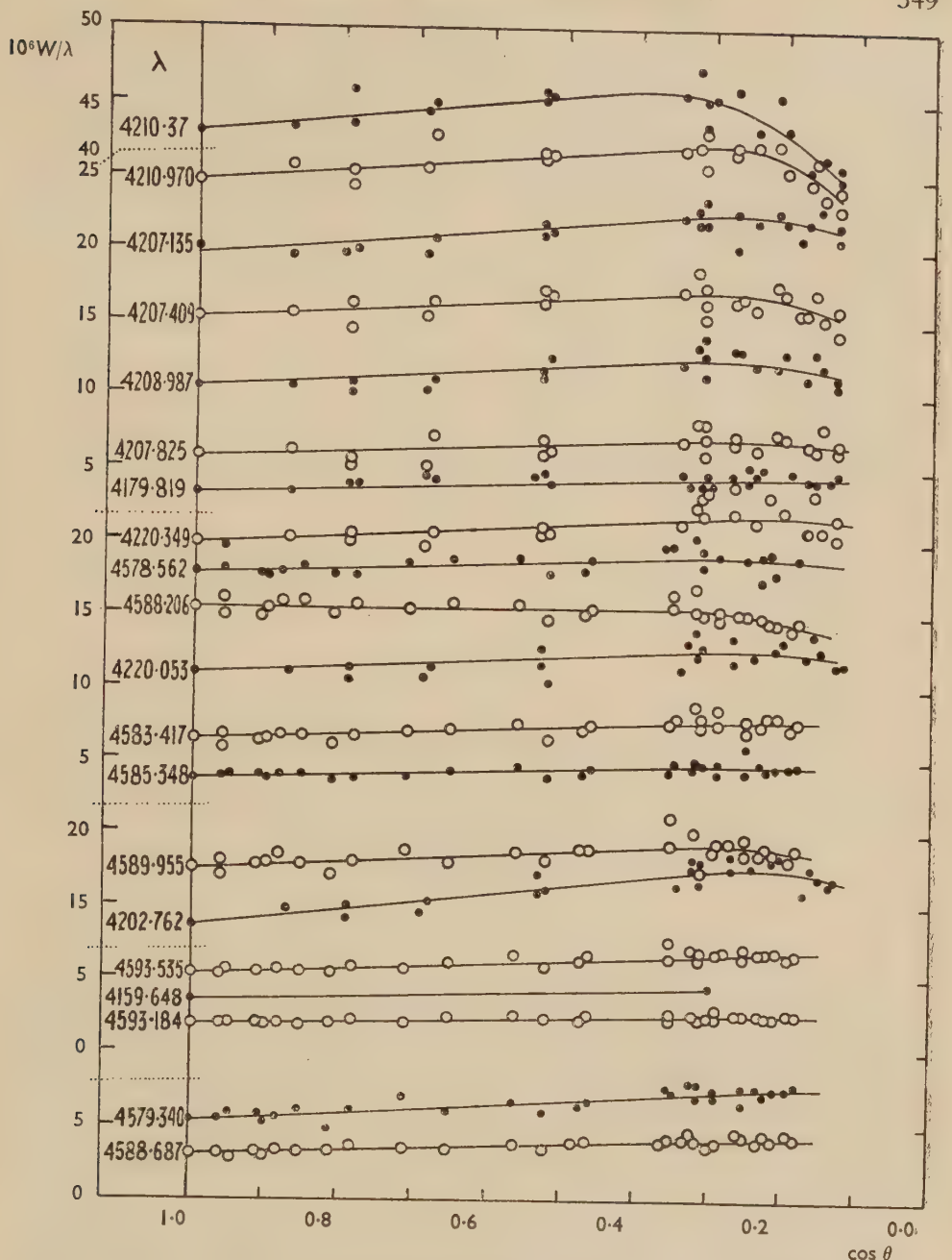

FIG. 2.—*Relation between equivalent breadth and position on the Sun's disk.*

strong evidence that there is a real difference between the blue-violet and yellow-green regions of the spectrum. If this change is associated with limb darkening, Houtgast's curves (**13**) (his Fig. 41) would suggest that line absorption was more effective than line scattering and that the ratio of line/continuous absorption was greater in the higher layers.

6. *Central Intensities.*—The instrumental corrections can be used to obtain the true central intensities r_c as explained in Section 2. Corrected central

intensities have been plotted against $\cos\theta$ and values for $\cos\theta$ equal to 1·0 and 0·3 obtained from such graphs are given in Table I. It can be seen that for weak lines ($10^6 W/\lambda < 10$) there is no appreciable change of central intensity with $\cos\theta$. There is actually a change in r_m but it is offset by the change in the correction. For the stronger lines there is an increase of r_c as one approaches the limb. The increase is approximately linear in $\cos\theta$ from 1·0 to 0·3, and nearer the limb becomes more rapid.

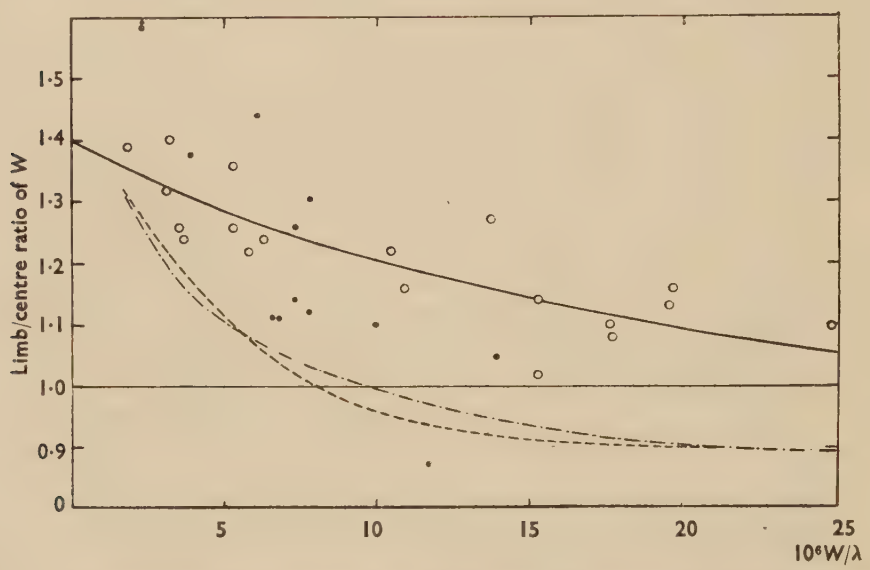

FIG. 3.—*The limb/centre ratio of equivalent breadth as a function of equivalent breadth at the centre.*

———○ *Allen* (4200 A. *and* 4600 A.).
● *Adam* (4100 A.).
– – – – – – – *Adam* (5100 A.).
— · — · — · *Nicholson* (5700 A.).

7. *Equatorial and Polar Limb Intensities.*—Observations by Abetti and Castelli (**15**) have led them to the conclusion that there are observable differences of Fraunhofer line intensities between the equatorial limb and the polar limb in the sense that the equatorial lines are weaker (both being much weaker than the lines from the centre of the disk). If this be true it is important in all centre-limb studies to be sure that observations are made at a specified solar latitude. The mounting of the Commonwealth Observatory Sun telescope makes this inconvenient and hence some investigation of the equator-pole variation was necessary. Plates of the region near 4200 A. were obtained on five different days during sunspot maximum. Active regions were avoided. At the time the Sun's equator was inclined at about 45° to the spectrograph slit. The Sun's image (of 12·5 cm. diameter) was projected on a screen and adjusted so that a hole in the screen in front of the slit was set 2·1 mm. from the limb (i. e. $\cos\theta = 0{\cdot}26$).

Table II gives the mean observed central intensities r_m of 16 lines for the centre of the disk and the equatorial and polar limbs. Each column represents the mean of 10 spectra and no significant difference between pole and equator can be found. Moreover the mean values of Δ_m for 9 lines were 1·84 mm. (on trace) for polar lines and 1·85 mm. for equatorial lines.

TABLE II

Values of r_m for the Sun's centre and for the equatorial and polar limbs

Wave-length	Centre	Equator	Pole	Wave-length	Centre	Equator	Pole
4200·455	0·598	0·597	0·600	4208·987	0·505	0·535	0·537
4200·934	0·248	0·319	0·312	4210·37	0·132	0·177	0·175
4202·042	0·085	0·115	0·115	4210·970	0·386	0·460	0·455
4202·762	0·406	0·452	0·452	4211·891	0·448	0·490	0·484
4205·546	0·302	0·373	0·373	4215·545	0·087	0·120	0·120
4207·135	0·267	0·325	0·327	4216·193	0·161	0·188	0·186
4207·409	0·542	0·559	0·555	4220·053	0·569	0·589	0·583
4207·825	0·734	0·727	0·732	4220·349	0·280	0·335	0·332

Since there is no difference in either r_m or Δ_m it is evident that there is also no difference in Δ_c, W or r_c, and we are justified in neglecting solar latitude in the present work.

Commonwealth Observatory,
Mount Stromlo, Canberra :
1948 *December* 24.

References

(1) C. W. Allen, *Ap. J.*, **85,** 165, 1937.
(2) P. ten Bruggencate, *Zs. f. Astrophys.*, **18,** 316, 1939.
(3) C. W. Allen, *Mem. Com. Sol. Obs. Canberra*, Nos. 5 and 6, 1934 and 1938.
(4) H. C. van de Hulst, *B.A.N.*, **10,** 79, 1946.
(5) M. W. Zemansky, *Phys. Rev.*, **36,** 219, 1930; F. Hjerting, *Ap. J.*, **88,** 508, 1938; H. C. van de Hulst and J. J. M. Reesinck, *Ap. J.*, **106,** 121, 1947.
(6) P. ten Bruggencate and J. Houtgast, *Zs. f. Astrophys.*, **20,** 149, 1940.
(7) M. G. Adam, *M.N.*, **98,** 112, 1937 ; **100,** 595, 1940.
(8) R. O. Redman, *M.N.*, **97,** 552, 1937.
(9) A. Unsöld, *Zs. f. Astrophys.*, **4,** 339, 1932.
(10) M. Minnaert, *B.A.N.*, **10,** 339, 1948.
(11) J. Evershed, *M.N.*, **94,** 96, 1934.
(12) This suggestion was made in conversation by L. Spitzer.
(13) J. Houtgast, "Variations in the profiles of strong Fraunhofer lines along a radius of the solar disc", Utrecht dissertation, 1942.
(14) The curve was extracted from unpublished observations kindly sent to me by Dr S. B. Nicholson.
(15) G. Abetti and I. Castelli, *Oss. e. Mem. R.O.A. Arcetri*, **13,** 27, 1935.

THE DAYTIME METEOR STREAMS OF 1948—I

Measurement of the Activity and Radiant Positions

A. Aspinall, J. A. Clegg and *A. C. B. Lovell*

(Communicated by A. C. B. Lovell)

(Received 1949 April 1)

Summary

The series of meteor streams incident on the sunlit side of the Earth between May and August, which were first studied in detail by the radio echo method during 1947, appear to be a recurrent phenomenon. Their radiant points lie in a narrow strip of the celestial sphere, situated somewhat to the north of the ecliptic, and extending from 330° to 120° in right ascension. They are unusually rich, giving hourly rates comparable with those of the Perseids and Geminids, and on many occasions two or three of these showers are active at the same time. In addition to confirming the 1947 observations during May and June, the work during 1948 led to the discovery of four further major showers in July and early August.

---

1. *Introduction.*—During the summer months of 1947 the radio echo observations of meteors led to the discovery of a hitherto unknown group of meteor streams falling on the sunlit side of the Earth.* Six major streams closely grouped in right ascension and declination, lying close to the ecliptic, were found in 1947 May and June. Although the daytime activity continued throughout 1947 July and August, the observational difficulties prevented the accurate delineation of further radiants. By comparison with the activity found in the summer of 1946 † it seemed possible that these streams were recurrent. This was found to be the case ‡ and in the present paper details are given of the 1948 observations covering the period 1948 May to August, and the results are compared with those for the same period in 1947.

2. *Technique.*—The essential features of the technique have been described previously. § In 1947 all observations were made visually from a cathode-ray tube display. In 1948 these visual observations were supplemented by photographic recording, using either the automatic recorder developed by Ellyett and Davies || or the moving-film method of the type described by Hey, Parsons and Stewart. ¶ The wave-length used for the investigation was 4·2 m. on which the main radio echo is obtained only when the meteor crosses the perpendicular from the receiving station to the direction of the trail.** This aspect property enables

* A. C. B. Lovell, *B.A.A. Circulars*, Nos. 282, 285, 1947. J. A. Clegg, V. A. Hughes and A. C. B. Lovell, *M.N.*, **107**, 369, 1947.

† J. P. M. Prentice, A. C. B. Lovell and C. J. Banwell, *M.N.*, **107**, 155, 1947.

‡ A full account of the observations during 1948 May has been given by J. A. Clegg, (*J.B.A.A.*, **58**, 271, 1948) and summaries of later results by A. C. B. Lovell, *B.A.A. Circulars*, Nos. 300, 305, 1948.

§ J. P. M. Prentice, A. C. B. Lovell and C. J. Banwell, *loc. cit.* A. C. B. Lovell, C. J. Banwell and J. A. Clegg, *M.N.*, **107**, 164, 1947.

|| C. D. Ellyett and J. G. Davies, *Nature*, **161**, 596, 1948. J. G. Davies and C. D. Ellyett, *Phil. Mag.*, **40**, 614, 1949.

¶ J. S. Hey, S. J. Parsons and G. S. Stewart, *M.N.*, **107**, 176, 1947.

** A. C. B. Lovell, C. J. Banwell and J. A. Clegg, *loc. cit.*

the coordinates of the meteor radiants to be determined from observations of the range and time of occurrence of the radio echoes as described by Clegg.* It has been demonstrated previously that on this apparatus the rate of occurrence of the radio echoes is closely related to the number of meteors seen by a visual observer under favourable conditions.†

3. *The development and radiants of the* 1948 *daytime streams.*—For each day the observational material consists of the measurement of the range and time of occurrence of the radio echoes with the directional aerial maintained on a constant bearing. A summary of the observations and the results of the delineation of the principal radiants for each day from 1948 May 1 to August 4 are given in Table I.

TABLE I

Date 1948		Limits of Observation (U.T.)		Number of Hours	Number of Echoes	Principal Radiants ($\alpha \pm \delta$)			
		h m	h m					C	C¹
May	1	10 15	13 00	2·8	36			19+20	
	2	09 10	13 45	4·5	58			19+20	30+20
	4	09 00	12 00	3·0	55	A	B		
	5	06 20	12 00	5·7	63	335±0	353	21+22	34+20
	8	05 00	11 30	6·5	32	337±0	354	22+22	
	9	10 00	14 30	4·5	38				
	10	08 40	13 00	4·2	43			24+22	34+20
	11	08 50	12 15	3·5	36		353		35+20
	13	09 05	11 50	2·8	41			26+24	36+20
	14	10 00	12 40	2·7	12			27+24	36+21
	16	09 05	13 30	4·3	35			28+24	36+21
	17	09 15	13 30	4·2	45			31+25	
	18	09 53	11 53	2·0	15			33+25	
	19	09 00	13 00	4·0	53		367	33+25	
	20	10 28	12 00	1·7	15			34+25	
	21	08 30	10 46	2·2	17				
	24	08 36	12 06	3·5	26	H		D	D¹
	25	08 59	13 00	4·0	85	27+20		41+25	57+27
	26	09 20	12 00	2·7	47	28+23		41+27	58+30
	27	10 54	11 58	1·1	8			43+27	
	28	08 35	13 17	4·7	51			44+27	
	30	09 10	14 00	5·0	63	32+23		45+29	61+32
	31	09 08	13 00	3·9	52				63+30
June	1	08 45	13 00	4·3	86	34+23		48+29	64+34
	2	09 17	13 46	4·5	116			48+29	
	3	10 30	13 00	2·5	39	36+25		49+29	65+30
	4	08 30	13 16	5·0	145	38+22		50+30	
	5	09 26	13 40	4·3	59	39+22		51+29	66+31
	6	09 40	13 38	4·0	50			52+29	66+31
	7	09 10	11 40	2·5	67			52+27	
	8	09 00	13 10	4·1	83	40+22		54+28	
	9	08 00	13 00	5·0	170			53+28	69+37
	10	09 25	13 05	3·7	26	43+22			
	11	08 50	11 30	2·8	108	44+22		52+28	
	12	09 50	10 50	1·0	72				
	13	10 40	14 15	3·6	43			54+27	74+33
	14	09 00	13 00	4·0	61			55+27	75+33
	16	06 00	12 15	6·3	230				76+33

* J. A. Clegg, *Phil. Mag.*, **39**, 577, 1948.
† J. A. Clegg, V. A. Hughes and A. C. B. Lovell, *loc. cit.*

Date 1948	Limits of Observation (U.T.)		Number of Hours	Number of Echoes	Principal Radiants ($\alpha \pm \delta$)			
	h m	h m						
June 17	08 47	13 00	4·2	63				
18	09 45	14 00	4·3	72				
20	11 44	14 00	2·2	27		F		
21	09 55	13 00	3·0	74		68+30		
22	09 35	13 22	3·7	76		68+30		
								G
23	09 10	13 06	3·9	31				86+26
24	09 22	11 12	1·8	51		68+33		
25	08 34	12 35	4·0	94		69+30		
27	08 47	12 06	3·2	99		71+34		
28	08 56	12 30	3·5	120		72+34		90+26
29	08 47	13 50	5·0	86		72+34		91+28
30	08 35	12 46	3·6	21				92+26
July 2	09 32	12 12	2·8	34				94+26
4	09 03	16 31	7·5	68				96+26
5	08 30	14 00	5·5	73				
6	09 00	13 51	4·9	38				
8	09 00	13 00	4·0	38				
11	09 22	14 30	5·2	26	J	K		L
12	08 45	14 30	5·8	81	85+11	96+21		108+15
13	08 40	14 30	5·8	69	86+11	97+21		109+15
14	09 10	13 10	4·0	41	87+11	98+21		111+15
15	08 44	13 40	4·8	48	88+13	99+21		
16	08 30	13 30	5·0	29				
17	) 13	12 00	2·8	51	88+13	100+21		113+15
18	09 20	13 30	4·2	55				
19	08 30	13 30	5·0	33				
20	07 45	09 30	1·7	18				
21	09 30	13 52	4·4	9				
22	07 00	11 50	2·6	41	M			
23	10 00	13 20	3·3	72	80+39			
24	08 37	17 00	7·3	67	81+39			
25	09 00	12 05	2·9	49	82+39			
26	08 25	13 01	4·6	69	84+38			
27	08 38	15 00	6·0	55	85+38			
28	08 38	14 30	5·9	88	87+38			
29	08 38	14 30	6·0	24	86+38			
30	08 52	14 30	5·7	86	87+38			
Aug. 1	06 00	14 30	8·5	46	89+38			
3	06 00	14 20	8·3	69	90+38			
4	06 00	14 45	8·5	75	91+38			
		Total	329·5	4437				

Colums 2, 3 and 4 of this table give the limits and duration of observation and the total numbers of echoes observed, and column 5 the principal radiants determined. The main radiants are plotted on a Mercator projection of the heavens in Fig. 1 and are discussed individually below. The notation of the showers (A, B, C...) is consistent with the notation used in Table II and Fig. 4 of the previous paper.*

(a) *The activity during* 1948 *May–June.*—The η-Aquarids (A), Piscids (C), ξ-Perseids (D), 54-Perseids (F) and β-Taurids (G), appeared at approximately

* J. A. Clegg, V. A. Hughes and A. C. B. Lovell, *loc. cit.*

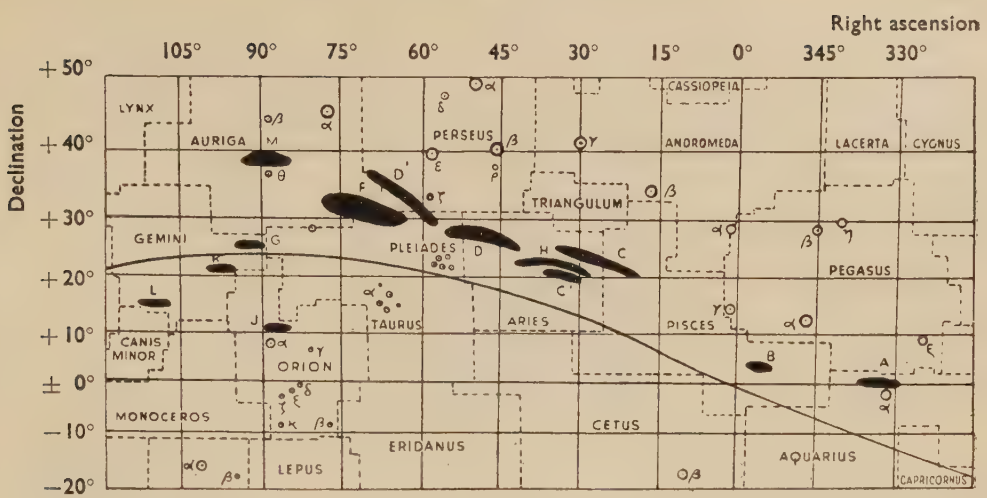

FIG. 1.—*Main areas of daytime activity* 1948 (*Mercator projection*).

Principal periods of activity.

A	*May* 1–9.	H	*June* 4–11.
B	*May* 4–10.	F	*June* 21–29.
C	*May* 1–21.	G	*June* 24–*July* 4.
C^1	*May* 2–16.	J	*July* 12–17.
D	*May* 25–*June* 14.	K	*July* 12–17.
D^1	*May* 25–*June* 16.	L	*July* 12–17.
		M	*July* 23–*August* 4.

the same dates and intensity as in 1947. Two radiants C and C^1 were determined for the Piscids, separated by some 13° of right ascension. Similarly the ξ-Perseids (D) were found to have two centres at $\alpha = 48°$, $\delta = +28°$ and $\alpha = 62°$, $\delta = +31°$ respectively, and a new stream (H) developed in the same area.

(b) *Three new radiants in Gemini and Orion.*—After the disappearance of the β-Taurid shower on July 4, the echo rate fell for several days and no well-defined streams could be recognized. On July 12, however, three new radiants became simultaneously active, one in Orion at $\alpha = 85°$, $\delta = +11°$(J) and two in Gemini at $\alpha = 96°$, $\delta = +21°$ (K) and $\alpha = 108°$, $\delta = +13°$ (L), each giving echo rates of 20 to 35 per hour. They remained until July 17, after which the separate centres became ill-defined, and the activity again fell to a relatively low level. Fig. 2 shows the plots for these three showers on July 12 with the aerial on azimuth 90°. The radiants appear as distinct centres culminating at $10^h 38^m$, $11^h 20^m$ and $12^h 15^m$.

(c) *The activity after July* 18. *New radiant in Auriga.*—Between July 18 and 23 the overall echo rate fell steadily, and although there was still an area extending from $\alpha = 70°$ to $\alpha = 130°$ over which the activity was markedly higher than in other parts of the sky, there were no well-defined radiants. On July 23 a weak and diffuse centre (M) appeared in Auriga, giving 5 to 15 echoes per hour. This new shower reached its peak on July 25, when its hourly rate rose to 30, and after this date it faded slowly, finally disappearing on August 5.

For the remainder of August the daytime rate was low, although the August Perseids, which were first detected on July 28, became very active. On several occasions during late July and August the apparatus was run continuously for 24 hours with the aerial maintained on a fixed bearing. The records show that in the last week of July the rate of meteoric activity at night became comparable

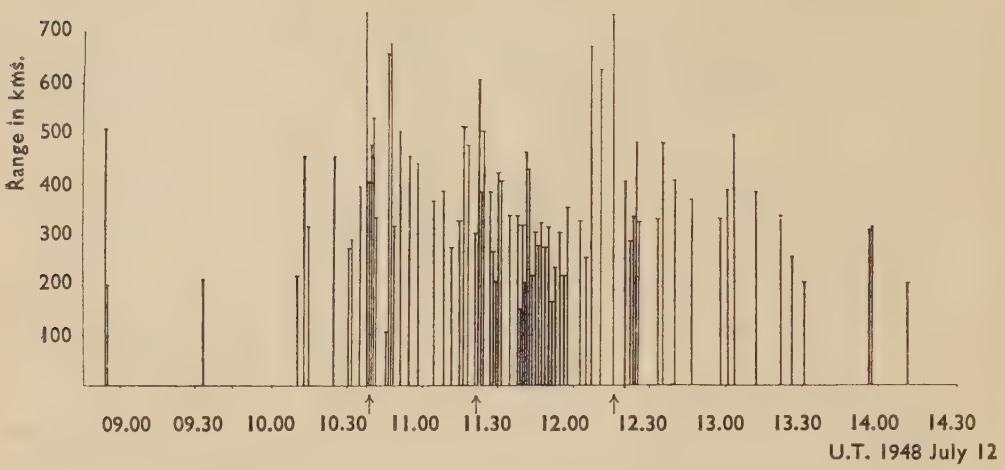

FIG. 2.—*Range/Time plots of echoes with aerial directed at azimuth* 90° *on* 1948 *July* 12.

with the daytime rate for the first time during the summer months. The night-time meteors were mainly from the known radiants near α Capricorni, α Cygni and δ Aquarii. The Perseids became by far the most prominent shower in early August and no further new daytime radiants of appreciable activity occurred until the close of the investigations in early September.

4. *The general level of activity of the* 1948 *daytime streams.*—The mean hourly rate per radiant throughout the summer of 1948 is shown in Fig. 3. There is a marked maximum at approximately June 9 during the ξ-Perseid shower and a steady decline from this time until early August. The contribution due to the

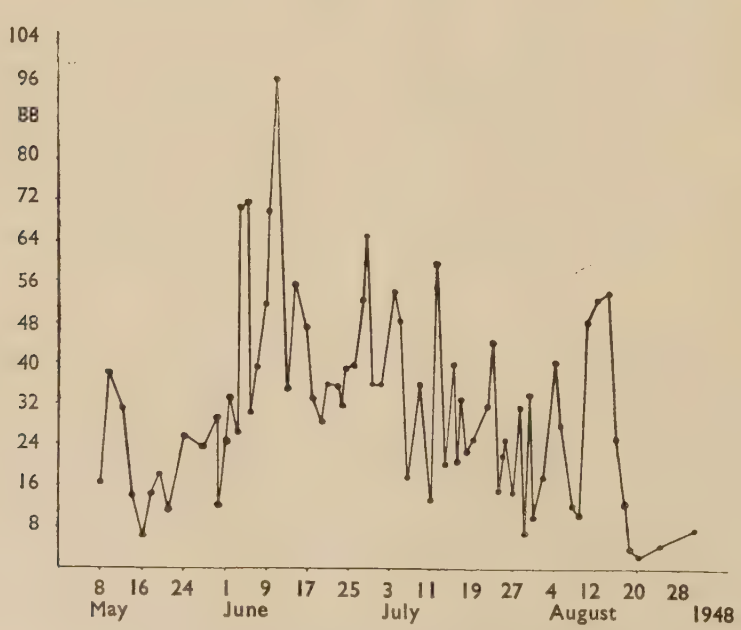

FIG. 3.—*Mean hourly rate per radiant* 1948 *May–August. Ordinates: Number of echoes/hour.*

Perseid activity in August has been included and the rate curve shows a subsidiary maximum on August 15.

5. *Discussion.*—A comparison of the 1948 and 1947 surveys shows that the development of the daytime activity of May to August followed the same general pattern in both years. The results of the observations in 1947 and 1948 are compared in Table II.

From these combined observations the most prominent streams which have occurred during 1947 and 1948 may be listed as follows :—

(i) *The η-Aquarids* (mean radiant position $\alpha = 337°$, $\delta = \pm 0°$) are active between May 1 and 10, with a rate of approximately 13 per hour. This stream is well known visually and the duration, hourly rate and radiant position quoted here, as obtained by the echo method, are in good agreement with the results of visual observations.

(ii) *The Piscids* (mean radiant position $\alpha = 37°$, $\delta = +22°$) occur between May 3 and May 18, with an average echo rate of 20 per hour, but at times the shower becomes much more active. Diffuse areas of activity precede and follow the radiant, and at times well-defined secondary radiants spring up to the east and west of the main centre.

(iii) *The ξ-Perseids* (mean radiant positions $\alpha = 50°$, $\delta = +28°$ and $\alpha = 65°$, $\delta = +30°$) consist of two radiants each giving an echo rate of 30 to 40 per hour. It seems somewhat doubtful whether these twin streams can be genetically related, but they show such marked similarity, being active over the same limits of time, with the same steady high echo rate during their period of activity and having radiants of the same sharply-defined type, that it is convenient to class them together.

(iv) *The Arietids* (mean radiant position $\alpha = 40°$, $\delta = +22°$) occur during the same period as the ξ-Perseids, but are somewhat shorter in duration and more intermittent in activity. This stream gives a mean echo rate of 30 per hour.

The Arietids and second ξ-Perseid radiant were not delineated in the 1947 observations. In retrospect, however, it is now evident that both these radiants existed in 1947 but the records were wrongly interpreted as indicating a radiant at $\alpha = 57°$, $\delta = +15°$. (Stream E in Table II.)

(v) *The 54-Perseids* (mean radiant position $\alpha = 69°$, $\delta = +30°$) are active between May 21 and May 29, diffuse in character and give a rate of 39 to 60 echoes per hour.

(vi) *The β-Taurids* (mean radiant position $\alpha = 90°$, $\delta = +26°$) occur between June 24 and July 4. The activity of this stream fluctuates considerably, varying between 0 and 65 echoes per hour.

(vii) *The α-Orionids* (mean radiant position $\alpha = 87°$, $\delta = +11°$) appear between July 12 and July 17, with an echo rate of 30 to 40 per hour. This radiant is active during the same period as two other centres of slightly lower activity, which have been listed in Table II as :

(viii) *The ν-Geminids ;* radiant at $\alpha = 98°$, $\delta = +21°$, and

(ix) *The λ-Geminids ;* radiant at $\alpha = 111°$, $\delta = +15°$.

(x) *The θ-Aurigids* (mean radiant position $\alpha = 87°$, $\delta = +38°$) are active from July 23 to August 4, with hourly rate reaching 20 at maximum.

It is hoped that future surveys will elucidate further the structure of these showers, particularly the somewhat less active radiants which culminate in the early morning during June and July and which have not yet been investigated in detail.

TABLE II

	SHOWER	1947 Radiant Coordinates	1947 Observed Duration	1947 Maximum Hourly Rate	1948 Radiant Coordinates	1948 Observed Duration	1948 Maximum Hourly Rate
A	η-Aquarids	339°±0° on May 5	May 1 to 10	13 on May 4	335°±0° on May 5	May 5 to 9	*
B		357°+5° on May 9	May 6 to 9	9 on May 8	360° †	May 4 to 10	7 on May 8
C	Piscids	27°+20° on May 9	May 5 to 14	28 on May 7	26°+24°	May 1 to 21	14 on May 10
C^1		Minor Radiants to West of C	May 7 to 12	...	36°+20° on May 13	May 2 to 16	30 on May 13
D	ξ-Perseids	51°+28° on June 10	May 30 to June 14	44 on June 6	49°+29° on June 3	May 25 to June 14	40 on June 5
‡D^1					65°+30° on June 6	May 25 to June 16	34 on June 1
‡E		57°+15° on June 6	June 2 to 13	40 on June 9			
‡H	Arietids				40°+22° on June 7	June 4 to 11	60 on June 4
F	54-Perseids	68°+35° on June 23	June 23 to 27	60 on June 25	69°+30° on June 25	June 21 to June 29	36 on June 26
G	β-Taurids	84°+25° on June 26	June 20 to 27	65 on June 27	90°+26° on June 28	June 24 to July 4	35 on July 3
J	α-Orionids				87°+11° on July 14	July 12 to 17	50 on July 12
K	ν-Geminids				98°+21° on July 14	July 12 to 17	60 on July 12
L	λ-Geminids				111°+15° on July 14	July 12 to 17	32 on July 12
M	θ-Aurigids				87°+38° on July 28	July 23 to Aug. 4	20 on July 25

* No reliable hourly rate was obtained.
† No declination measurements were made in 1948.
‡ Streams D^1 and H existed in 1947 but were wrongly interpreted as radiant E (see p. 357).

6. *Acknowledgments.*—This work was carried out at the Jodrell Bank Experimental Station of the University of Manchester and we are indebted to several of our colleagues for help in making the observations, in particular to J. G. Davies and C. D. Ellyett for the use of the information obtained during the course of their work on the velocity measurements. One of the authors (A. A.) wishes to acknowledge the receipt of a Maintenance Grant from the D.S.I.R. The authors wish to thank J. P. M. Prentice for his constant interest and invaluable advice on this work and its presentation.

Physical Laboratories,
University of Manchester:
1949 *March* 29.

THE DAYTIME METEOR STREAMS OF 1948—II

Measurement of Velocities

C. D. Ellyett

(Communicated by A. C. B. Lovell)

(Received 1949 April 1)

Summary

The paper describes measurements of the velocities of 61 daytime meteors observed between 1948 June 25 and August 6. A comparison is made between the dates of occurrence of the relevant streams described in Part I of the paper and the meteor velocities covering the same dates. The probable velocity values for two of the main showers are deduced, and it is shown that these showers possess elliptical orbits.

---

1. *Introduction.*—The work on the daytime meteor showers described in Part I of this paper indicates that the summer daytime showers are recurrent phenomena, and that several possess well-defined radiants. It is therefore desirable to measure the velocities of these meteors in order that information can be obtained about the orbits of the streams. The present paper describes the velocity measurements made during the course of the work discussed in Part I. Unfortunately the technique could not be applied until 1948 June 25 and hence the information obtained refers only to the showers active between this date and early August.

2. *Technique and treatment of records.*—The basic radio equipment was the same as described in Part I, but for the velocity measurements an additional automatic recorder was used. This instrument, which has been described by Davies and Ellyett*, gives an automatic photographic record of the range and individual amplitudes of the first 60 pulses returned from the meteor trail.† It has been shown that as the meteor trail crosses the foot of the perpendicular from the station, the amplitude of the returned pulses varies in a manner analogous to the Fresnel pattern for diffraction of light at a straight edge.‡ The angular diameter of a given zone is known from theory, and range is an observed parameter, hence the linear length of any zone can be calculated. The time taken in crossing the zone is obtained from the number of pulses and hence the velocity is determined directly. The chief uncertainty in the velocity calculation lies in the evaluation of the number of pulses between specified zone maxima or minima in the photograph of the successive echo pulse amplitudes. Small pulse-to-pulse random amplitude variations generally occur, which require to be smoothed out. From each zone measurement a velocity value is calculated and the mean of the zone velocities and the standard deviation obtained for the meteor. Meteors

* J. G. Davies and C. D. Ellyett, *Phil. Mag.*, **40**, 614, 1949.

† Pulse recurrence frequency = 620·8 per sec. The time base duration limits the number of individual pulses seen to 60.

‡ A. C. B. Lovell and J. A. Clegg, *Proc. Phys. Soc.*, **60**, 491, 1948. C. D. Ellyett and J. G. Davies, *Nature*, **161**, 596, 1948.

giving less than four zone measurements, including multiple zones, have been excluded in the following analysis. By this technique velocity determinations have already been made for ten Geminid meteors, giving a mean value of 34·4 ± 1·45 km./sec.*, which is in good agreement with Whipple's photographic results.†

3. *The distribution of velocities.*—The technique was first applied to the daytime shower on 1948 June 25 and Table I gives details of the 61 velocity determinations made between this date and August 6.

TABLE I

Meteor velocities obtained during the 1948 daytime shower

Date 1948	Time (U.T.)	Range (km.)	No. of zone measurements	Apparent geocentric velocity (km./sec.)
	h m s			
June 25	09 17 30	355	6	40·5±0·7
	10 39 15	195	4	24·1±0·6
	10 59 45	395	6	43·6±2·3
	11 11 00	**355**	**4**	**35·8±0·6**
	11 20 00	**345**	**4**	**37·3±1·9**
	11 22 30	**320**	**9**	**38·9±2·3**
	11 31 15	**365**	**9**	**36·2±2·5**
	11 41 00	**340**	**6**	**40·0±2·3**
June 27	09 08 30	395	6	33·9±2·6
	09 20 00	395	6	32·4±3·3
	10 25 30	310	9	24·2±1·7
	10 43 30	**590**	**6**	**38·0±0·7**
	10 46 30	**335**	**4**	**36·6±1·0**
	11 07 30	**345**	**12**	**36·3±3·7**
	12 01 50	**325**	**6**	**40·2±1·5**
June 28	09 17 10	305	6	46·6±1·3
	09 43 30	185	4	33·3±2·1
	09 50 15	195	7	28·1±1·1
	10 08 10	230	9	26·6±1·7
	10 09 00	**500**	**9**	**38·5±2·8**
	10 22 40	**320**	**9**	**34·4±2·1**
	10 44 45	**350**	**4**	**41·4±1·4**
	11 24 20	**320**	**9**	**38·4±3·2**
	12 19 05	135	6	32·4±2·8
	12 21 15	415	6	29·1±2·7
June 29	**11 34 00**	**175**	**4**	**34·0±1·0**
	11 47 00	**320**	**6**	**39·9±3·6**
July 2	09 31 20	375	6	49·3±2·1
	10 18 35	370	9	49·3±1·4
	11 59 05	290	4	24·9±1·4
July 6	09 33 24	350	12	39·1±4·7
	10 24 40	330	6	43·3±1·8
	10 27 30	340	4	30·5±3·7
July 8	09 52 32	130	12	22·8±2·9
	11 11 47	400	7	36·9±1·5
	11 17 05	195	6	18·0±0·5
	11 30 11	235	7	38·2±0·7
	12 32 25	320	4	31·3±1·7

* J. G. Davies and C. D. Ellyett, *loc. cit.*

† F. L. Whipple, *Proc. Amer. Phil. Soc.*, **79**, 499, 1938.

TABLE I.—*Continued*

Date 1948	Time (U.T.)	Range (km.)	No. of zone measurements	Apparent geocentric velocity (km./sec.)
	h m s			
July 9	10 53 15	230	12	20·5±1·5
	11 03 50	430	9	29·9±1·4
	11 40 45	340	12	17·0±1·2
July 13	08 39 40	395	6	38·6±2·3
	11 01 51	195	12	22·9±1·1
July 14	10 53 59	205	6	25·8±2·0
	11 12 49	320	6	35·3±3·5
July 15	09 39 42	395	6	46·1±2·0
July 23	11 47 05	370	9	27·0±2·5
	11 58 01	180	4	23·5±3·3
July 24	10 50 21	235	4	30·4±2·2
	12 36 10	310	4	26·0±1·5
July 27	08 53 15	355	7	61·8±4·6
	11 38 14	320	9	26·6±2·1
	14 28 54	165	4	19·7±1·6
July 28	08 45 14	400	6	40·6±1·6
	09 09 06	275	4	32·7±0·6
	09 49 25	360	9	35·5±1·6
	10 40 15	415	6	32·2±2·8
	11 46 17	195	6	38·6±1·3
	12 29 53	415	4	31·5±0·6
Aug. 5	09 13 01	270	4	30·4±0·4
Aug. 6	06 46 08	560	4	54·0±1·1

The velocity values are shown in Fig. 1A, and the total number of velocities in each group of 5 km./sec. in Fig. 1B.

The spread of the group is wide, with a maximum in the region of 35–40 km./sec. At least two values appear to be well above the main group. However, little significance can be attached to a single velocity value in the absence of any knowledge of the meteor path. As the period of observation totalled $81^h\,29^m$ it is very likely that a few sporadic meteors were received along with the main daytime groups. The background rate for the equipment is

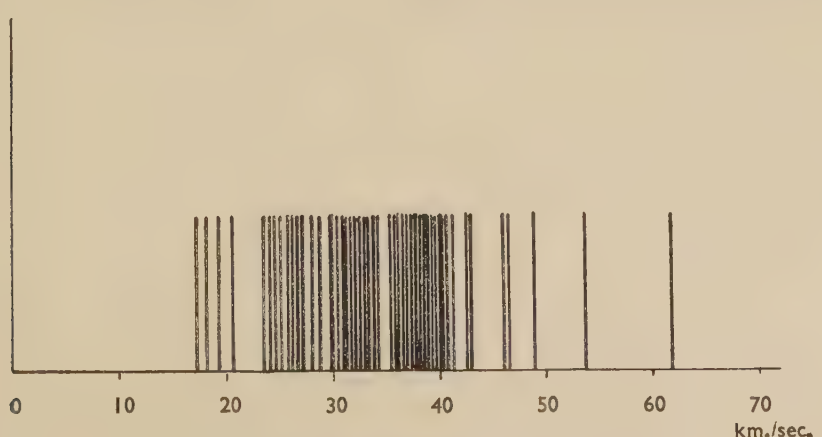

FIG. 1A.—*Individual velocity values—daytime stream*

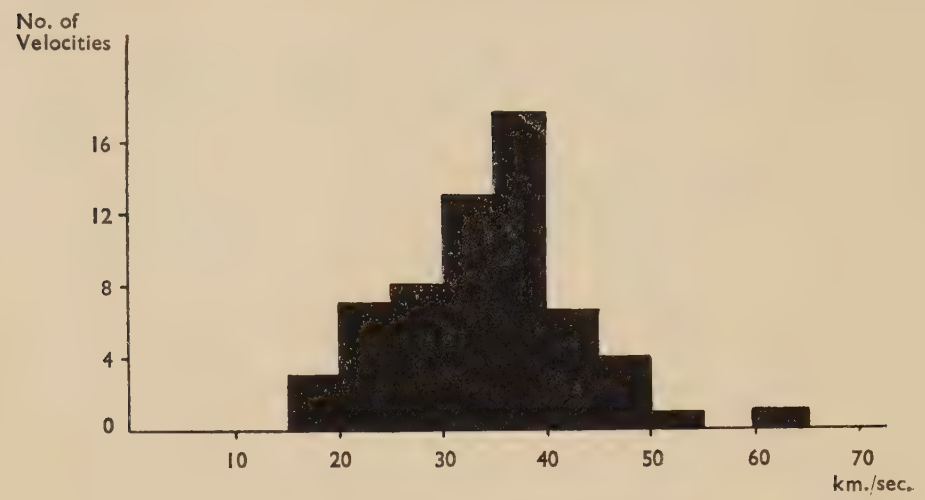

FIG. 1B.—*Spread of meteor velocities—daytime stream.*

known to be about 1·5 per hour *, and 7·5 per cent of the echoes in the daytime showers give velocity values †, so nine of the present group could be attributed to sporadic meteors. The isolated high-velocity values could arise from this source. Groups of similar-valued velocities however would be less likely to come from random sporadic sources. The two high values have therefore been deleted.

4. *The velocities of particular radiant groups.*—The records have been analysed to determine whether it is possible to associate velocity groups, for the period under review, with the specific radiants described in Part I. For this purpose the distribution of velocities with date is shown in Fig. 2. Taking into account the duration of transit of the radiant through the aerial beam ‡, only those velocities occurring in the interval from 0·5 hours before transit to 1·5 hours after transit can be attributed to a given radiant.

Between July 6 and July 15 the radiant structure is complex and only weakly represented in Table I, so the analysis has been confined to the two periods (*a*) June 25 to July 2 and (*b*) July 23 to August 5.

Period (*a*).—Between June 25 and July 2 thirty velocities were obtained. At the commencement of this period the two radiants 54-Perseid ($\alpha = 69°$, $\delta = +30°$, H.R. 36, Transit $10^h 40^m$ U.T.) and β-Taurid ($\alpha = 90°$, $\delta = +26°$, H.R. 35, Transit $11^h 40^m$ U.T.) were already active. The 54-Perseid stream terminated on June 29, but the β-Taurid stream continued until July 5. Seven of the thirty velocities occurred at times outside the permissible limits of either of these radiants and have been excluded from the discussion. These seven values are shown in outline only in Fig. 2.

Of the remaining 23 velocities, 15—shown in heavy type in Table I—have their mean values contained within $37·5 \pm 3·7$ km./sec. Further, although the activities of the two radiants overlap in time, six velocities in the group of 15 occurred before the β-Taurid radiant had entered the radio beam, so it is reasonable to attribute the groups to the 54-Perseid radiant.

* A. C. B. Lovell and J. P. M. Prentice, *J.B.A.A.*, **58**, 140, 1948.
† J. G. Davies and C. D. Ellyett, *loc. cit.*
‡ J. A. Clegg, *Phil. Mag.*, **39**, 577, 1948.

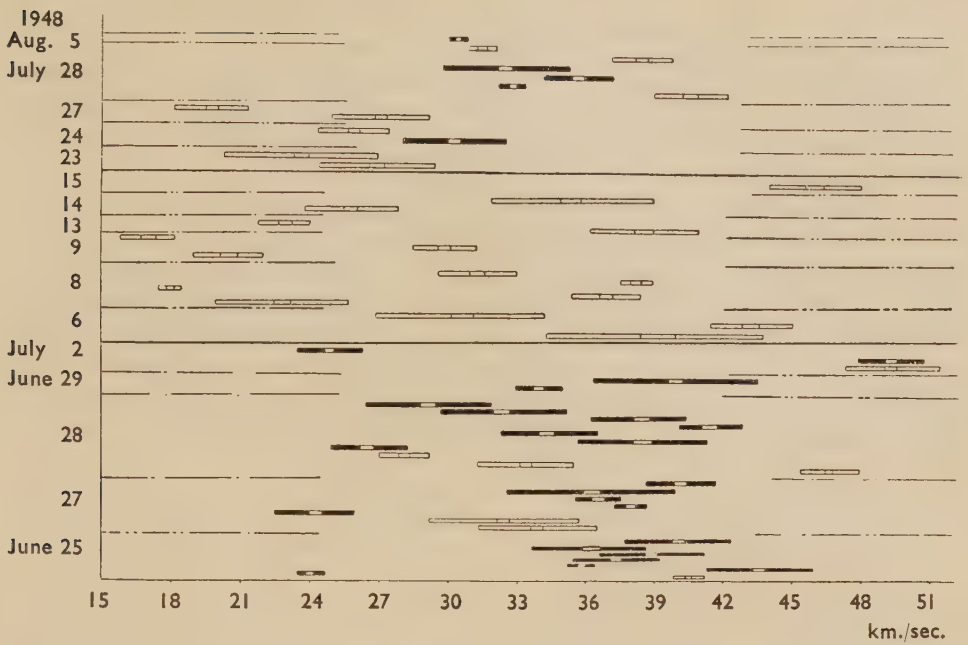

FIG. 2.—*Distribution of meteor velocities with date.*

The evidence is insufficient to attribute a velocity to the β-Taurid shower, as only two velocity values were obtained when this radiant alone was active.

Period (*b*).—Throughout this period the θ-Aurigid radiant alone was active ($\alpha = 87°$, $\delta = +38°$, H.R. 20, Transit $9^h\ 27^m$ U.T.). Thirteen velocities were obtained, of which eight, however, lie outside the time limits for the transit of the radiant through the beam. The remaining five, contained within $32{\cdot}9 \pm 2{\cdot}7$ km./sec., can be attributed to the θ-Aurigids. There also appears to be evidence of a low-velocity group on these days, in transit about 2–3 hours after the Aurigids. This group does not correspond to any major shower listed in Part I.

5. *Calculation of heliocentric velocities and orbits.*—As the time of transit is known for the two streams to which apparent geocentric velocities have been ascribed, it is possible to make an approximate calculation of their heliocentric velocities. The results are given in Table II.

TABLE II

Approximate heliocentric velocities

Meteor Stream	Transit time (U.T.)	Apparent geocentric velocity (km./sec.)	Approximate heliocentric velocity (km./sec.)
54-Perseid	$10^h\ 40^m$	$37{\cdot}5 \pm 3{\cdot}7$	$39{\cdot}1 \pm 2{\cdot}6$
θ-Aurigid	$9^h\ 27^m$	$32{\cdot}9 \pm 2{\cdot}7$	$27{\cdot}5 \pm 1{\cdot}4$

The accuracy of these determinations is insufficient to justify the introduction of detailed corrections for the retardation in the atmosphere and the gravitational acceleration. However, the gravitational attraction introduces the larger correction

and the overall effect would be to lower the value of the heliocentric velocity by approximately 1 km./sec.

It is clear from Table II that the two meteor streams under review possess elliptical orbits and, in the absence of further information at this date, it is reasonable to assume that the other sections of the daytime showers will likewise possess elliptical orbits.

6. *Acknowledgments.*—The author is particularly indebted to his colleague J. G. Davies, who took a large part in the collection of the records ; to Dr A. C. B. Lovell, Director of the Jodrell Bank Experimental Station of the University of Manchester, where this work was carried out, for his assistance in the collection of data and his valuable advice on the presentation of the paper ; and to J. P. M. Prentice, Director of the Meteor Section of the British Astronomical Association, for his helpful criticism of the results. Grateful acknowledgment is made to the Imperial Chemical Industries Ltd. for the award of a Research Fellowship.

Physical Laboratories,
University of Manchester:
1949 *March* 29.

ON THE COSMOLOGICAL PROBLEM

F. Hoyle

(Received 1949 January 14)

Summary

Earlier work on the continuous creation of matter is generalized, and criticisms of certain aspects of this work by Bondi and Gold are answered. The aesthetic issues that arise in the cosmological problem are briefly discussed.

---

1. *Introduction.*—Einstein's general theory of relativity places the restrictions

$$G^{\mu\nu} - \tfrac{1}{2}g^{\mu\nu}G + \lambda g^{\mu\nu} = -\kappa T^{\mu\nu} \qquad (1)$$

on the ten independent components of $g_{\mu\nu}$, which define a four-dimensional Riemannian space in accordance with the following line element

$$ds^2 = g_{\mu\nu}dx^\mu dx^\nu. \qquad (2)$$

The constant κ is expressed in terms of the Newtonian constant of gravitation γ by the relation $\kappa = 8\pi\gamma/c^4$, where c is a constant velocity (3×10^{10} cm. per sec.), λ is a "cosmical constant" and $T^{\mu\nu}$ is the material energy tensor defined by

$$T^{\mu\nu} = \rho v^\mu v^\nu, \qquad (3)$$

where the matter at the point x^μ has velocity v^μ and proper density ρ (it is assumed that there is only one hydrodynamic streamline through x^μ).

This scheme is invariant both in the sense that (1) and (3) are tensor equations, and also in that no special property distinguishes any one coordinate system. Such a scheme cannot lead uniquely to a description of the observed universe, since the observed motions of material particles are markedly non-invariant. For example, at each point of space-time a preferred direction is defined by the observed motion of matter. Weyl has pointed out that the preferred directions, obtained in this way, are consistent with the statement that the world lines of material particles can be represented approximately, but not exactly, as geodesics radiating from a particular point of space-time. It was therefore proposed that, for cosmological purposes, the consideration of (1) should be restricted to solutions satisfying the latter condition. The non-invariant character of this condition is clearly shown by the mathematical result that in all such solutions the adoption of a geodesic form for the line element provides a system of universal time.

In the usual cosmological models the solutions of (1) are further restricted by taking ρ to depend solely on the time coordinate. This is an expression of the observed approximate constancy of average values of ρ, the averages being taken over space volumes that are large enough to contain many extragalactic nebulae.

Even when these special conditions are imposed on (1), there remains an infinity of solutions. As Robertson (**1**) has shown, the resulting models may be divided into a number of categories, the physical properties of which can be determined. It turns out that in all cases there are serious discrepancies with the results of theoretical and observational astrophysics (**2**). This difficulty cannot be due to the restrictions, mentioned above, that are placed on (1), since these restrictions

are derived from observed characteristics of the universe. If the conclusions of astrophysics are accepted, the discrepancies can only be resolved by a modification of (1), or by an entirely new theory.

The point of view adopted by the writer is that a search for a new system of cosmology is fully warranted by the astrophysical evidence. It seems reasonable, however, to restrict modifications of (1), at any rate in the first place, to the minimum necessary to give a satisfactory system of cosmology.

Equations (1) lead to $(T^{\mu\alpha})_\alpha = 0$, since the divergence of the left-hand side is zero. Thus the solutions of (1) can only represent physical systems in which matter and momentum are conserved. This means that the adoption of (1) involves the assumption that a solution of the cosmological problem can be obtained without reference to the creation of the universe. This assumption is valid if the universe were created in the remote past, but must be invalid if matter is created continuously. Thus, since the mode of creation cannot be decided on *a priori* grounds, it is clear that the equations (1) are of a restricted nature. Accordingly, it is a natural step to seek a modification of (1) that removes this restriction.

An attempt to carry out this project has recently been made by the writer (**3**). Equations were obtained that led to a model for the expanding universe free from immediate observational objections.

This model has, however, been criticized by Bondi and Gold (**4**), partly on mathematical grounds and partly from an aesthetic point of view. One of the objects of the present paper is to discuss these criticisms. The mathematical criticisms refer to the theory in its most general form. This was not given in the previous paper (**3**), which works in terms of an approximation in which the material in the extragalactic nebulae is taken as being smeared out into a uniform background. Thus, prior to a discussion of the arguments of Bondi and Gold, the general theory, free from approximation, is given in Section 2. It is then shown in Section 3 that the difficulties anticipated by Bondi and Gold do not arise. Aesthetic questions are discussed in Section 4.

2. *The general theory.*—The vector $(T^{\mu\alpha})_\alpha$ is described in terms of the components of a symmetrical tensor $C^{\mu\nu}$ by the relation

$$-\kappa(T^{\mu\alpha})_\alpha = (C^{\mu\alpha})_\alpha. \tag{4}$$

Thus we can write

$$-\kappa T^{\mu\nu} = C^{\mu\nu} + (\text{Tensor of zero divergence}). \tag{5}$$

In accordance with the normal relativity theory $(G^{\mu\nu} - \frac{1}{2}g^{\mu\nu}G)$ is chosen as the tensor of zero divergence. Accordingly,

$$G^{\mu\nu} - \tfrac{1}{2}g^{\mu\nu}G + C^{\mu\nu} = -\kappa T^{\mu\nu} \tag{6}$$

represent the general field equations (the cosmical constant is taken to be zero).

The non-invariant character of the universe is introduced by the following geometrical determination of the direction of the vector $(C^{\mu\alpha})_\alpha$. It is assumed that a three-dimensional surface S_0 can be found, such that a tangent plane is defined everywhere on S_0. Then at each point of S_0 draw the geodesic normal to the corresponding tangent plane. This set of geodesics can be used to define a system of coordinates. If the same absolute length from S_0 be laid off along each geodesic the locus of the end points, S say, is a surface orthogonal to the geodesics themselves. A coordinate system t, x_1, x_2, x_3 can then be chosen, such that S_0 is the surface $t = 0$, and the surface S is defined by the equation

$$ct = (\text{absolute length laid off along the geodesics}). \tag{7}$$

In this coordinate system the line element is given by

$$ds^2 = c^2 . dt^2 + g_{ij}(t, x_1, x_2, x_3) dx_i dx_j \; ; \; i,j = 1, 2, 3. \tag{8}$$

The above process enables a t-coordinate to be determined for each point of space-time. Moreover, a preferred direction is defined at each point by the particular member of the set of geodesics that passes through the point. (For the moment singular points will be ignored. This question is discussed in the following section.) The direction of $(C^{\mu\alpha})_\alpha$ is identified with this preferred direction. We regard S_0 as being a given surface, so that $(C^{\mu\alpha})_\alpha$ is a vector with a specified direction. Accordingly, three conditions are placed on the ten independent components of $C^{\mu\nu}$. Further, we put

$$C^\alpha_\alpha = \text{constant}, \tag{9}$$

thereby giving four conditions on $C^{\mu\nu}$. This is sufficient, if $C^{\mu\nu}$ is constructed from a vector $^*C^\mu$ in accordance with the relation

$$2C^{\mu\nu} = {}^*C^{\mu\nu} + {}^*C^{\nu\mu}, \tag{10}$$

to complete the mathematical scheme.

In the smoothed-out problem the present scheme has the same steady-state solution as that given previously (**3**).

The constant in (9) can be adjusted to give agreement with the observed Hubble-Humason velocity-distance relation. In terms of the previous notation, (9) then takes the form

$$C^\alpha_\alpha = 9/a^2. \tag{11}$$

The line element for the steady-state solution can be reduced to the well-known de Sitter form

$$ds^2 = c^2 dt^2 - e^{2ct/a}(dx_1^2 + dx_2^2 + dx_3^2). \tag{12}$$

The density ρ is again constant and is given by $3/\kappa c^2 a^2$. Moreover, it can be shown that the steady-state solution is stable against fluctuations of the coefficient of $(dx_1^2 + dx_2^2 + dx_3^2)$ from the value $e^{2ct/a}$ given in (12).

Although the present theory reduces to that given previously for the case of physical interest, a mathematical difference arises from the adoption of (11). This condition is not a generalization of the previous work, which leads to the alternate invariant condition

$$^*C_\alpha (C^{\alpha\beta})_\beta + C_{\alpha\beta} C^{\alpha\beta} = 0. \tag{13}$$

For mathematical purposes (11) is preferable to (13), since (11) preserves linearity in the components of $^*C^\mu$. (This much simplifies the treatment of singular points.)

A second difference arises from the use of the basic surface S_0 in place of the point O adopted in the earlier work. The advantage of the present treatment is that the de Sitter line element can be discussed without introducing geodesics of infinite length.

3.—Provided t is sufficiently large, singular points can occur on the S surfaces. An infinity of geodesics of the basic set pass through such points. The theory can be extended to include these points because the linearity of (6), (10) and (11) in the components of $^*C^\mu$ enables the necessary creation properties to be established by a continuity process. Bondi and Gold (**4**) have suggested that physical difficulties may arise from the behaviour of newly created matter at singular points. Their argument would seem to imply that, when t becomes very large,

all points of S may become singular. This is not the case, for there are at most ∞^2 singular points on an S surface, as compared with the ∞^3 points of the surface itself.

It has also been suggested by Bondi and Gold that, even in the absence of electromagnetic fields, the general orbits of particles are not geodesics in the present theory. This view appears to have arisen from an oversight, as will be seen from the following argument.*

It can be shown by a well-known procedure that, when the expression (3) for $T^{\mu\nu}$ is used in (4), the equations of motion of material of density ρ are

$$\frac{dv^\mu}{ds} + \{\alpha\beta, \mu\} v^\alpha v^\beta = \frac{1}{\kappa\rho c^2}[v_\alpha v^\mu (C^{\alpha\beta})_\beta - (C^{\mu\alpha})_\alpha]. \tag{14}$$

The terms in $C^{\mu\nu}$ tend to reduce the angle between v^μ and $(C^{\mu\alpha})_\alpha$ except when these vectors are parallel, in which case the right-hand side of (14) vanishes. Accordingly, it might be expected that, except in this special case, the orbits of particles in a purely gravitational field are not geodesics. This conclusion is erroneous, however, on account of the important assumption, involved in adopting (3) for $T^{\mu\nu}$, that there is only one hydrodynamic streamline through each point. When v^μ and $(C^{\mu\alpha})_\alpha$ are not parallel this assumption requires newly created particles, which initially move in the direction $(C^{\mu\alpha})_\alpha$, to be absorbed into the v^μ stream. Such an absorption involves a collisional mechanism between the particles. The terms on the right-hand side of (14) are due to the electromagnetic or nuclear forces arising in the collisions. In a purely gravitational field the newly created matter would form a stream separate from the v^μ stream, and the particles in each stream follow geodesics.

4. *The general cosmological problem*

4.1. *Theories that are wholly invariant.*—It has been suggested to the writer on several occasions that it would be preferable to replace the non-invariant conditions on $(C^{\mu\alpha})_\alpha$, as defined in Section 2 (invariance is destroyed, not by a departure from tensor equations but through a preferred direction being defined by geometrical considerations at each point of space-time) by corresponding invariant conditions. The following discussion shows that such a procedure leads to grave difficulties.

Wholly invariant systems can be obtained by taking $(C^{\mu\alpha})_\alpha$ and v^μ to be parallel vectors (in a single stream region). Since it would be unsatisfactory for $(C^{\mu\alpha})_\alpha$ to depend on the velocity of matter but not on its density, we take

$$(C^{\mu\alpha})_\alpha = (\text{constant}) \,.\, \kappa\rho v^\mu \tag{15}$$

as giving a natural choice for $(C^{\mu\alpha})_\alpha$. In the smoothed-out problem (15), taken together with (6) and (10), leads to the same steady-state solution as the theory of Section 2. The situation is not satisfactory, however, when local condensations are considered. For it can be shown that (15) requires all bodies to double their masses in a time less than 10^9 years (the constant in (15) being chosen to give agreement with the observed velocity-distance relation). This result leads to serious difficulties, notably in the theory of white dwarfs and in planetary theory. These difficulties are so severe as to dispose of (15).

* Unfortunately I did not notice this oversight when Mr Bondi and Mr Gold showed me the manuscript of their paper.

A further possibility, suggested by Bondi, is given by writing

$$(C^{\mu\alpha})_{\alpha} = (\text{constant}) \cdot \sqrt{\kappa\rho}\, v^{\mu}. \tag{16}$$

In the smoothed-out problem this relation, together with (6) and (10), again leads to a steady state identical with that given by the theory of Section 2. Moreover, the weakening of the dependence on ρ avoids the astrophysical objections to (15).

But even so, there is, in the writer's view, an overriding objection to the adoption of any wholly invariant scheme such as that given by (15) or (16). For (6), (10) and (16) cannot lead uniquely to a satisfactory cosmological theory, since, as pointed out above, the universe is a markedly non-invariant structure. Thus to obtain the required solution it would be necessary to impose severe restrictions on (6), (10) and (16). Such a procedure could only be satisfactory if answers could be given to the following questions.

Why are these restrictions adopted, and what is their special significance?

What is the significance of the unwanted solutions of the equations?

Unless answers to these inscrutable questions can be given, wholly invariant schemes seem unacceptable on aesthetic grounds. This view has been emphasized by Bondi (**5**) in a recent review of cosmology.

The non-invariant creation process given in Section 2 was deliberately adopted to avoid this difficulty. The constancy of C^{α}_{α}, as given by (11), leads to a creation rate effectively independent of ρ (there is a slight dependence through the $g_{\mu\nu}$). Thus (11) preserves the uniformity of average values of ρ, the averages being taken over large spatial volumes. That is, the adoption of (11) ensures that large-scale homogeneity is reached and maintained within the S subspaces. By working in the smoothed-out approximation it can then be shown that a unique stable steady state, given by the line element (12), must be attained. Accordingly, apart from the details of localized condensation, the theory of Section 2 would appear to lead to a unique steady state for the universe.

This result, in the writer's view, gives the theory an advantage over any wholly invariant formulation of the creation properties. Moreover, it is important to notice that non-invariance applies only to the creation properties. Once matter has been created the full invariance of Einstein's general theory of relativity is required to describe the states occurring in local condensations. That is, a distinction is drawn between the creation of matter and its subsequent behaviour.

4.2. *Theories that are not invariant.*—The aesthetic objections of Bondi and Gold to the theory outlined in Section 2 are based, not on the non-invariance of the creation process, but on the invariance of the equations describing the properties of matter subsequent to its creation. Thus these authors agree with the arguments of 4.1, that a wholly invariant scheme cannot be accepted, since such a scheme cannot lead to a unique description of the large-scale properties of the universe, and they infer that an entirely non-invariant theory should be adopted. The idea employed by the writer, of introducing non-invariance only through the creation of matter, is regarded by them as an artificial device. Further discussion of this question depends upon a closer investigation of the point of view maintained by Bondi and Gold.

The acceptance of complete non-invariance rejects the postulate of relativity whereby all observers, no matter how different their environments, must find that the same basic equations are capable of describing their various observations. Thus Bondi and Gold express the view that the equivalence of observers should

hold only for observers placed in similar environments (4). Instead of the postulate of relativity, they accept a postulate due to Mach, whereby inertial properties of matter have significance only when measured relative to matter. The distinction between the two postulates is clearly shown by the following example. Consider a universe in which the only material content is a rigid sphere. According to relativity theory, as in Newtonian dynamics, significance can be attached to the statement that the sphere possesses rotation. A Foucault pendulum set up by an observer on the surface of the sphere would determine the rate of rotation (time being measured by an atomic clock). According to Mach's postulate, on the other hand, it is meaningless to speak of the sphere being in rotation, because this would involve measuring the inertial property of rotation, not against matter but against space. On this view, a pendulum set up on the surface of the sphere would not show the Foucault property but would behave as a simple pendulum.

This example shows that, according to Mach's postulate, the observations of terrestrial physics would have to be strongly coupled to the universe as a whole. Although this view is in contradiction to the general outlook of terrestrial physics, it can be argued that, provided the coupling is sufficiently constant over the region of space-time accessible to a terrestrial observer, it is impossible to decide by experiment whether or not such a coupling exists. Thus, there is some ground for the claim that no experiment can be wholly contrived or controlled ; that we can only contrive experiments in so far as the large-scale properties of our environment permit us to do so. Although this possibility cannot be denied, it is important to notice that such ideas must necessarily involve an entirely new theoretical development. In particular, it seems likely that electromagnetic forces and nuclear forces would have to be assigned natural places in such a theory. For modern physics indicates that the inertial properties of matter are intimately connected with electromagnetic and nuclear forces. This requirement is not necessarily a disadvantage to Mach's postulate. It is one of the least satisfactory features of general relativity that no adequate generalization of the theory, capable of including electromagnetic and nuclear forces, has yet been found (for example, there is no simple geometrical description of the orbits of charged particles in an electromagnetic field).

The remarks of the previous paragraph show that the quantitative formulation of the ideas of Bondi and Gold is likely to be a matter of considerable difficulty. While the writer is not in principle opposed to these ideas, it seems preferable that the question of the continuous creation of matter should be discussed by a modification of existing theory rather than by attempting simultaneously to build an entirely new description of the universe. That Einstein's general theory of relativity may ultimately be replaced by a theory of wider scope is no argument against this procedure. The situation is in many ways analogous to Eddington's work on the stellar mass-luminosity-radius relation. By adopting a simplified theory, several features of which are now known to be erroneous, Eddington was able to direct attention to the important features of the problem in a manner that would not have been possible if he had insisted from the outset in searching for a theory perfect in every detail.

Bondi and Gold (4), in discussing the continuous creation of matter, have avoided the introduction of a quantitative theory by making the hypothesis that the universe, when taken on a sufficiently large scale, satisfies the wide (perfect)

cosmological principle. Since the wide cosmological principle is very far from being satisfied over regions with linear dimension less than about 10^{24} cm., such a hypothesis immediately raises the following questions :

What considerations determine the scale necessary for the wide cosmological principle to be approximately satisfied ?

Why should the cosmological principle not be strictly satisfied ?

Quite apart from these questions, which Bondi and Gold do not answer, their imposition of the wide cosmological principle as a primary axiom deserves comment. Physical science is based on axioms that usually consist in associating observational quantities with the symbols appearing in certain mathematical equations. The choice of the equations is guided by the requirement that the observed interrelations between the physical quantities concerned must be correctly represented by the equations. So far, those equations that have become generally accepted are of field form. That is, for each separate point of space-time, relations are given between physical quantities and their derivatives. It is clear, therefore, that the imposition, as a primary axiom, of the wide cosmological principle, which is a statement concerning the behaviour of the universe as a whole, is a radically new departure. The situation is not similar to that of the narrow cosmological principle in relativistic cosmology (**1**), for in the latter case the narrow cosmological principle is used as an arbitrary criterion for obtaining special solutions of the field equations, which themselves represent the primary axioms. This feature of the work of Bondi and Gold is, in the writer's view, open to serious question. It is believed that the wide cosmological principle should follow as a consequence of primary axioms of the field form, as in the scheme of Section 2, and should not appear itself as a primary axiom.

Finally, it may be mentioned that the aesthetic value of Mach's postulate is to some extent weakened in a universe with continuous creation of matter. For "empty space" possesses physical properties in such a universe, since no region of space can remain permanently empty. Accordingly it is far from being clear that "inertia against space" is an absurd conception.

St. John's College,
Cambridge :
1949 *January* 12.

References

(**1**) H. P. Robertson, *Rev. Mod. Phys.*, **5**, 71, 1933.
(**2**) F. Hoyle, *Nature*, **163**, 196, 1949.
(**3**) F. Hoyle, *M.N.*, **108**, 372, 1948.
(**4**) H. Bondi and T. Gold, *M.N.*, **108**, 252, 1948.
(**5**) H. Bondi, *M.N.*, **108**, 104, 1948.

A NOTE ON HEAT TRANSFER IN THE UPPER CHROMOSPHERE AND CORONA

R. G. Giovanelli

(Received 1949 January 10*)

Summary

A consideration of the problem of heat transfer in the Sun's atmosphere indicates that while thermal conduction is adequate to transfer heat through the corona, the heat conducted from the corona to the upper chromosphere cannot be transmitted through the chromosphere solely by conduction nor by radiation and conduction together. Therefore heat must be transferred through the upper chromosphere mainly by convection. The transition from convection to conduction as the main agent of heat transfer seems to mark the boundary between the chromosphere and corona.

1. *Introduction.*—The outer layers of the Sun are known to be at temperatures higher than that of the visible surface, and the source of heat has recently been the subject of considerable discussion. Alfvén (**1**) attributes the heating to the action of granules which, moving perpendicular to the Sun's general magnetic field, set up magneto-hydrodynamic waves which are propagated into the outer atmosphere where they are damped, the energy being converted into heat; while Bondi, Hoyle and Lyttleton (**2**) have shown that accretion of interstellar material may be the source of the heating.

Whatever the mode of heating, the temperature distribution depends also on the rate of transfer of heat. Alfvén (**3**) and Woolley (**4**), using classical formulae for the thermal conductivity, concluded that thermal conduction is more important than radiation in transferring heat in the corona and Alfvén estimated the temperature distribution in the corona for a source of heat at a given elevation. Bondi, Hoyle and Lyttleton showed that radiation is inadequate to transfer the heat they expected from accretion. They deduced, on the basis of classical formulae, that if conduction alone operated, the temperature gradients would be so high that the thickness of the transition layer from a temperature of 10^4 to 10^6 deg. K. could not exceed 10 km. This, they contended, would result in an unstable high radial pressure gradient (although this does not seem to follow) and they were led to postulate convection as the mode of heat transfer in the corona and chromosphere, obtaining good agreement between theory and the observed temperature distribution.

The details of Bondi, Hoyle and Lyttleton's analysis apply specifically to an atmosphere in which the effects of magnetic fields are negligible. If, however, the Sun's general magnetic field extends into the outer corona—and it seems difficult to avoid such a conclusion—it appears that important modifications in their theory may be required ; for in magnetic fields of a few gauss, as expected in the corona, the radius of gyration of a proton having thermal energy is of the order of only a few metres, while the mean free path in the corona is of the order of 10^3 km. Thus, since the transport of matter across lines of force is greatly reduced,

* Received in original form 1948 November 10.

it is difficult to see how the circulation necessary for continuity in a convection system can occur in the corona.

It is the purpose of this note to reconsider the problem of heat transfer in the upper chromosphere and inner corona, taking into account the large increase with temperature of the thermal conductivity of a highly ionized gas. It can be shown that some of the difficulties which the presence of the Sun's general magnetic field introduces into a theory of heat transfer by convection can be avoided, for we find that thermal conduction is by itself adequate to transfer heat in the corona, and that it accounts for the sharp temperature rise between the chromosphere and corona. Thermal conduction is greatly restricted in directions perpendicular to lines of magnetic force and so heat flow occurs mainly in the direction of the magnetic field. If the Sun's general field approximates to that of a dipole the flow of heat is thus radial near the poles (being there independent of the presence of the magnetic field) and approximately parallel to the surface near the equator. While this necessitates higher temperatures near the equator than near the poles, the order of magnitude of the temperature should be the same throughout the corona because of its high thermal conductivity.

We discuss first the simpler case of the temperature of the corona in the higher magnetic latitudes, subsequently showing that conduction can also account for the temperature distribution in equatorial zones.

In the upper chromosphere, however, we find it impossible to account for heat transfer solely on the basis of conduction and radiation, and we are forced to conclude that most of the heat must be transferred through this region by convection; difficulties associated with the existence of convection in these denser regions in the presence of a magnetic field are expected to be much less than in the corona and, indeed, observation indicates that the chromosphere is in turbulent motion.

2. *The Observed Temperature Distribution.*—The temperature distribution in the chromosphere and corona, as far as is at present known, is shown in Fig. 1 by the solid lines and crosses. The photosphere is at a temperature of about 6×10^3 deg. K. Between 500 and 3000 km. above the base of the chromosphere the temperature appears to have a uniform value of about 3×10^4 deg. K. (**5, 6**). At 12,000 km. it is about 10^5 deg. K., and above 20,000 km. it is about 10^6 deg. K. It has not yet been possible to derive intermediate values from observation. It is evident that there is a steep temperature gradient between 12,000 and 20,000 km., but the width of the transition region is not known.

3. *The Thermal Conductivity of a Highly Ionized Medium.*—The thermal conductivity of a highly ionized medium is not known with great accuracy. In a binary gas, heat conduction results mainly from the diffusion of the lighter constituent, so that heat conduction in a highly ionized gas is due mainly to the electrons. The approximate thermal conductivity of a gas, whose particles repel one another according to an inverse square law, is known, and this enables the conductivity of an electron gas to be deduced. However, in a highly ionized gas such as the Sun's atmosphere (assumed for simplicity to be pure hydrogen) electrons and protons are present in equal concentrations. Thus heat flow is impeded by collisions not only of electrons with electrons (as in an electron gas) but of electrons with protons. The approximate thermal conductivity due to the lighter constituent of a binary gas when collisions between the lighter particles are neglected (this being then known as a Lorentzian gas) and when collisions between

lighter and heavier particles take place according to an inverse square law of attraction is also known. Consideration of an electron and a Lorentzian gas enables the thermal conductivity of a highly ionized gas to be deduced with sufficient accuracy for our purpose.

(i) *Electron gas.*—Using Chapman and Cowling's notation (**7**), the thermal conductivity λ_e of an electron gas is given approximately by

$$\lambda_e = \frac{25}{32}\left(\frac{km\theta}{\pi}\right)^{\frac{1}{2}}\left(\frac{2k\theta}{e^2}\right)^2 \cdot \frac{c_v}{A_2(2)}, \tag{1}$$

where k is Boltzmann's constant, m and e are the mass and charge (e.s.u.) of an electron, θ is the temperature, $c_v (=3k/2m)$ is the specific heat, and

$$A_2(2) = 2\left\{\log_e(1+v_{01}^2) - \frac{v_{01}^2}{1+v_{01}^2}\right\}, \tag{2}$$

where

$$v_{01} = 4dk\theta/e^2, \tag{3}$$

d being the mean distance between pairs of neighbouring electrons. It is sufficient for our purposes to replace d by $N_e^{-\frac{1}{3}}$, where N_e is the electron concentration. For electron concentrations and temperatures such as are found in the Sun's atmosphere, we find that $A_2(2)$ ranges from 28·2 for $N_e = 3 \times 10^8$ per c.c., $\theta = 10^6$ deg. K., to 15·8 for $N_e = 10^{12}$ per c.c., $\theta = 3 \times 10^4$ deg. K., and so is roughly constant. A convenient mean value for present purposes is $A_2(2) = 24$.

Inserting numerical values for physical constants,

$$\lambda_e = 2{\cdot}1 \times 10^{-6}\theta^{\frac{5}{2}} \text{ c.g.s. units.} \tag{4}$$

(ii) *Lorentzian gas.*—The thermal conductivity λ_l of a Lorentzian gas when the lighter and heavier particles are present in equal concentrations and are electrons and protons respectively (collisions between electrons and electrons being neglected) is given (**8**) by

$$\lambda_l = k\left(\frac{2k\theta}{m}\right)^{\frac{1}{2}}\left(\frac{2k\theta}{e^2}\right)^2 \frac{\Gamma(5)}{3\pi^{\frac{1}{2}}A_1(2)}, \tag{5}$$

where

$$A_1(2) = \log_e(1+v_{01}^2). \tag{6}$$

In cases of interest to us, $A_2(2) \doteqdot 2A_1(2)$, whence we find $\lambda_l/\lambda_e \doteqdot 6$. It is clear that in a highly ionized gas, electrons collide mainly with electrons, and the thermal conductivity does not differ greatly from that of an electron gas. We therefore take the thermal conductivity to be as given by (4).

4. *The Temperature Distribution.*—The presence of a magnetic field prevents the flow of heat by conduction other than in the direction of lines of magnetic force, in which direction the thermal conductivity is not significantly affected by the presence of the field. Thus the direction of heat transfer depends upon the inclination of the lines of magnetic force to the Sun's surface and varies with latitude. For simplicity, we first restrict consideration to heat flow perpendicular to the Sun's surface, as in high latitudes, but other cases may be readily treated.

With vertical heat flow, the equation of thermal transfer in the absence of convection is

$$\frac{d}{dz}\left(A\theta^{\frac{5}{2}}\frac{d\theta}{dz}\right) + H = R, \tag{7}$$

where H is the rate of production of heat per unit volume per second, R is the quantity of heat radiated per unit volume per second and A equals $2{\cdot}1 \times 10^{-6}$. In the upper chromosphere and corona absorption of radiation is negligible compared with R.

The magnitude of H is unknown. In that region of steep temperature gradient between the upper chromosphere and inner corona we may, however, suppose that the heat production is small compared with the heat flowing in from higher elevations, so that H may be neglected.

The temperature distribution as maintained by conduction alone is found by putting $R=0$ in equation (7), whence for a constant flow of heat across all sections

$$\frac{d}{dz}\left(A\theta^{\frac{5}{2}}\frac{d\theta}{dz}\right)=0, \tag{8}$$

the solution of which is

$$\theta^{\frac{7}{2}}=7C(z+z_0)/2A, \tag{9}$$

where C is an integration constant equal to the rate of flow of heat across unit section and z_0 is an integration constant which may be omitted by a suitable redefinition of the origin of coordinates. The temperature is fairly uniform when θ is high, but the gradient is steep for the lower temperatures. We may compare (9) with observation, according to which the temperature rises from small values to 10^6 deg. K. in not more than 10^9 cm. between the chromosphere and corona. Thus

$$C=6\times 10^5 K \text{ erg/cm.}^2\text{/sec.}, \tag{10}$$

where $K \geqslant 1$. The temperature distribution as maintained by conduction alone is shown in Fig. 1, for the case in which $K=1$.

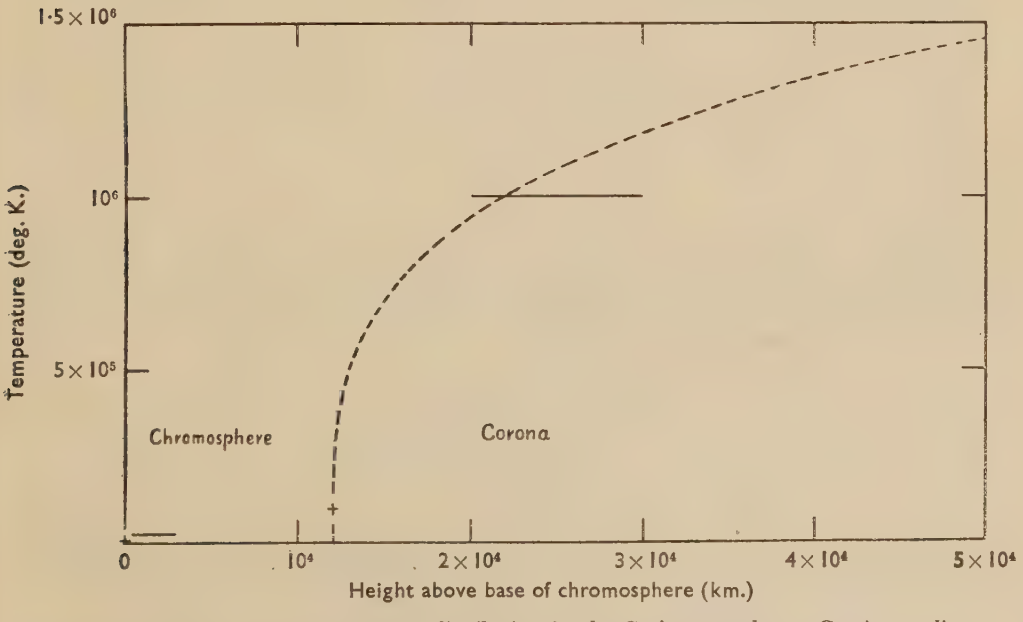

FIG. 1.—*The known temperature distribution in the Sun's atmosphere. Continuous lines indicate the regions in the chromosphere and corona which appear to be approximately isothermal. The temperature at 12,000 km. is an estimate from the electron concentration, derived from observations of the elevation to which Hα can be observed at eclipses. The broken line is obtained from equation* (9), *with* $C=6\times 10^5$ *erg/cm.*^{2}*/sec.*

The inflow of heat in the above region cannot be less than that due to conduction, so that (10) gives a lower limit to its magnitude. It is easy to see, however, that conduction cannot account for the temperature distribution in all regions, for (9) and (10) indicate that the temperature falls from 3×10^4 deg. K. to zero in less than half a kilometre. This is due to the increasingly sharp temperature gradient required to conduct a given quantity of heat as the temperature falls. We shall therefore investigate the hypothesis that radiation becomes significant in reducing the quantity of heat to be conducted as the temperature falls.

It is first necessary to obtain an estimate of R, the heat radiated per unit volume per second. This can be derived from a knowledge of the populations of the excited atomic states and of the rate of recombination. Consideration has been given elsewhere (**9**) to the populations of some of the substates of hydrogen when conditions depart markedly from thermodynamic equilibrium. It was found that the populations depend on the spectral energy density of any incident radiation; but this is largely due to the process of scattering, in which a quantum is absorbed and re-emitted without energy gain or loss to the gas. We obtain a fair estimate of the rate of line emission by neglecting the effect of the radiant energy incident on the gas. Over the range $2{\cdot}5 \times 10^4 \leqslant \theta \leqslant 10^5$ deg. K., $10^9 \leqslant N_e \leqslant 10^{11}$ per cc., the sum of the energies emitted in the $L\alpha$, $L\beta$ and $H\alpha$ lines may be expressed roughly as $2 \times 10^{-14} N_e^2 \theta^{-2}$ erg/c.c./sec.

Again, most of the energy radiated in recombination processes is in the Lyman continuum. In the range $5 \times 10^4 \leqslant \theta \leqslant 10^6$ deg.K., the rate of radiation in the Lyman continuum is about $1{\cdot}0 \times 10^{-19} N_e^2 \theta^{-1}$ erg/c.c./sec.

At high temperatures, radiation becomes relatively unimportant compared with conduction, and we see that below 10^5 deg. K., line emission is more important than emission by recombination. It is probable that the rate of radiation in all lines and continua is not far from

$$R = \eta N_e^2 \theta^{-2} \text{ erg/c.c./sec.}, \tag{11}$$

where $\eta \approx 4 \times 10^{-14}$, over the ranges of N_e and θ considered in this note.

If we now integrate the energy radiated below a height such that $\theta = \theta_1 = 10^6$ deg. K., at which $N_e = N_1 \approx 4 \times 10^8$ per c.c., we find

$$\int R dz = \eta \int_{\theta}^{\theta_1} N_e^2 \theta^{-2} dz. \tag{12}$$

Since the pressure changes only slowly over large distances when θ is of the order of 10^6 deg. K., and since the distances involved are small when θ is much lower, we may regard the pressure as constant. Thus from (9) and (12)

$$\begin{aligned} \int R dz &= \eta (N_1 \theta_1)^2 (A/C) \int_{\theta}^{\theta_1} \theta^{-\frac{3}{2}} d\theta \\ &= -2\eta (N_1 \theta_1)^2 (A/C) [\theta^{-\frac{1}{2}}]_{\theta}^{\theta_1} \\ &= (45/K)[10^3 \theta^{-\frac{1}{2}} - 1]. \end{aligned} \tag{13}$$

If the amount radiated in the region between two planes whose temperatures are 10^6 deg. K. and θ equals a fraction f of the total heat flowing past the upper of these planes, we can thus write

$$(45/K)[10^3 \theta^{-\frac{1}{2}} - 1] = 6 \times 10^5 Kf. \tag{14}$$

The fraction f cannot have any appreciable magnitude for any temperature for which this relation is valid (say, $\theta > 2{\cdot}5 \times 10^4$ deg. K.). For example, with

$K=1, f=0{\cdot}1$, equation (14) gives θ to be about 1 deg. K. We deduce that radiation cannot significantly dispose of the inflowing heat. Since the heat cannot be conducted at the comparatively low temperature of the chromosphere, we are forced to the conclusion that convection processes must be responsible for transferring a considerable fraction of the heat through the highest part of the chromosphere. Radiation becomes important in somewhat lower regions of the chromosphere, as pointed out by Bondi, Hoyle and Lyttleton, who showed that the chromosphere emits as radiation almost all the inflowing heat.

5. *Thermal Conduction in Low Latitudes.*—We now consider the temperature distribution in the corona in equatorial zones. There the Sun's general magnetic field, if it approximates to that of a dipole, will be only slightly inclined to the surface, and so, neglecting transverse conduction and other modes of heat transfer, the flow of heat in the corona will be almost parallel to the Sun's surface. We may thus expect a temperature maximum in equatorial zones. This is in conformity with observation; for the intensity of the 5303 A. line is a maximum in equatorial zones and a minimum near the poles, as may be seen from results in the *Quarterly Bulletins on Solar Activity*, while Waldmeier's eclipse measurements (**10**) indicate that the temperature increases with the intensity of this line.

To see the order of magnitude of the temperature expected when heat transfer is solely by conduction along lines of force, we note that the equation of a line of force in a dipole field, the axis being parallel to the solar axis, is

$$y^2 = Cr^3,$$

where y is the distance from the polar axis and r the distance from the centre of the Sun, C being a constant. It can readily be shown that a line of force passing a distance a above the Sun's surface at the equator, where $a \ll r_0$, meets the Sun's surface at two points $2\sqrt{ar_0}$ apart. If $a=3\times10^4$ km., this separation is $2{\cdot}9\times10^5$ km. Now suppose, for simplicity, that a tube of force has constant cross-section of 1 cm.^{2}, and that a total amount of heat of 6×10^5 erg/sec. is generated uniformly along its length. Putting $R=0$, the solution of equation (7) is

$$\theta^{\frac{7}{2}} = -\frac{7Hz^2}{4A} + bz + g,$$

where z is now measured along the tube of force, and b and g are integration constants. The length of the tube of force above the Sun's surface is approximately $2\sqrt{ar_0}$. With θ small (≈ 0) when $z=0$, and $d\theta/dz=0$ when $z=\sqrt{ar_0}$, then

$$\theta^{\frac{7}{2}} = -\frac{7H}{4A}z^2 + \frac{7H\sqrt{ar_0}}{2A}z.$$

Inserting numerical values, and putting $a=3\times10^4$ km., we find the maximum value of θ along the tube of force to be $1{\cdot}7\times10^6$ deg. K., of the order of magnitude of that observed. It follows that conduction can adequately account for heat transport in the corona both in the absence of a general magnetic field and in the presence of a dipole field.

The radial temperature gradient between the upper chromosphere and inner corona is difficult to predict for equatorial zones. In addition to the unknown rate of heating, it depends on the transverse thermal conductivity and so on the strength of the general magnetic field. It also depends on the effectiveness of convection in the upper chromosphere. The gradient should not be less than that in polar regions, where the magnetic field is approximately radial.

Our conclusions may be summarized as follows :—

(1) The corona is a region where heat transfer seems to be due mainly to conduction.

(2) In the highest parts of the chromosphere heat transfer is mainly by convection.

(3) The transition region where the main agent of heat transfer changes from convection to conduction is a region of high temperature gradient. It is reasonable to identify this with the boundary between the chromosphere and the corona.

These deductions differ from those of Bondi, Hoyle and Lyttleton, who invoked convection to explain the transfer of heat in the corona as well as in the chromosphere.

This work has been carried out as part of the research programme of the Commonwealth Council for Scientific and Industrial Research.

Division of Physics,
National Standards Laboratory,
Chippendale, N.S.W. :
1949 *January* 4.

References

(1) H. Alfvén, *M.N.*, **107,** 211, 1947.
(2) H. Bondi, F. Hoyle, and R. A. Lyttleton, *M.N.*, **107,** 184, 1947.
(3) H. Alfvén, *Ark. Mat. Astr. Fys.*, **27 A,** No. 25, 1941.
(4) R. v. d. R. Woolley, *Aust. J. Science*, Supplement to Vol. **10,** No. 2, 1947.
(5) R. O. Redman, *M.N.*, **102,** 140, 1942.
(6) R. G. Giovanelli, *Aust. J. Sci. Res.*, **1,** 360, 1948.
(7) S. Chapman and T. G. Cowling, *The Mathematical Theory of Non-Uniform Gases*, Cambridge, 1939, p. 179.
(8) S. Chapman and T. G. Cowling, *loc. cit.*, p. 191.
(9) R. G. Giovanelli, *Aust. J. Sci. Res.*, **1,** 289, 1948.
(10) M. Waldmeier, *Astronomische Mitteilungen der Eidgenössischen Sternwarte Zürich*, No. 149, 1947.

FAINT STARS WITH PROPER MOTIONS EXCEEDING 0″·15 PER ANNUM IN HYDERABAD ASTROGRAPHIC ZONES, LIST VI

(Communicated by the Director)

(Received 1949 March 2)

Summary

This paper gives a list of 50 faint stars with relative proper motion exceeding 0″·15 per annum.

The present list is a continuation of the previous work. The Hyderabad Serial number is continued from the fifth list of this series.* For details of method of comparison and reduction of proper motions, reference may be made to the above cited papers.

The plates were mainly blinked by Mr S. Aravamuthan and measured by Mr U. S. Rao; the reductions were carried out by Messrs M. V. V. Sastry and S. Aravamuthan.

Proper motions exceeding 0″·15 per annum in Hyderabad Astrographic Zones :—VI

Serial No.	Ptg. Mag.	R.A. (1900)	Decl. (1900)	μ_α	μ_δ
		h m s	° ′	″	″
242	11·4	0 0 35	−19 17·7	−0·156	−0·057
243	11·5	0 14 02	−20 6·2	+0·129	−0·200
244	11·1	1 42 20	−19 58·0	+0·156	−0·085
245	12·7	2 26 30	−20 8·1	+0·082	−0·151
246	12·8	6 57 51	−17 59·1	+0·027	−0·164
247	12·9	8 11 16	−17 33·8	+0·177	−0·027
248	12·8	8 47 43	−17 22·3	+0·068	−0·163
249	10·8	9 28 47	−19 57·6	−0·114	−0·114
250	11·6	9 30 41	−19 11·4	−0·128	+0·156
251	11·3	9 42 30	−19 52·3	+0·110	+0·110
252	10·9	9 48 34	−19 48·4	+0·129	−0·171
253	12·9	9 49 49	−18 52·5	+0·063	−0·142
254	12·6	9 53 09	−18 57·6	−0·028	+0·185
255	12·5	10 19 24	−19 41·6	−0·114	−0·142
256	13·1	10 19 31	−18 2·8	−0·158	−0·095
257*	11·9	10 23 11	−17 59·2	−0·164	+0·092
258*	11·3	10 23 25	−19 6·9	−0·166	−0·038
259	10·5	10 31 02	−19 5·2	−0·170	+0·114
260	11·4	10 32 27	−19 1·0	−0·126	+0·141
261	13·0	10 40 58	−18 34·3	−1·809	−0·645
262	12·3	10 43 38	−19 40·4	−0·205	−0·110
263	12·7	11 04 21	−20 0·0	−0·141	−0·079
264	8·8	11 15 25	−20 7·7	−0·184	+0·014
265	10·8	11 16 07	−18 59·3	−0·071	+0·127
266	11·8	11 19 50	−19 12·1	+0·057	−0·142
267	12·2	11 44 45	−18 39·5	+0·095	−0·126
268	12·2	11 54 26	−19 35·9	−0·173	+0·110

* *M.N.*, 107, 397, 1947.

Serial No.	Ptg. Mag.	R.A. (1900)	Decl. (1900)	μ_α	μ_δ
		h m s	° ′	″	″
269*	11·8	12 0 43	−18 18·6	+0·029	−0·313
270	12·7	12 35 42	−20 5·4	−0·063	−0·189
271	12·0	12 37 19	−18 24·9	−0·158	+0·047
272	11·7	13 36 41	−19 58·5	−0·456	−0·016
273	12·7	21 59 36	−16 22·5	−0·095	−0·191
274	12·8	22 0 12	−17 2·0	−0·300	−0·232
275	12·0	22 0 31	−18 46·7	−0·164	−0·055
276	13·1	22 6 49	−17 42·6	+0·191	−0·136
277	10·1	22 7 35	−16 14·5	+0·232	−0·150
278*	11·4	22 7 58	−19 52·2	+0·014	−0·218
279	11·7	22 10 42	−19 37·0	−0·165	0·000
280	12·8	22 13 54	−18 36·4	−0·164	−0·082
281	10·6	22 40 39	−16 6·9	−0·041	−0·190
282	12·6	22 56 20	−19 41·5	−0·071	−0·214
283	9·4	22 57 38	−19 10·6	+0·014	−0·214
284	11·2	23 03 09	−18 46·7	+0·143	−0·086
285	11·3	23 19 38	−18 10·4	−0·014	−0·157
286	9·4	23 27 30	−18 21·8	+0·171	+0·029
287	12·6	23 32 2	−19 17·9	+0·299	0·000
288	10·6	23 34 49	−20 0·2	+0·269	−0·224
289*	11·8	23 40 29	−18 18·2	+0·071	−0·160
290	12·0	23 46 56	−17 34·2	+0·082	−0·137
291*	11·2	23 49 41	−19 8·6	−0·226	−0·120

Nizamiah Observatory,
Hyderabad, Deccan, India :
1948 *December* 31.

OCCULTATIONS OF STARS BY THE MOON OBSERVED AT THE NIZAMIAH OBSERVATORY, HYDERABAD, DURING THE YEAR 1947

(Communicated by the Director)

(Received 1949 March 2)

TABLE I

No.	Star	Mag.	Phase	Date 1947	U.T. h	m	s	Obs.
1	η Leon	3·6	R	Jan. 10	0	21	55·2	V.
2	*A* Gemi	5·1	D	Feb. 3	19	31	46·9	V.
3	τ Taur	4·3	D	,, 28	13	15	25·2	V.
4	η Leon	3·6	D	Mar. 5	20	37	31·8	V.
5	η Leon	3·6	R	,, 5	21	15	49·5	V.
6	τ Virg	4·8	R	,, 9	20	40	49·8	M.G.
7	118 Taur *f.*	5·9	D	,, 28	13	42	25·2	V.
8	B.D.+19° 2250	9·2	D	Apr. 1	17	57	0·5	M.G.
9	B.D.+19° 2251	6·6	D	,, 1	18	11	31·0	M.G.
10	θ Ophi	3·4	D	,, 10	19	19	10·1	V.
11	θ Ophi	3·4	R	,, 10	20	30	40·8	V.
12	35 Capr	6·0	R	May 12	21	37	24·3	M.G.
13	B.D.+26° 1410	8·6	D	,, 23	13	46	28·9	V.
14	40 Gemi	6·3	D	,, 23	13	51	25·1	V.
15	B.D.+12° 2284	6·4	D	,, 27	14	49	5·3	V.
16	66 Virg	5·8	D	,, 30	13	41	49·6	M.G.
17	14 Taur	6·3	R	Sept. 6	21	24	54·2	M.G.
18	376 B Aquar	6·3	D	Oct. 26	16	18	39·7	M.G.
19	134 B Gemi	6·5	R	Nov. 3	20	48	13·5	M.G.
20	125 Taur	5·0	R	,, 29	15	57	38·8	M.G.
21	ω Canc	5·9	R	Dec. 1	20	27	18·0	M.G.
22	ξ Canc	5·2	R	,, 2	23	35	48·4	M.G.
23	79 Canc	6·1	R	,, 2	23	59	50·8	M.G.
24	72 Virg	6·1	R	,, 7	23	47	7·4	M.G.

The last column indicates the following observers :
V. : M. V. V. Sastry.
M.G. : Mahomed Ghouse.

TABLE II

No.	$\sigma'-\sigma$ ″	cos $(\rho-\chi)$	sin $(\rho-\chi)$	No.	$\sigma'-\sigma$ ″	cos $(\rho-\chi)$	sin $(\rho-\chi)$
1	−2·9	−0·92	+0·40	13	−1·2	+0·79	−0·61
2	−1·8	+0·59	−0·81	14	+0·8	+0·83	−0·56
3	−0·5	+0·68	+0·73	15	−2·3	+0·84	−0·55
4	−2·1	+0·72	+0·69	16	−0·9	+0·98	+0·18
5	−0·3	−0·34	+0·94	17	+1·1	−0·98	−0·20
6	+1·0	−1·00	−0·02	18	−1·0	+0·85	+0·53
7	−0·8	+0·85	+0·52	19	+1·5	−0·98	+0·19
8	+0·6	+0·86	+0·51	20	[+4·2]	−0·98	−0·21
9	−2·7	+0·70	+0·71	21	+2·2	−0·92	−0·39
10	+0·9	+0·96	+0·27	22	+1·2	−0·66	+0·75
11	+0·4	−0·72	+0·70	23	+0·3	−0·36	+0·93
12	−3·2	−0·75	−0·66	24	+1·1	−0·94	+0·34

The instrument used throughout was the 15-inch visual refractor. The corrections to the standard clock were determined from observations with the transit instrument. The reductions were carried out by M. V. V. Sastry, assisted by S. Aravamuthan. No correction was applied to the observed time.

The mean places for 1947·0 of two stars (Nos. 8 and 13) are given in the following table. For star No. 13, proper motions have been applied to the coordinates given in the catalogue in computing the mean place for use in the reduction.

TABLE III

No.	R.A. (1947·0)			Dec. (1947·0)			Remarks
	h	m	s	°	′	″	
8	9	41	17·65	+19	5	58·7	A. G. Berlin 3913
13	6	55	57·93	+25	59	7·5	A. G. Cambridge 3644 $\mu_\alpha - 0^s{\cdot}0002$; $\mu_\delta + 0''{\cdot}011$

Nizamiah Observatory,
Hyderabad, Deccan, India:
1948 *December* 31.

OCCULTATIONS OF STARS BY THE MOON OBSERVED AT THE NIZAMIAH OBSERVATORY, HYDERABAD, DURING THE YEAR 1948

(Communicated by the Director)

(Received 1949 March 23)

TABLE I

No.	Star	Mag.	Phase	Date 1948	U.T. h	m	s	Obs.
1	B.D.+14° 469	6·8	D	Jan. 20	16	26	19·5	M.G.
2	95 Taur	6·2	D	,, 22	17	51	8·4	V.
3	η Leon	3·6	D	,, 27	15	54	41·6	V.
4	η Leon	3·6	R	,, 27	16	12	9·3	V.
5	46 Virg	6·1	R	,, 30	22	59	0·7	V.
6	B.D.+18° 459	7·3	D	Feb. 17	14	37	58·4	V.
7	v^1 Canc	5·7	D	,, 22	14	14	13·6	M.G.
8	v^2 Canc	6·4	D	,, 22	15	01	51·3	M.G.
9	B.D.+6° 228	6·7	D	Mar. 13	13	38	52·5	V.
10	53 Arie	6·1	D	,, 15	15	03	25·5	V.
11	B.D.+27° 943	6·8	D	,, 18	15	40	3·0	M.G.
12	B.D.+27° 1296	7·2	D	,, 19	13	48	32·0	M.G.
13	47 Gemi	5·6	D	,, 19	19	27	27·2	M.G.
14	B.D.+26° 1481	6·8	D	,, 19	19	39	30·7	M.G.
15	ξ Canc	5·2	D	,, 21	14	29	51·0	M.G.
16	79 Canc	6·1	D	,, 21	15	12	4·4	M.G.
17	90 H′ Canc	6·1	D	,, 21	17	30	18·0	M.G.
18	A Sgtr	5·0	R	Apr. 29	22	50	28·3	M.G.
19	B.D.+24° 1968	6·8	D	May 14	16	34	1·6	M.G.
20	46 Leon	5·7	D	,, 16	15	53	34·8	M.G.
21	27 Pisc	5·1	D	Oct. 15	21	59	33·7	M.G.
22	B.D.+24° 674	6·3	R	,, 21	18	07	54·7	M.G.
23	B.D.−2° 31	7·2	D	Nov. 12	13	33	2·9	M.G.
24	54 Ceti	5·9	D	,, 14	18	50	42·5	M.G.
25	χ^2 Aqar	4·6	D	Dec. 8	13	04	54·3	N.P.
26	29 Pisc	5·2	D	,, 9	15	00	15·1	M.G.
27	ξ Canc	5·2	R	,, 19	17	48	1·1	N.P.
28	79 Canc	6·1	R	,, 19	18	17	26·4	N.P.
29	90 H′ Canc	6·1	R	,, 19	20	55	7·1	N.P.
30	η Leon	3·6	R	,, 20	18	37	18·9	N.P.

The last column indicates the following observers :

V. : M. V. V. Sastry.
M.G. : Mahomed Ghouse.
N.P. : Nataraj Pillay (under training from Trivandrum Observatory).

The instrument used throughout was the 15-inch visual refractor. The corrections to the standard clock were determined from observations with the transit instrument. The reductions were carried out by S. Aravamuthan assisted by K. B. Shameem. No correction was applied to the observed time.

TABLE II

No.	$\sigma'-\sigma$	cos $(\rho-\chi)$	sin $(\rho-\chi)$	No.	$\sigma'-\sigma$	cos $(\rho-\chi)$	sin $(\rho-\chi)$
	"				"		
1	−0·3	+0·81	−0·59	16	−2·3	+0·77	+0·64
2	+0·9	+0·75	−0·67	17	−2·9	+0·94	−0·33
3	+1·5	+0·31	−0·95	18	−1·3	−0·53	+0·85
4	+1·5	−0·22	−0·98	19	−0·6	+0·66	+0·75
5	+2·2	−0·33	+0·94	20	0·0	+0·94	−0·34
6	+0·1	+0·79	+0·62	21	+0·4	+0·97	−0·25
7	−1·5	+1·00	−0·03	22	+2·0	−0·97	+0·22
8	+0·4	+0·98	+0·20	23	−0·1	+0·66	−0·75
9	−2·2	+0·93	−0·35	24	+1·1	+0·82	+0·57
10	−0·5	+0·80	−0·60	25	−2·3	+0·93	−0·36
11	−0·8	+0·87	+0·49	26	−1·8	+0·67	+0·74
12	−3·1	+0·93	−0·36	27	−0·6	−0·45	+0·89
13	−1·4	+0·70	+0·71	28	−0·5	−0·42	+0·91
14	−0·1	+0·51	−0·86	29	+1·1	−0·79	−0·62
15	−1·3	+0·89	+0·45	30	+1·4	−1·00	+0·10

Nizamiah Observatory,
Hyderabad, Deccan, India :
1949 *February.*

ON THE NATURE OF THE EARTH'S CORE*

W. H. Ramsey

(Received 1949 June 5)

In a previous paper (*M.N.*, **108**, 406, 1948) the author has suggested that the density jump at the boundary of the Earth's core is due to a phase transition under pressure, and not to the appearance of a new material such as iron. A metallic type of structure was proposed for the material in the core. In the present paper the transition to the metallic phase is explained in greater detail. Seismological data are used to prove that the core cannot be composed of either iron or an alloy of nickel and iron. It is shown how the theory removes certain difficulties arising from the hypothesis of an iron core, and how it can account for features not hitherto explained.

* The full text of this paper is published in *M.N., Geophys. Suppl.*, **5**, No. 9, 1949.